

# POLITECNICO DI TORINO

Department of Chemical and Materials Engineering

**Master of Science course  
In Materials Engineering**

Master of Science Thesis

## **Cationic photopolymerization and hot lithography technology: characterization and 3D printing study of epoxy-based photopolymers**



**Tutor**

prof. Marco Sangermano  
prof. Jürgen Stampfl

**Candidate**

Corrado Dall'Argine

March 2020





## ***Sommario del lavoro di tesi***

### **1. Obiettivo del progetto e stato dell'arte**

Il processo di fotopolimerizzazione consente, tramite l'emissione di un certa lunghezza d'onda da parte di una sorgente di luce, di ottenere un network polimerico partendo da una resina, solitamente allo stato liquido. Grazie alle reazioni chimiche foto-indotte, la fotopolimerizzazione evidenzia numerosi vantaggi rispetto ai tradizionali processi di indurimento di monomeri di termoindurenti: assenza di solventi, trattamenti a temperatura ambiente, utilizzo di prodotti meno inquinanti, rapidità di processo e riduzione di costi. Grazie a queste peculiarità, le applicazioni della fotopolimerizzazione sono cresciute negli anni: originariamente presente nel settore della finitura superficiale del legno, i fotopolimeri sono oggi impiegati nella creazione di rivestimenti protettivi e vernici, nel settore medicale, in particolare dentale, e nel settore dei materiali compositi come matrici. Questo tipo di polimeri costituiscono ancora il principale materiale venduto e conseguentemente impiegato nel settore della fabbricazione additiva: essenzialmente utilizzati per la prototipazione rapida, i polimeri foto-curabili rappresentano una potenziale risorsa da sviluppare e migliorare parallelamente allo studio e alla crescita delle tecnologie di stampa 3D.

Questo progetto si inserisce in questo panorama proponendo una caratterizzazione di una formulazione fotopolimerica a base epossidica: tale sistema risulta curabile tramite fotopolimerizzazione cationica, un meccanismo di fotopolimerizzazione meno conosciuto e sfruttato rispetto a quello radicalico soprattutto in ambito di stampa 3D. L'obiettivo di questo lavoro è modificare e caratterizzare dal punto di vista termo-meccanico tale formulazione foto-curabile, dimostrandone la stampabilità grazie all'impiego di un innovativo approccio di stereolitografia, che sfrutta l'aumento di temperatura di processo. Tramite tale caratterizzazione, il lavoro svolto mira ad introdurre la fotopolimerizzazione cationica come metodo affidabile per lo sviluppo di nuovi ed innovativi fotopolimeri, processabili tramite tecniche basate sulla stereolitografia. La formulazione di partenza, costituita da una resina epossidica a base bisfenolo A (BADGE/BDGE) e da un fotoiniziatore di tipo cationico (sale di triarilsolfonio esafluoroantimoniato), verrà modificata inserendo un agente di trasferimento di catena, opportunamente selezionato tra diversi composti chimici: tale aggiunta dovrebbe garantire migliore controllo sulla formazione del network della resina polimerizzata e portare ad una reattività maggiore del sistema ad alte temperature. Una volta caratterizzate le diverse formulazioni preparate tramite test meccanici, prove foto-termiche e foto-reologiche, quella considerata più idonea verrà scelta per essere sottoposta ad un processo di stampa 3D all'interno della macchina. Al fine di dimostrarne la processabilità tramite un processo di stereolitografia a caldo, campioni per prove meccaniche verranno stampati e successivamente testati per confrontarli con i risultati precedenti, in modo da conoscere l'influenza che il processo di stampa ha sulle caratteristiche del fotopolimero. Infine nell'ottica di migliorare le proprietà di tale fotopolimero, alcuni additivi tenacizzanti verranno introdotti nella formulazione e verrà indagata la loro capacità di modificare opportunamente il materiale finale.

Per poter comprendere meglio il lavoro qui presentato, una visione d'insieme dei meccanismi alla base della fotopolimerizzazione cationica verrà data di seguito; in aggiunta una descrizione del metodo di fabbricazione additiva sfruttato si rende necessaria per capire il lavoro svolto.

La fotopolimerizzazione cationica è stata scoperta dal professor Crivello negli anni '70 a seguito dell'osservazione del comportamento di alcuni sali di iodonio e solfonio ("onium salt") irradiati con sorgente UV: la formazione di una forte soluzione acida, conseguentemente all'interazione con l'emissione di luce, permetteva la polimerizzazione cationica di un

monomero di tipo vinilico. Questo tipo di fotopolimerizzazione desta crescente interesse nella ricerca di nuovi fotopolimeri grazie ai suoi evidenti vantaggi rispetto alle formulazioni fotopolimerizzabili per via radicalica: nessun blocco della reazione dovuto all'interazione con ossigeno o aria, bassa sensibilità verso l'acqua, processo di cura al buio ("dark curing"), processo privo di solventi o prodotti tossici ed inquinanti. Alcuni monomeri come per esempio quelli a base epossidica o vinilica possono essere fotopolimerizzati solo grazie a tale metodo: il meccanismo attraverso il quale fotopolimerizza un monomero di tipo epossidico è riportato in figura 2.4. Grazie all'apertura dell'anello epossidico, il polimero ottenuto da questo tipo di polimerizzazione mostrerà un'alta stabilità dimensionale e un basso ritiro volumetrico, tale caratteristica costituisce un ulteriore vantaggio rispetto alla fotopolimerizzazione radicalica di acrilati e metacrilati, solitamente caratterizzati da forti distorsioni dimensionali a seguito della polimerizzazione. Oltre al monomero di partenza, l'altro componente fondamentale in una formulazione fotocurabile di tipo cationico è il fotoiniziatore: osservando la figura 2.8, ove sono riportati alcuni esempi di fotoiniziatori cationici e schematicamente il meccanismo di formazione dell'acido. Un sale di iodonio o solfonio, come quelli studiati dal prof. Crivello, è in grado di generare una specie fortemente acida ( $\text{HMX}_n$ ) a seguito di complesse reazioni fotoindotte dalla sorgente di luce, la quale emette solitamente nell'UV. La struttura del sale è composta da una specie di tipo anionico e di tipo cationico: quest'ultima definisce la fotochimica del composto, ovvero l'assorbimento e l'efficienza del fotoiniziatore, ed anche la stabilità termica. La controparte anionica determina in maniera diretta le proprietà chimiche del sale: la forza dell'acido formato e la sua stabilità, l'efficienza del fotoiniziatore e la cinetica della propagazione della reazione. Una volta generata la specie acida a seguito della radiazione assorbita, il meccanismo di propagazione della reazione, nel caso di un monomero epossidico, è di tipo crescita a catena, come riportato in figura 2.4: il carbocatione, altamente reattivo, che si forma a seguito dell'interazione con l'acido generato porta la catena a crescere per conseguente attacco di monomeri epossidici, i quali, aprendo l'anello, propagano la reazione. Le terminazioni della catena in questo genere di fotopolimerizzazione sono limitate, per tale motivo la conversione dei gruppi funzionali all'interno del fotopolimero risulta essere elevata e procede persino rimossa la fonte di luce: questo è il meccanismo di cura al buio tipico di tale polimerizzazione. Tale meccanismo di crescita della catena può essere regolato e modificato inserendo un cosiddetto agente di trasferimento della catena: il suo ruolo all'interno della reazione è spostare il sito attivo di crescita della catena dal monomero a tale agente, il quale potrà proseguire la crescita di una nuova catena attivando un altro monomero. A titolo di esempio in figura 2.13 è visibile la differente propagazione della catena polimerica, partendo da un monomero di natura epossidica, in assenza ed in presenza dell'agente di trasferimento della catena. I composti che possono svolgere tale ruolo in presenza di monomeri di tipo epossidico sono essenzialmente alcoli organici: scegliendo l'agente corretto è possibile modificare il network del fotopolimero e controllare le sue proprietà, adattandole alle esigenze; in aggiunta la reattività e la cinetica stessa della fotopolimerizzazione sono modificate in presenza di tale aggiunta nella formulazione. A seconda delle applicazioni può rendersi necessario assorbire radiazioni a lunghezze d'onda maggiori, questo è reso possibile impiegando un fotosensibilizzatore: il quale, accoppiato al fotoiniziatore, è in grado di assorbire radiazioni a lunghezze d'onda maggiori e tramite il meccanismo di trasferimento dello stato eccitato mostrato in figura 2.16 è in grado di indurre la formazione della specie acida da parte del fotoiniziatore.

Il principio alla base delle tecniche di fabbricazione additiva è la creazione di un oggetto o un componente partendo dal file dello stesso realizzato tramite software di modellazione CAD: una volta definito l'oggetto, il file viene convertito in formato STL, successivamente si svolgono l'eventuale aggiunta di supporti e l'orientamento dell'oggetto, seguite poi dall'operazione di slicing, che definisce la divisione in strati che assemblati tra loro dalla

stampante lungo la direzione di crescita (asse zeta) porteranno alla realizzazione della parte desiderata. L'operazione svolta dalla stampante di sovrapposizione dei singoli layer precedentemente definiti, differenzia la fabbricazione di oggetti in maniera additiva (addizione di strato su strato) dai metodi produttivi tradizionali di fusione o di sottrazione di materiale (vedi figura 3.1). Il vantaggio di tale metodo produttivo è rappresentato dall'elevata libertà concessa nel realizzare il design e le funzionalità del componente da stampare, scongiurando problematiche e aumento dei costi di processo. Gli svantaggi tutt'ora collegati al processo di additive manufacturing derivano dal fatto che tale tecnologia era stata inizialmente pensata per la costruzione di prototipi: la velocità di costruzione del pezzo e i volumi di lavoro sono limitati, i materiali stampabili sono in numero ridotto e le proprietà meccaniche dei materiali stampati risultano insufficienti per certe applicazioni, infine la precisione e la risoluzione dei prodotti stampati risultano spesso non idonee per reali applicazioni e quindi una finitura superficiale è sempre richiesta. Ad oggi la fabbricazione additiva permette di processare principalmente metalli e polimeri, in quest'ultimo ambito comprende svariate tecniche che si differenziano per lo stato fisico della materia prima utilizzata per la stampa: le tecnologie che processano il polimero in polvere, quelle che stampano partendo da un filamento polimerico ed infine le stampanti che partono da liquido, possibile esclusivamente per polimeri. Tra le tecniche di stampa tridimensionale che sfruttano i polimeri in forma liquida, la più vecchia è la stereolitografia a laser (SLA): la piattaforma di lavoro è sommersa in una vasca di resina liquida, al di sopra di essa si trova il sistema di specchi che direziona il fascio laser. Il componente viene costruito strato per strato, di spessori definiti, con progressivo abbassamento della piattaforma: la figura 3.4 mostra le possibili varianti del sistema base della stereolitografia a vasca piena, che risulta affetto da tempi lunghi di processo e spreco di materiale dovuto al riempimento della vasca. Ad oggi la stereolitografia rimane il processo che assicura le migliori prestazioni in termini di finitura superficiale e del rispetto delle tolleranze dimensionali dei pezzi, il suo impiego in applicazioni diverse dalla prototipazione è limitato dal fatto che i materiali stampabili con tale tecnica sono essenzialmente polimeri termoindurenti, che in forma liquida sono caratterizzati da una bassa viscosità: questo insieme di fattori limita grandemente le prestazioni meccaniche del prodotto finale della stampa. Il processo di stereolitografia a caldo, sviluppato da Cubicure, punta a trovare una soluzione al problema di coniugare precisione di stampa tipica della SLA insieme a polimeri con proprietà meccaniche tipiche dei termoplastici, processabili con tecniche a filo o a letto di polveri. Uno schema del processo di stampa è presente in figura 3.8: la piattaforma di lavoro, il piano trasparente di stampa e l'unità di stratificazione dei layer sono riscaldabili sino a temperature di circa 120 °C: questo permette di processare resine altamente viscosi o scarsamente reattive a temperatura ambiente, normalmente non processabili nelle normali macchine SLA. La macchina lavora esattamente allo stesso modo di una stereolitografia a configurazione rovesciata: in cui il laser irradia il polimero da sotto attraverso un piano di lavoro trasparente, il componente viene costruito strato per strato alzando la piattaforma di lavoro; l'assenza di una vasca di materiale limita lo spreco di materiale e velocizza i tempi di stampa, accelerando le operazioni tra la costruzione di un layer e l'altro. Lo studio di nuove formulazioni fotopolimerizzabili basate su monomeri altamente viscosi o addirittura solidi a temperatura ambiente non prima stampabili può aprire la strada allo sviluppo di fotopolimeri con caratteristiche meccaniche migliorate e modificate opportunamente per ogni applicazione ed esigenza.

## **2. Materiali e metodi**

### *2.1 Materiali*

La formulazione di base, indicata come Reference, è composta da diglicidil etere di bisfenolo A o BADGE e dal 3% in peso di fotoiniziatore di tipo cationico triarilsolfonio

esafluoroantimoniato in soluzione con carbonato di propilene al 50% in peso. Gli agenti di trasferimento di catena inseriti nella formulazione di base per poter studiare la loro influenza sulla regolazione del network sono: trimetilolpropano, polipropilenglicole, politetraidrofurano e Boltorn H20 (polimero iper-ramificato). Le percentuali in cui tali composti sono stati aggiunti sono molari, tenendo conto del rapporto tra gruppi epossidici e gruppi idrossido: la nomenclatura completa delle formulazioni è riportata nel paragrafo 5.2. Il fotosensibilizzatore, utilizzato in questo caso per aver un maggior controllo sulla precisione di stampa dei singoli layer, è l'antracene, aggiunto nelle formulazioni per la stampa in percentuale in peso non oltre lo 0,5%, limite di solubilità dell'antracene nella resina BADGE. L'influenza positiva dell'antracene presente nella formulazione durante il processo di stampa è testimoniata dalla figura 6.8. Nel capitolo 7 sono stati studiati gli effetti di alcuni additivi al fine di migliorare le prestazioni meccaniche del fotopolimero: nanoparticelle di silice (fumed silica), particelle di gomma di tipo core-shell e polisilossani contenenti gruppi idrossido nella catena.

## *2.2 Metodi di analisi*

Le tecniche di analisi delle proprietà meccaniche usate per testare e confrontare tra loro i diversi polimeri derivanti dalla fotopolimerizzazione delle varie formulazioni sono state: la prova di trazione, l'analisi termica dinamo-meccanica (DMTA) e l'analisi di rilassamento degli sforzi. La foto-DSC e la foto-reologia sono i due strumenti utilizzati per studiare in situ la reazione di fotopolimerizzazione cationica in presenza di diverse concentrazioni dell'agente di trasferimento di catena. La foto-reologia è un'analisi sviluppata presso la TU appositamente per studiare la fotopolimerizzazione di resine per applicazioni nella SLA: il settaggio di tale strumento, visibile nella figura 4.9, prevede il collegamento di un reometro a piatti piani e paralleli con una lampada UV e un sistema in grado di emettere ed analizzare segnali IR (vicino e lontano).

## *2.3 Stampante 3D*

La stampante presente nei laboratori della TU, visibile in figura 4.12, è molto simile a quella commercializzata dall'azienda Cubicure: l'unica limitazione in questo caso sono le temperature massime a cui i componenti posso essere riscaldati, la piattaforma di lavoro raggiunge massimo 80 °C, mentre il piano trasparente può essere scaldato sino a 100 °C, così come l'unità di stratificazione e distribuzione della resina. Il processo di stampa è uguale alla versione commercializzata da Cubicure: il funzionamento di base è identico a quella di una SLA in configurazione rovesciata, in questo caso non è presente alcuna vasca per il contenimento del liquido, il quale viene mantenuto in temperatura dall'unità di stratificazione e distribuzione della resina.

# **3. Risultati e discussione**

La discussione dei risultati del lavoro sperimentale è divisa in 3 capitoli per una maggiore chiarezza di esposizione, perciò in questa sintesi verrà fatto lo stesso.

## *3.1 Selezione della formulazione per il processo di stampa*

Inizialmente si è scelto di confrontare tramite DMTA, in configurazione flessione a 3 punti, gli effetti dei differenti agenti di trasferimento di catena inseriti nella formulazione di base: i grafici nelle figure 5.6 e 5.7 permettono un confronto completo di tutte le formulazioni preparate (ad esclusione di quelle contenenti il Boltorn, il quale ha mostrato insolubilità nella resina). L'effetto atteso dalla presenza di questi componenti è la regolarizzazione del network polimerico, questo effetto è osservabile nella modifica dell'andamento della curva del modulo conservativo ricavata, la quale mostra, rispetto alla curva della formulazione Reference, una caduta del modulo netta e definita in corrispondenza della temperatura di transizione vetrosa ( $T_g$ ). Le curve relative al  $\tan \delta$  mostrano un picco in corrispondenza della  $T_g$  più ristretto e spostato a

temperature inferiori, tali effetti sono collegati alla presenza dell'agente di trasferimento di catena. La tabella 5.1 riassume i risultati principali ricavati dalla prova dinamo meccanica: la temperatura di transizione vetrosa diminuisce all'aumentare della concentrazione dell'agente di trasferimento di catena, a parità di concentrazione la diminuzione della  $T_g$ , rispetto al valore della formulazione Reference, risulta molto pronunciata nel caso del polipropilenglicole e del poliTHF, meno considerevole nel caso del trimetilolpropano. Il modulo conservativo, misurato a 25 °C, diminuisce in funzione della concentrazione dell'agente, eccetto in presenza del 20% molare di polipropilenglicole; il valore del modulo conservativo a fine curva, nella zona di plateau, può essere visto come un'indicazione della densità di reticolazione del fotopolimero, la quale diminuisce all'aumentare della concentrazione dell'agente regolatore del reticolo. Per poter processare correttamente la resina all'interno della stampante e mantenere buone proprietà e stabilità termica, il fotopolimero da stampare deve avere una regolazione efficace del network, direttamente visibili dalle curve di modulo conservativo e  $\tan \delta$ , ed una  $T_g$  non inferiore ai 120 °C: per questo si è scelto di testare nelle prove successive solamente le formulazioni contenenti 10%, 20% e 30% di trimetilolpropano.

Successivamente la prova di trazione ha mostrato come la presenza del trimetilolpropano non abbia sostanzialmente alterato le proprietà meccaniche del fotopolimero: un leggero peggioramento rispetto alla formulazione di base è riscontrabile, soprattutto nel caso in cui il trimetilolpropano sia presente al 30% molare. La tabella 5.2 e la figura 5.8 mostrano i risultati ottenuti dalla prova.

La prova di rilassamento degli sforzi svolta su un provino per flessione a 3 punti è stata condotta in acqua a 37 °C, dopo aver messo il provino a mollo per 30 minuti. Questa tipologia di misurazione ha messo in evidenza come all'aumentare della concentrazione di trimetilolpropano il rilassamento del fotopolimero aumenti: questo comportamento è in accordo con all'andamento dei moduli conservativi e delle temperature di transizione vetrosa, misurati tramite DMTA, ed è quindi possibile confermare che la presenza dell'agente di trasferimento di catena selezionato porta ad una generale maggior flessibilità del network polimerico, dovuta all'azione di regolarizzazione del network operata dal trimetilolpropano. I grafici in figura 5.10 mostrano i risultati della prova di rilassamento.

La foto-DSC eseguita sempre sulle formulazioni allo stato liquido, di modo da poter comprendere come la reazione di fotopolimerizzazione è influenzata dalla presenza del trimetilolpropano; le 4 formulazioni considerate sono state confrontate tra loro a 3 diverse temperature: 25 °C, 50 °C e 80 °C. A 25 °C la formulazione di base si mostra più reattiva, ovvero raggiunge in minor tempo il picco massimo esotermico, mentre le altre formulazioni mostrano un'area e un'altezza del picco esotermico maggiore, però spostato a tempi maggiori. Aumentando la temperatura la situazione cambia: in particolare la formulazione contenente il 20% di trimetilolpropano mostra ad 80 °C uno spiccato aumento di reattività rispetto alle altre come testimoniato dai dati in tabella 5.6 e dai grafici in figura 5.13. La presenza del trimetilolpropano aumenta la reattività e la velocità di polimerizzazione del fotopolimero.

La foto-reologia abbinata ad analisi IR permette di seguire l'evoluzione nel tempo dei parametri reologici di modulo conservativo e dissipativo, forza normale per definire la trasformazione del network mentre la fotopolimerizzazione è in corso: grazie all'analisi dei segnali IR è possibile registrare allo stesso momento la conversione dei gruppi epossidici nel tempo. In tabella 5.7 sono raccolti i dati principali della prova, eseguita in questo caso a 80 °C: l'effetto positivo sulla cinetica di reazione è evidente in presenza del 20% di trimetilolpropano, difatti la conversione dei gruppi epossidici aumenta (sia finale sia al punto di gel), il modulo conservativo aumenta e il tempo di gelazione diminuisce e la forza normale in valore assoluto diminuisce, quindi ci si attende un restringimento inferiore. Tali effetti evidenziano un netto

miglioramento della formulazione base in termini complessivi della reazione di fotopolimerizzazione in presenza dell'agente di trasferimento di catena: la temperatura di 80 °C può essere considerata la temperatura di processo durante la stereolitografia della resina, che grazie ai miglioramenti evidenziati da tale prova risulterà stampabile.

Al termine di questa sezione di prove si è deciso di scegliere come formulazione da processare nella stampante la CDA\_1\_20% (ovvero con il 20% di trimetilolpropano), in quanto considerata la migliore come bilancio tra proprietà termiche legate alla reazione di fotopolimerizzazione cationica e proprietà meccaniche del materiale, poi migliorabili in seguito tramite l'aggiunta di additivi, che non rechino problemi in fase di stampa.

### *3.2 Stereolitografia a caldo*

I parametri macchina da impostare per poter eseguire un lavoro di stampa sono: la velocità di scansione del laser, l'orientazione e la distanza di hatching (distanza che intercorre tra una passata e l'altra del laser) del fascio durante il riempimento dello strato, la velocità di movimento, lungo l'asse zeta, della piattaforma di costruzione dell'oggetto, la velocità del piano trasparente di stampa al di sotto dell'unità di stratificazione del liquido e la forza massima applicabile dalla piattaforma sul piano trasparente di lavoro. Lo spessore e il numero dei layer necessari per ottenere l'oggetto desiderato sono presenti nel file caricato per avviare il processo di stampa e sono quindi impostati in fase di progettazione nel programma Autodesk Netfabb, il quale permette di posizionare l'oggetto sulla piattaforma di costruzione e di modificare la parte prima della conversione in formato leggibile per il software di controllo della stampante. Le temperature delle parti riscaldabili sono i parametri macchina principali che consentono la stampabilità di tale resina alle alte temperature.

Il primo passo per la definizione dei parametri di stampa è capire quale velocità di scansione del laser risulta migliore per stampare la formulazione: questo è possibile attraverso test di semplice esposizione a fascio laser a varie velocità ed osservare quale permette di ottenere uno strato di materiale solido sufficientemente resistente per poter sostenere un processo completo di stampa. Inizialmente si è dimostrato fisicamente in macchina come la presenza del trimetilolpropano renda più reattiva la formulazione, questo è confermato dai dischi ottenuti per semplice esposizione del laser come mostrato in figura 6.1, difatti a parità di velocità del laser il fotopolimero ottenuto dalla formulazione CDA\_1\_20% risulta più solido e resistente rispetto a quello ottenuto dalla formulazione di base. Successivamente si è dimostrato che la formulazione CDA\_1\_20% è stampabile sino a velocità di 500 mm/s del laser (vedere immagine in figura 6.3). L'effetto della presenza dell'antracene nel regolarizzare la polimerizzazione durante il passaggio del laser è visibile in figura 6.8.

Durante le prove di stampa della resina alcuni problemi si sono riscontrati: come prima problematica, il sistema di distribuzione del nuovo strato della resina è stato impossibile da utilizzare in quanto la resina liquida non veniva efficacemente posizionata al fine di cominciare la formazione di un nuovo layer: l'operazione di ridistribuzione è stata eseguita manualmente mettendo in pausa il lavoro di stampa e controllando che la resina fosse sufficiente per stampare un ulteriore strato. In secondo luogo essendo la reazione di fotopolimerizzazione cationica fortemente esotermica, si è notato la formazione di bolle al di sotto dello strato anti-adesivo a seguito della sovrapposizione di strati consecutivi localizzati in una zona precisa del piano trasparente di stampa, visibile chiaramente in figura 6.4. Queste bolle sono probabilmente collegate all'evaporazione localizzata del solvente del collante che tiene insieme il film anti-adesivo con lo strato sottostante di silicone del piano trasparente: unitamente alla pressione esercitata dalla piattaforma e al fatto che il piano è mantenuto ad 80 °C queste bolle tendono prima a rialzare il film e poi a romperlo portando quindi all'impossibilità di concludere il lavoro di stampa. Tale problema è stato particolarmente evidente durante la stampa dell'oggetto in

figura 6.7, il quale è stato ottenuto alla fine rimuovendo il film anti-adesivo come mostrato in figura 6.5.

I provini stampati come in figura 6.6 sono stati ottenuti stampando a velocità del laser di 350 mm/s e strati di spessore 100  $\mu$ m: per verificare l'influenza del processo di stampa sul materiale sono stati stampati provini a trazione e a flessione per DMTA e RSA. Tutti i provini hanno subito un trattamento termico al termine della stampa per eliminare le tensioni e completare la conversione dei gruppi epossidici: il trattamento scelto prevede 4 ore a 250 °C in forno, il risultato è mostrato in figura 6.6. La DMTA del provino stampato e post-trattato è confrontato con le curve ricavate precedentemente di Reference e CDA\_1\_20% in figura 6.8 e 6.9: il fotopolimero stampato risulta aver mantenuto in questo caso le proprietà evidenziate per la stessa formulazione non sottoposta al processo di stampa, i risultati sono riassunti in tabella 6.1. La prova di trazione ha mostrato un leggero miglioramento delle proprietà meccaniche: aumento del modulo e della resistenza a trazione unitamente ad un leggero aumento dell'allungamento a rottura (quasi un punto percentuale in più), come testimoniato dal grafico in figura 6.10. L'aumento del modulo e della resistenza a trazione sono correlabili con il post trattamento termico come evidenziato dal grafico in figura 6.11. La prova di rilassamento degli sforzi ha mostrato un miglioramento nel caso del materiale stampato e trattato termicamente: difatti il rilassamento della formulazione CDA\_1\_20% stampata è in linea con quello della formulazione Reference, in cui è assente il trimelolpropano. Il grafico in figura 6.12 mostra tali andamenti dei provini.

In conclusione da questi risultati è possibile dire che il processo di stampa ha generalmente una buona influenza sul fotopolimero ottenuto dalla formulazione CDA\_1\_20%: le proprietà ricavate dai test sono mantenute e in alcuni casi migliorate rispetto allo stesso fotopolimero non stampato. La stampabilità di tale formulazione è comprovata dagli oggetti ottenuti e mostrati nella figura 3.1 sottostante.



**Figura 3.1:** Oggetti stampati tramite stereolitografia a caldo, quella a destra è incompleto a causa della rottura del film anti-adesivo che ha impedito la corretta sovrapposizione dei layer.

I problemi evidenziati precedentemente possono essere risolti progettando un diverso settaggio delle parti coinvolte durante la stampa: un nuovo tipo di incollaggio per collegare il film anti-



adesivo del piano di trasparente di stampa ed anche una diversa impostazione di tale piano inserendo una vasca di contenimento della resina liquida per poter meglio controllare la formazione di un nuovo strato al passaggio della lama dell'unità di distribuzione, similmente a quanto è previsto in sistemi DLP presenti nel laboratorio.

### *3.3 Miglioramento prestazioni meccaniche*

Gli additivi scelti al fine di migliorare meccanicamente, in particolare tenacizzando il materiale di partenza, sono stati: particelle di gomma di tipo core-shell solubili in resine di tipo epossidico, polisilossani con gruppi idrossido e nanoparticelle di silice. Le particelle di gomma e di silice sono state aggiunte alla formulazione precedentemente selezionata per il processo di stampa (CDA\_1\_20%): le particelle di tipo core-shell sono state inserite al 1%, 2%, 3%, 5% e 10% in peso, la nanosilice è stata aggiunta in percentuali del 1% e 2% in peso (oltre tali aggiunte la formulazione risultava molto viscosa persino alla temperatura di processo di 80 °C). I polisilossani selezionati sono appartenenti a tre famiglie di prodotto differenti: Tegomer H-Si 2311, Tegomer H-Si 6440P (vedere figura 7.1) e Wax OH 350D, tutti e tre i prodotti sono state aggiunti in percentuali in peso del 1%, 3% e 5% prima alla formulazione base (Reference) e successivamente alla formulazione CDA\_1\_20%, ma solo quelle considerate di interesse dai risultati ottenuti sulla resina di base. Le analisi eseguite su queste formulazioni sono state prova di trazione, DMTA, RSA e foto-DSC.

I risultati complessivi della prova a trazione sono riassunti per le formulazioni CDA\_1\_20% modificate in tabella 7.1: le caratteristiche meccaniche del materiale di base risultano migliorante in maniera evidente dalla presenza del 2% di nanosilice, in particolare l'allungamento a rottura quasi raddoppia, la resistenza a trazione risulta anch'essa migliorata come testimoniato dal grafico in figura 7.1. Meno interessanti sono i miglioramenti ottenuti con l'aggiunta dei polisilossani Tegomer 2311 al 5% e del 1% di Wax OH 350D, vedere grafico in figura 7.7. L'effetto atteso tenacizzante collegato all'aggiunta delle particelle di gomma non è stato riscontrato nelle curve a trazione, come visibile nella figura 7.2. I risultati della prova di trazione eseguita sulle formulazioni Reference contenenti i diversi silossani sono raccolti in tabella 7.2: i miglioramenti più significativi, anche se in misura limitata, si sono riscontrati nel caso del 5% di Tegomer 2311 e del 1% Wax 350D, per tale motivo si è deciso di provare ad aggiungerli anche alla formulazione CDA\_1\_20% per tentare di migliorare la performance meccanica.

La DMTA è stata eseguita sulle stesse formulazioni testate precedentemente a trazione: i risultati per i polimeri ottenuti dalla polimerizzazione delle varie formulazioni a base CDA\_1\_20% sono riassunti in tabella 7.3, mentre quelli relativi alle aggiunte fatte alla formulazione Reference sono riportate in tabella 7.4. Da tale analisi i campioni contenenti particelle di gomma mostrano andamenti del modulo conservativo e di  $\tan \delta$  differenti rispetto alla formulazione CDA\_1\_20%: la transizione netta del modulo conservativo in corrispondenza della temperatura di transizione vetrosa osservata precedentemente scompare oppure è appena accennata, come visibile in figura 7.10, allo stesso modo le curve  $\tan \delta$  presentano un comportamento differente, nel quale l'effetto del trimetilolpropano tende ad essere meno visibile. Per quanto riguarda l'aggiunta dei polisilossani e della nanosilice, la situazione rimane invariata rispetto alla formulazione di base CDA\_1\_20%, con soltanto un aumento del valore del modulo conservativo nel caso di silice e Wax OH 350D: il motivo di tale invarianza è legato al fatto che la silice e i silossani scelti fungono anch'essi da agenti di trasferimento di catena grazie alla presenza di gruppi OH, i quali permettono di partecipare alla reazione di fotopolimerizzazione cationica e, nel caso di silice, realizzano un forte legame tra la superficie della nanoparticella e il network polimerico. Per quanto riguarda le formulazioni Reference con l'aggiunta dei polisilossani selezionati, i quali data la presenza di gruppi idrossido dovrebbero



agire da agenti di trasferimento di catena nella fotopolimerizzazione: gli effetti dovuti alla presenza di gruppi OH che operano come tali agenti risultano maggiormente pronunciati nel caso dell'aggiunta del 1% di Wax OH 350D, vedi figura 7.13.

La prova di rilassamento degli sforzi è stata eseguita su campioni derivanti dalla fotopolimerizzazione delle formulazioni CDA\_1\_20% contenenti 1%, 2% di nanosilica, 1% di Wax OH 350D e 5% di Tegomer H-Si 2311: le curve sono visibili in figura 7.14, tutti gli additivi selezionati portano i campioni a diminuire la tendenza a rilassarsi del network rispetto alla formulazione CDA\_1\_20% pura. I risultati migliori sono ottenuti grazie all'inserimento nella composizione del 2% di nanoparticelle di silice e del 5% di Tegomer H-Si 2311, i cui rilassamenti a fine prova risultano maggiori di quello registrato per la Reference. Similmente a quanto esposto precedentemente per la CDA\_1\_20%, le formulazioni di Reference modificate con polisilossani in generale mostrano un minor rilassamento rispetto alla formulazione pura, eccetto nel caso in cui sia presente 1% e 3% di Wax OH 350D, come si può osservare guardando la figura 7.15.

La foto-DSC è stata eseguita per indagare il ruolo di agenti di trasferimento di catena dei polisilossani scelti all'interno della formulazione Reference: i risultati sono esposti in tabella 7.7 e dalle curve in figura 7.20. L'effetto, legato alla presenza di gruppi idrossido nella catena di questi additivi, sulla velocità di polimerizzazione e la reattività termica della fotopolimerizzazione della resina epossidica è inferiore rispetto a quello operato dal trimetilolpropano. La stessa analisi è stata eseguita sulle formulazioni CDA\_1\_20% contenenti 1% di Wax OH 350D, 5% di Tegomer 2311 e 2% di nanoparticelle di silice: i risultati sono riportati in tabella 7.6 e le curve mostrate in figura 7.16. Da segnalare anche in questo caso come le nanoparticelle di silice grazie alla presenza di gruppi idrossido sulla superficie partecipino attivamente alla reazione di fotopolimerizzazione aumentando i valori legati al picco esotermico registrato, tale effetto conferma il suo ruolo come agente di trasferimento di catena.

La maggiore reattività registrata tramite foto-DSC è confermata dai test di esposizione al fascio laser eseguiti in stampante: la formulazione è in grado di fotopolimerizzare se esposta ad un fascio a velocità di 1000 mm/s. Nonostante la rimozione del film anti-adesivo (ed anche lo strato rovinato dalle precedenti stampate) un campione per la RSA è stato stampato e successivamente trattato termicamente in forno. Il risultato della prova di rilassamento degli sforzi è riportato in figura 7.22, la quale mostra un maggior rilassamento del polimero stampato rispetto a quello semplicemente foto-curato; tale prova non può essere considerata rappresentativa delle caratteristiche della resina processata nella stampante in quanto le condizioni di stampa non erano ottimali come nel caso di studio esposto nella precedente sezione. In conclusione la presenza delle nanoparticelle di silice non impedisce la reale stampabilità della formulazione processata precedentemente, ma anzi ne aumenta la reattività e soprattutto migliora le proprietà meccaniche e di rilassamento degli sforzi rispetto alla formulazione pura. In figura 3.2 è riportata l'evoluzione delle proprietà meccaniche dalla Reference alla CDA\_1\_20% con il 2% di nanoparticelle di silice all'interno.

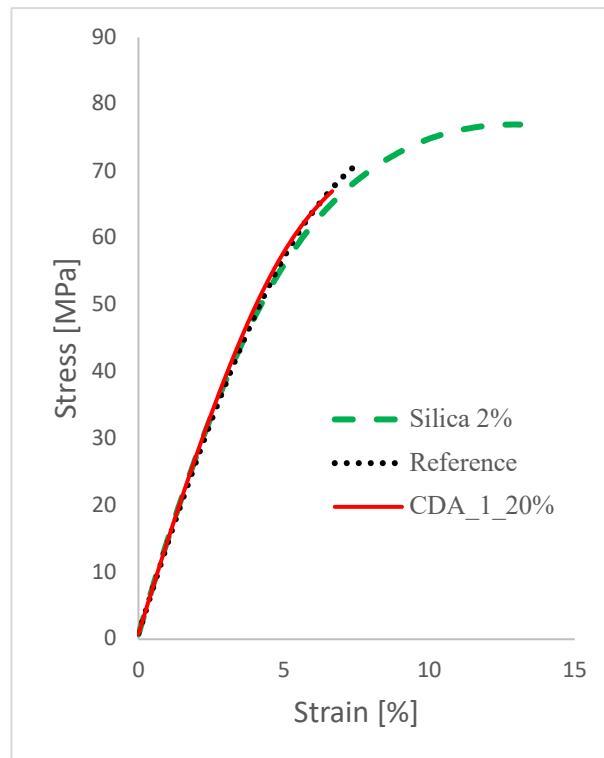


**Figura 3.2:** Proprietà meccaniche di Reference, CDA\_1\_20% e CDA\_1\_20%+2%Silice

#### 4. Conclusioni finali

Essendo il lavoro sperimentale suddiviso in 3 capitoli: nei paragrafi 5.4, 6.5 e 7.4 sono riportate le conclusioni preliminari di ogni parte del lavoro, le quali saranno riprese in maniera organica nel capitolo 8. L'obiettivo primario era provare la reale stampabilità della resina BADGE, modificata con l'aggiunta di un agente di trasferimento di catena, sfruttando una stampante basata sul processo di stereolitografia a caldo. La formulazione CDA\_1\_20% ha mostrato buona processabilità in macchina, permettendo di stampare provini ed oggetti come mostrato nelle sezioni apposite contenute nel capitolo 6, inoltre le proprietà dei provini ottenuti tramite processo di stereolitografia a caldo sono risultate coerenti con quelle del materiale caratterizzato precedentemente tramite DMTA e migliorate leggermente nel caso di comportamento di rilassamento e delle proprietà meccaniche ricavate dalla prova di trazione. Le proprietà meccaniche di tale materiale, ovvero quelle di un polimero termoindurente, sono state migliorate in maniera efficace grazie alla presenza di nanoparticelle di silice: la quale interagisce direttamente con il network polimero in formazione grazie alla presenza di gruppi idrossido sulla superficie delle particelle. Tale meccanismo di interazione diretto durante la fotopolimerizzazione produce anche una maggiore reattività termica della resina, registrata tramite foto-DSC: unitamente alla dimensione nanometrica la presenza di questo additivo nella resina liquida non inficia la processabilità durante la stereolitografia.

Futuri studi legati alla modifica della composizione della formulazione potranno permettere di selezionare ed ottenere le proprietà specifiche per ogni applicazione, come mostrato da tale lavoro: utilizzando il metodo di stereolitografia a caldo, il quale assicura la precisione tipica dei metodi stereolitografici, la processabilità di fotopolimeri eccessivamente viscosi o scarsamente reattivi termicamente a temperatura ambiente è assicurata.



## **Index**

1. Work introduction	1
2. Photocuring technologies overview	3
2.1 Photopolymerization principles	3
2.2 Formulations for cationic photopolymerization	8
2.2.1 Epoxy monomers	8
2.2.2 Chain transfer agents	10
2.2.3 Other additives	11
2.2.4 Cationic photoinitiators	12
2.2.4.1 Photosensitizers	13
3. Additive manufacturing process	15
3.1 Introduction to additive manufacturing technique	15
3.2 Stereolithography	18
3.2.1 Hot lithography approach	20
4. Materials and methods	23
4.1 Materials	23
4.1.1 BADGE resin	23
4.1.2 Cationic photoinitiator	24
4.1.3 Chain transfer agents	25
4.1.4 Photosensitizer	25
4.1.5 Additives for thermoset modification	26
4.2 Analysis methods and machines	27
4.2.1 Thermal dynamic mechanical analysis	27
4.2.2 Tensile test	28
4.2.3 Stress relaxation analysis	30
4.2.4 Photo differential scanning calorimetry analysis	31
4.2.5 Photo-rheology	31
4.3 Formulations and samples preparation	32
4.4 Hot lithography machine	35
5. First part: selection of chain transfer agent for BADGE cationic photopolymerization	37
5.1 Central focus of the first part of the project	37
5.2 List of formulations	37
5.3 Experimental results and discussions	37

5.3.1 DMTA	38
5.3.2 Tensile test	43
5.3.3 RSA	45
5.3.4 Photo-DSC	46
5.3.5 Photo-rheology	50
5.4 Preliminary conclusions	54
6. Second part: 3D printing of cationic photopolymer using hot lithography approach	55
6.1 Central focus of the second part of the project	55
6.2 Formulations preparation for printing	55
6.3 3D printing of the resin	55
6.3.1 Irradiation tests	55
6.3.2 Definition of process parameters	58
6.3.3 Printing of parts	58
6.4 Test results and discussion	62
6.4.1 DMTA	62
6.4.2 Tensile test	64
6.4.3 RSA	66
6.5 Preliminary conclusions	67
7. Third part: properties modification of the thermoset through different additives addition	67
7.1 Central focus of the third part of the project	68
7.2 List of formulations	68
7.3 Test results and discussions	69
7.3.1 Tensile test	69
7.3.2 DMTA	75
7.3.3 RSA	82
7.3.4 Photo-DSC	84
7.3.5 Brief printability study	89
7.4 Preliminary conclusions	90
8. Final conclusions	91
9. Bibliography	92



## 1. Work introduction

UV curing based technologies are increasing rapidly in the industrial applications and processes, introducing new monomers and formulations, which enable the exploitation of new properties and features in the final products. From the initial application in the wood-finishing coatings, the UV curable monomers are, nowadays, extended to creation of several and complex surface treatments, coatings and adhesives used in medical, electronics field, material protection or composites. The main feature of UV curing, which is the light irradiation in order to obtain a solid material, gives enormous advantage respect to the classic thermal curing of film on a substrate: rapid curing, low energy requirements, room-temperature treatment, non-polluting and solvent free formulations and reduction of costs. Basically the photocured thermoset can be polymerized thanks to two different mechanisms (that start from light irradiation): the radical photopolymerization, intensely employed, and the cationic photopolymerization, which, lately, is getting more interesting because of its peculiarity respect to the radical one [1]. Schematic photopolymerization mechanism is reported in figure 1.1.

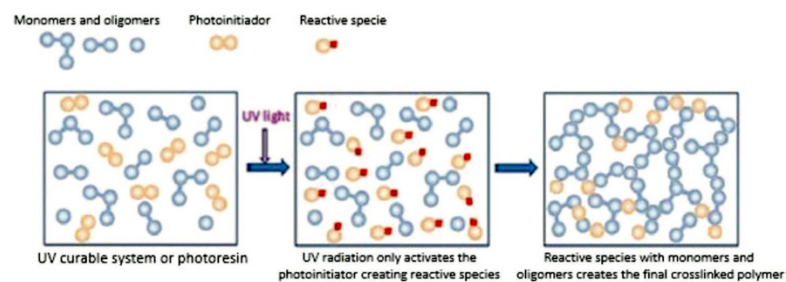


**Figure 1.1:** Photopolymerization process [2].

Another technological revolution, in the last years, is represented by the rising of additive manufacturing or rapid prototyping machine: originally developed for accelerate and reduce the costs related to the prototype creation. From that moment the patents and the articles related to 3D printing application are enormously increased in the years [3], as explained in the figure 1.2. The advantages of additive manufacturing machine are several and, thanks to the continuous development in this field, the importance of this production method is growing. The 3D printing gives the possibility of almost limitless design freedom, easy error correction starting from the CAD model, minimum material waste and costs reduction in some cases. The additive manufacturing techniques, anyway, are still characterized by some critical aspects that need to be overcome: the building speed related to the object construction is slower than traditional industrial process, the resolution, not for all machine, is rather low and the materials portfolio and their properties are quite limited.

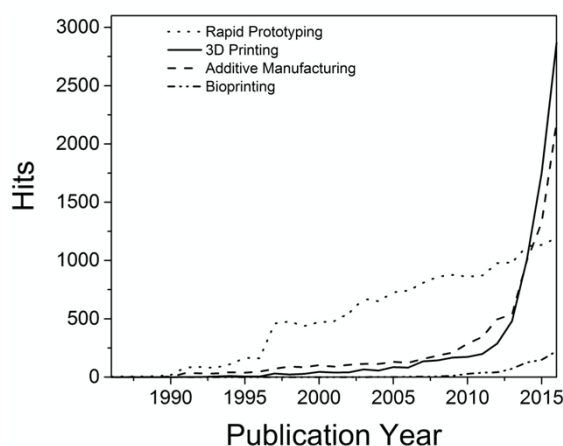


**Figure 1.2:** Growing of additive manufacturing related publications [3].

The photopolymers, anyway, still represent the most valuable and most sold material for the additive manufacturing market, because of their application in rapid prototyping [3]. Combining the new research in the UV curable monomers and the possibility of design and production gave by the 3D printing machines, it could be possible to introduce new materials with more interesting and performing characteristics, giving the chance to apply the novel techniques of UV curing and 3D printing combination in new industrial sectors.

The purpose of this work is the study of a cationic photopolymerizable system, based on an epoxy resin, in order to obtain proper structural properties of the final thermoset polymer and to allow formulation printability through high temperature 3D printing technology. The idea behind this project is to take advantage of the cationic photopolymerization, which has some positive aspects respect to the radical photopolymerization, usually applied to acrylates and methacrylates, which are normally involved in 3D printing processes. And since the epoxy resins are the best choice among cationic photopolymers, the final goal is to expand the list of printable photopolymers, though improvement of the epoxy-based cationic photocured systems.

For achieving this, the basic formulation (that will be the Reference in the further description of the work), which is composed by a BADGE resin (epoxy resin based on bisphenol A) and a cationic photo-initiator (salt of triarylsulfonium hexafluoroantimonate in a solution of propylene carbonate), will be modified by selecting a polyol-based chain transfer agent, after scanning different of them, which should allow a control on reactivity and on the thermo-mechanical performances of the material. The selection could be possible by testing these resins through different thermo-mechanical analysis: first of all, thermal dynamic mechanical analysis (DMA) will help showing how the glass transition temperature ( $T_g$ ) changes in relation with different chain transfer agents and how the storage module curve should have a different behaviour because of the chain transfer agent presence [4, 5, 6, 7, 8]. Secondly the tensile test will show the mechanical properties of the thermosets, another mechanical test will be the stress relaxation analysis (RSA), which tells how much the polymer will relax during time after a certain load is applied on it. These tests are performed on the solid resins which, in this first part, are photopolymerized in a silicone mould by UV lamp in an UV chamber. In order to understand the reactivity and kinetic of the reaction, which is fundamental for the additive manufacturing process, the liquid resins will be studied using Photo-DSC and Photo-Rheology methods [9, 10]. After all these analysis the result of this first part will be the selection of the formulation that should have a good balance between thermal reactivity, higher than the pure resin and the photoinitiator, and final mechanical properties.



After the first part of tests which will provide the most promising formulation, the next step of the work is represented by focusing on the optimal parameters of the 3D-Printer in order to having a 3D-printed material that can maintain the same properties of the one produced by UV photopolymerization. The machine that will fulfil this aim is based on the Hot Lithography method, particularly suitable for all that high viscous and low reactive resin at room temperature [11, 12]. Once proven the printability of the formulation, the tests performed on the solid material in the first part of the work will be repeated in order to characterized the printed photopolymer and see which is the influence of the additive manufacturing process on the thermoset properties [13, 14].

In the last part of the project the selected formulation in the previous steps will be modified by mixing different additives to have a better structural material which could remain printable. To achieve this result the chosen modifiers are: core-shell rubber particles, fumed silica (nanoparticles) and different kind of siloxane based additives (solid or liquid) [15, 16, 17, 18, 19, 20, 21, 22, 23, 24, 25]. The effects of these materials addition will be investigated in the reference (BADGE resin and photo-initiator) and in the selected formulation from the first study of the project. The characterization of these new formulations will be carried out performing the same test done previously and finally, once selected the most suitable formulation, this new resin will be printed using the same 3D-printing process.

Before starting with the discussion of the results of the different analysis the next chapters will focus on:

- The description of the material chemistry involved.
- The hot lithography machine and process.
- The detail of the test and analysis executed.
- The preparation of formulations and samples.

The work is been entirely carried out in the laboratories of TU Wien, with a cooperation between the chemistry department and the 3D printers lab.

## 2. Photocuring technologies overview

### 2.1 Photopolymerization principles

“Photopolymers are hardly new materials. The photosensitivity of Judean asphalt...was known from antiquity,...due to sunlight induced cross-linking” [26]. Thanks to this so called old process the “microelectronics revolution” [26] is been possible and today the research in UV based process still remains a field in continuous growing. A photopolymer polymerizes thanks to the light irradiation interaction and this light absorption starts the reaction that will create the cross-linked network which defines the thermoset characteristics (see figure 1.1).

There are two different types of photopolymerization: one is the radical based reaction and the other is the cationic based reaction. The common principal in both mechanism is the light absorption in the UV region of the light spectrum (200-400 nm), see figure 2.1. The energy associated to a certain radiation (see formula 2.1), which is characterized by its own frequency ( $\nu$ ) or wavelength ( $\lambda$ ) (inversely correlated to frequency by the speed of light  $c=3 \times 10^8 \text{ms}^{-1}$ ), is:

$$E = h\nu \text{ (where is } h=6.626 \times 10^{-34} \text{ Js}^{-1}) \quad (2.1)$$

The quantum of energy carried by the radiation can be absorbed by a molecule that becomes energetically excited: this energy should be equal to energy difference between the ground energy state  $E_0$  and the excited state  $E_1$ . The electronically state of this excited molecule can evolve according to Perrin-Jablonskis diagram, visible in figure 2.2: the processes that can occur are fluorescence, phosphorescence, internal conversion of states, intersystem crossing.

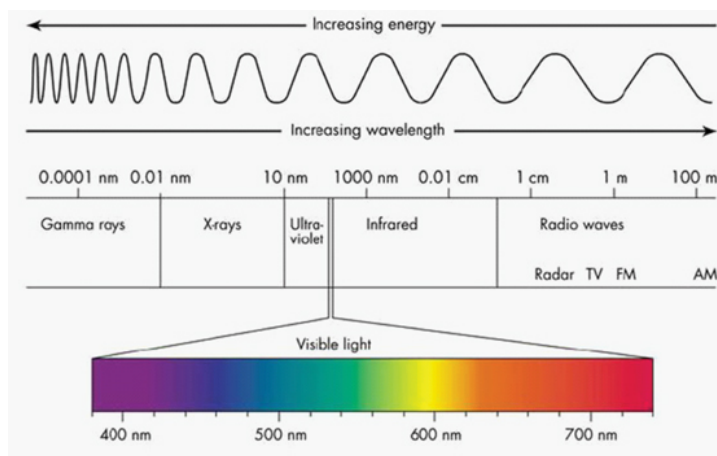


Figure 2.1: UV-visible spectrum region [27].

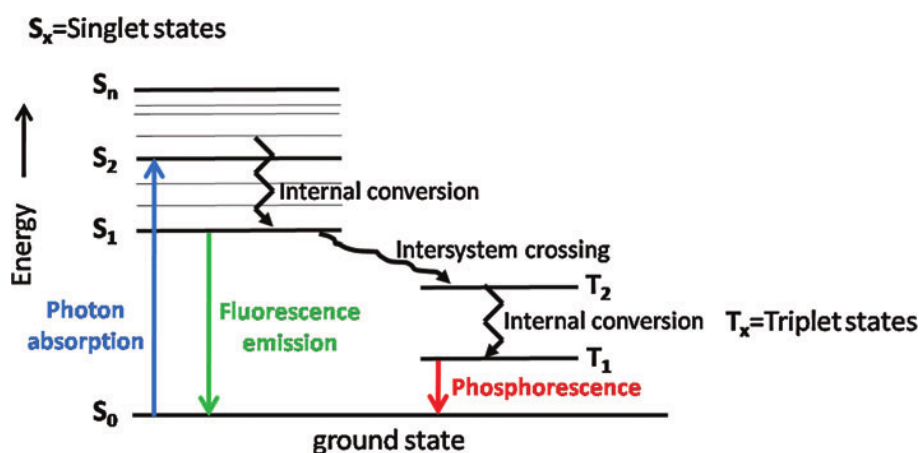


Figure 2.2: Perrin-Jablonskis diagram [28].

In order to obtain a photocurable polymer material, the starting formulation should contain essentially:

- A photoinitiator, which absorbs light, defines the curing rate and its spectral absorption determine the light source and efficiency of the reaction.
- A monomer or oligomer, which is the multifunctional molecule that leads after the photopolymerization to the final polymer and it defines the final properties of material.
- Other additives for adjusting some specific features, for example a reactive diluent for controlling the viscosity or in this work a chain transfer agent for increasing reactivity and obtaining a well-regulated network.

To sum up the important role for the starting of the photopolymerization reaction is played by the photoinitiator, which, through the light interaction, generates the first reactive species that

starts the monomer propagation. The type of the reactive species is different if we consider a radical photoinitiator or cationic one: the first, after light absorption, produces a radical species which starts the monomer propagation by radical mechanism (scheme in figure 2.3), the latter generates, thanks to light excitation, a very strong Brønsted or Lewis acid (sometimes called super-acid) that starts the reaction from a proton or carbocation (see figure 2.4).

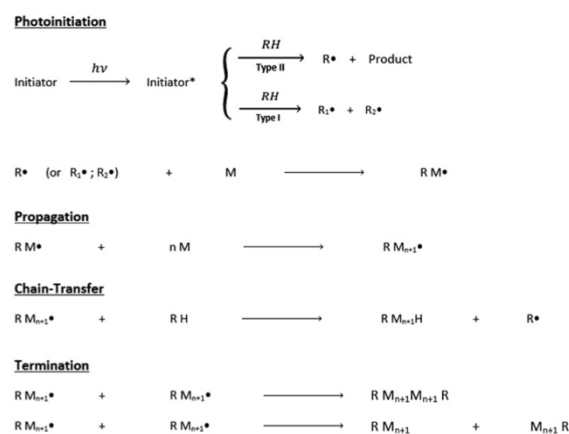


**Figure 2.3:** General scheme of radical photopolymerization reaction in presence of carbon-carbon double bond [2].

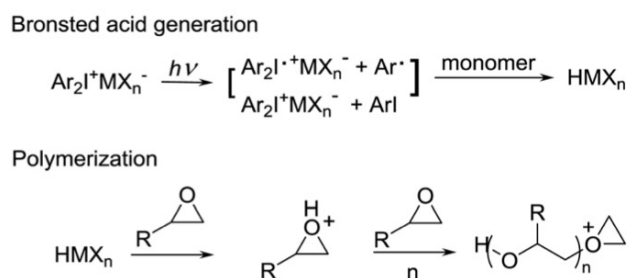


**Figure 2.4:** Scheme of cationic photopolymerization reaction in presence of epoxy ring. [26].

The radical photoinitiated reaction is usually very fast, this advantage makes the radical systems particularly suitable for rapid prototyping and additive manufacturing technology. The radical photoinitiator is excited by the light and promoted to the first excited singlet state which is converted to the triplet state by fast intersystem crossing: this determines the formation of the radical species ( $R^\bullet$ ) which can start the reaction rapidly with monomer. The triplet state could be deactivated by oxygen quenching, by radiative or not products or by interaction and reaction with other molecules. Commonly the radical photoinitiators are classified taking in to account two different reaction mechanism: photolysis process or Norrish type I and hydrogen abstraction reaction or Norrish type II. In figure 2.5 the Darocur 1173 photoinitiator is presented, Norrish type I ( $\alpha$ -cleavage) initiators (like Darocur) are molecule based on benzoyl chromophore, mostly present in stereolithography patents, that cleave into radical fragments once exposed to radiation with a certain wavelength. Other examples of radical Norrish type I are in the figure 2.6, usually this type of radical initiators are very reactive.

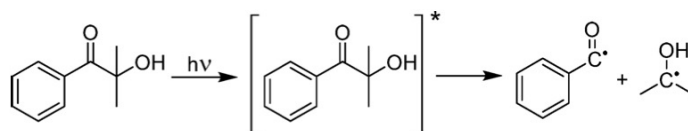


**Figure 2.5:** Darocur 1173 photocleavage mechanism [3].

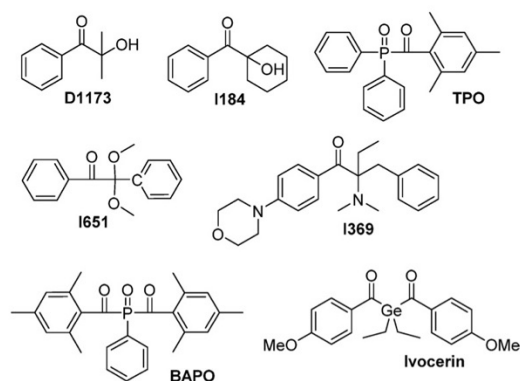


**Figure 2.6:** Norrish type I radical photoinitiators [3].

Norrish type II photoinitiators are characterized by two components: an absorbing molecule or sensitizer, which can interact with light, and a co-initiator or synergist, which, after light irradiation, donates a hydrogen atom to the excited sensitizer leading to the radical species formation. The co-initiator is usually tertiary amine with alkyl substituent, the sensitizers are commonly benzophenone, thioxantone and benzyl derivatives, example of this Norrish type II initiator is shown in figure 2.7.

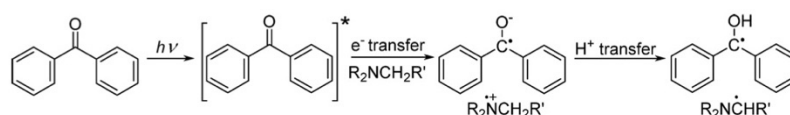


**Figure 2.7:** Norrish type II photoinitiator, Benzophenone and amine [3].

Methacrylate and Acrylate monomers are usually photopolymerized through radical mechanism and they are well known and mostly applied in the stereolithography (or SLA) based application thanks to the rapidity of the reaction, to the availability of lots of different compositions and photoinitiators and to the good processability. Although some issues related to them are: the shrinkage and the distortion occurring are high, crosslinked network is usually very brittle and heterogeneous, this leads to a material with poor characteristics, and oxygen reaction inhibition; nowadays solution has been proposed for avoiding and controlling some of these characteristics [3, 5, 6, 13, 26, 29].

Recently [1] cationic photopolymerized systems are becoming more interesting in several application field, including additive manufacturing, due to their intrinsic advantages respect to free radical photopolymer: no oxygen and air inhibition, this means that inert atmosphere for curing is not necessary, minimal sensitivity to water and dark cure process[3, 26], which described the ability of a cationic systems to continue the polymerization until the protonic acid

is active, even though the light source is turned off. In addition cationic photopolymerization can be considered an environmental-friendly process because of the absence of toxic and irritating products, like solvents. First discovery of a cationic photoinitiator was made by Prof. Crivello in the late 1970s; this initiator (see figure 2.8) was aryl iodonium salts ( $\text{ArI}^+\text{X}^-$ ) with different counterions: the class of onium salts are the widely applied photoinitiator groups thanks to their great reactivity and thermal stability.

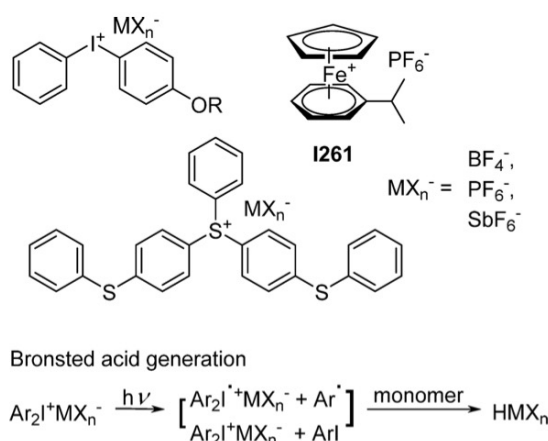


**Figure 2.8:** Example of cationic photoinitiators and the general scheme of acid formation reaction [3].

The cationic photoinitiator is composed of two essential parts (figure 2.8): a cationic side and an anionic part (counterion). The first is responsible for absorbing the incident light, and the structure of this molecule determines all the photochemistry of the initiator, which includes the quantum yield and the UV absorption behaviour, and also the whole molecule's thermal stability. In fact, changing chromophores on the aromatic rings allows the tuning of the wavelength and the intensity of light absorbance; this peculiarity gives the chance of having high efficiency matching easily the light emission spectrum with the photoinitiator's specific absorbance. For reaching wavelengths higher than 350 nm, it is better to use a photosensitizer coupled with the cationic photoinitiator, like anthracene [3, 26, 30]. The anionic part determines the chemical strength and stability of the photoacid generator or PGA (common name for cationic photoinitiator) and it influences the efficiency and the kinetics of the polymerization reaction.

The generation of a super-acid by these salts is quite a complex process: the reaction mechanism is shown in figure 2.9. After UV irradiation, the initiator decomposes into a mixture of different intermediates, which react with monomer or solvent, leading to the formation of the strong acid species  $\text{HMX}_n$ . The scheme in figure 2.9 gives a better idea of the complexity of products which are originated by the photoexcitation and consequently decay, with heterolytic and homolytic cleavages, of singlet state; these species are extremely reactive with the surrounding environment and they are responsible for the initiation of the polymerization. The anionic parts of the salt directly influence the strength of the photoacid generated: in fact, bigger counteranions, lower is the nucleophilicity and so higher is the reactivity of the acidic species; the order of reactivity of the most common counteranion is:  $\text{SbF}_6^- > \text{AsF}_6^- > \text{PF}_6^- > \text{BF}_4^-$  [3, 26].

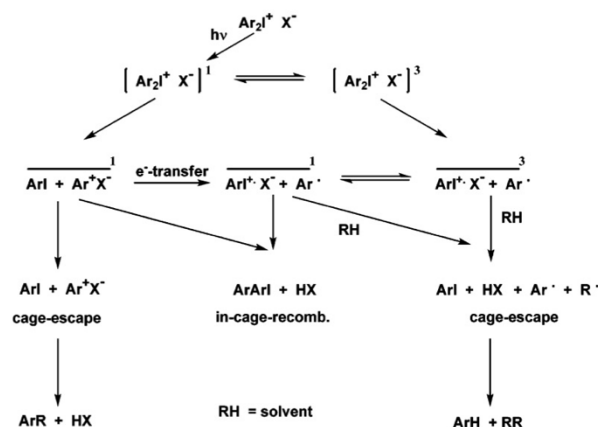


**Figure 2.9:** Mechanism of the diaryliodonium salts photolysis reaction [26].

Photoinduced cationic polymerization has been applied, with good success and efficiency, in ring-opening polymerization of epoxy systems and other strained ring systems such as cyclic ethers, lactones and acetals, as well as aliphatic unsaturated monomers as vinyl ethers, which are inactive toward radical species. Virtually the cationic photopolymerization could be synthesized polymers with a wide range of heteroatoms backbone. The most representative cationic photopolymerized monomers are the epoxy functionalised oligomers, which due to high reactivity and excellent chemical and physical properties find several application in coatings, adhesives and inks. There is another advantage that coming from the ring-opening process operated by cationic photoreaction: the shrinkage linked to the material are significantly lower than the one associated to free-radical photopolymers. Mixing epoxy or vinyl based monomers with acrylates is very common [3, 26], especially in additive manufacturing application involving stereolithography machine, in order to reduce the shrinkage and the distortion linked to the radical photopolymerization reaction. The two reaction do not interfere each other, in fact the radical polymerization is faster than the cationic one, this helps in controlling the shrinkage and also the oxygen inhibition, in addition to a higher conversion: the final polymer is not a copolymer, but it is defined as interpenetrating network.

To sum up, the cationic photopolymerization shows substantially benefits respect to the free-radical reaction:

- Absence of oxygen/air inhibition.
- Dark curing.
- Polymers with different backbone structures.
- Lower shrinkage thanks to ring-opening mechanism.

## 2.2 Formulations for cationic photopolymerization

In this paragraph the principal components of a cationic photocurable polymer will be described in the next sections, also focusing on the materials studied in this project. As mentioned before the polymers that can be synthesized by cationic photopolymerization are various, but the next section will be taking into account the epoxy functionalised monomer family, which represents the most interesting and performing material, already applied in lots of different research and industrial fields.

### 2.2.1 Epoxy monomers

An epoxy monomer is characterized by a functional group called epoxide ring: the group is a 3-membered ring composed by an oxygen atom bonded to two adjacent carbon atoms, as it is shown in the figure 2.10.

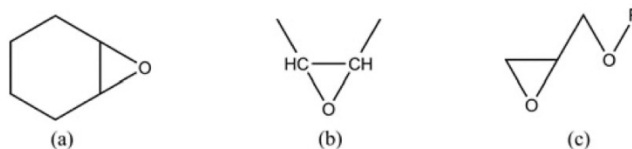


**Figure 2.10:** Examples of epoxy monomers (a) cycloaliphatic, (b) aliphatic and (c) glycidyl ether [22].

This ring is highly strained and could be open by adding a nucleophile: like for example amines, ammonia, alkoxides or hydroxides [31, 32]. In order to create a crosslinked network, difunctional epoxides react in combination, for examples, with secondary amines, that are called crosslinkers: a typical step growth reaction is shown in figure 2.11. Usually this kind of crosslinking is obtained by thermal curing of the formulations, otherwise the reaction would be slow, the ring-opening reaction is very exothermal and gives better dimensional stability of the final material, in fact the volumetric shrinkage due to the crosslinking is reduced.

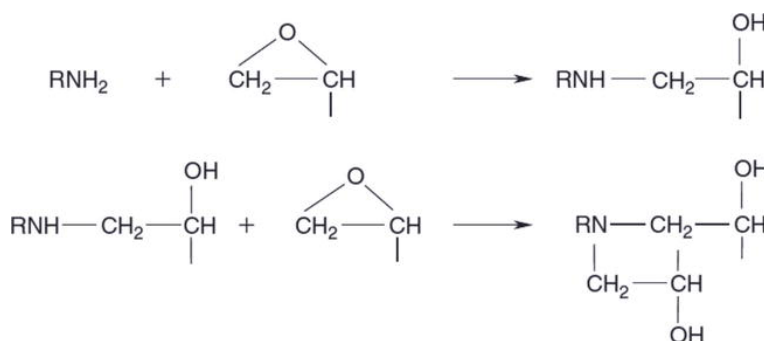


**Figure 2.11:** Epoxy resin crosslinking reaction in presence of amine [32].

In this work the epoxy resin, taking into account for preparing the different formulations, is the diglycidyl ether of bisphenol-A or BADGE/DGEBA (see figure 2.12 for the structure), derived from the reaction between bisphenol-A and epichlorohydrin: it is the most known type of epoxy resin, frequently employed in composites as the matrix and also in lots of coatings and adhesives application, because of its good mechanical property, thermal stability, chemical resistance and hardness.

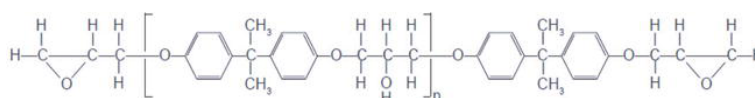


**Figure 2.12:** Backbone structure of BADGE resin [32].

Among the cationic photopolymers, again, the BADGE resin is the most important photomonomer: although the rate of polymerization of difunctional epoxides is by one order lower than that of diacrylate monomers, probably because of a lower propagation rate constant. The reactivity of an epoxy resin is strongly related to the molecular structure: for example epoxy resin with cycloaliphatic groups with high double ring strain can crosslinked faster than the one which contains ether groups like BADGE [3].

The cationic photopolymerization mechanism (see figure 2.4) of the epoxy resin is different from the thermal curing with amines: the first is a chain growth reaction, the latter is a step growth one (see figure 2.11). After the formation of the strong acid by light irradiation of photoinitiator, the propagation of the reaction is thermally driven and the kinetics changes with temperature: first the protonic species leads to formation of oxonium ion, highly reactive and instable, that immediately reacts with a monomer in order to form a tertiary oxonium ion in a ring opening reaction. The propagation of the reaction continues thanks to subsequent attack of next monomers to the terminal tertiary oxonium group: the mechanism of polymerization is chain growth type. The termination steps in cationic photoinitiated reaction are limited: recombination is possible between counteranion of initiator and the reactive species or between the propagating ends and a nucleophilic impurities (like water for example). For this reason the cationic photopolymerization can propagate after UV irradiation, reaching high conversion efficiency that could be increased by thermal post-treatment: this rate of conversion is not achievable in the free radical photopolymerization, characterised by high probability of termination reactions during the polymerization.

Since the difference mechanism of chain growing during the synthesis of the thermoset material, the network originated from the cationic photopolymerization is different from the one created by amine curing reaction: the high cross-link density leads to an embrittlement of the polymer [3, 26]. In order to counteract this behaviour and to regulate the network formation, polyols are often used as chain transfer agents, whose function will be explained afterwards: the weight percentage of this additive has direct effects on the mechanical and thermal properties of the polymer, if it's too high could strongly decrease the polymer performance [3].

### *2.2.2 Chain transfer agents*

A chain transfer agent (CTA) is a chemical compound that can be called modifier or regulator and it has at least one weak chemical bond: thanks to this it can react with the active site of a propagating polymer chain and stop the growing. With the addition of chain transfer agent, the reactive spot of the polymerization is located on this agent that can transfer it to another monomer for starting a new chain. The main advantages, when this kind of chain transfer molecule is involved in the cationic photocuring, are: control over the chain length, regulation of cross-linked network, changing in the kinetics reaction and modification of mechanical properties. These agents are frequently found in both cationic and radical photocurable formulations: of course different types of molecules can act specifically and efficiently as chain transfer agent if only they are coupled with the correct monomers.

As described before polyols are often applied in addition to epoxy monomers: in figure 2.13 it is shown the different reaction mechanism occurring in the presence of a chain transfer agent during cationic photopolymerization of an epoxy monomer.



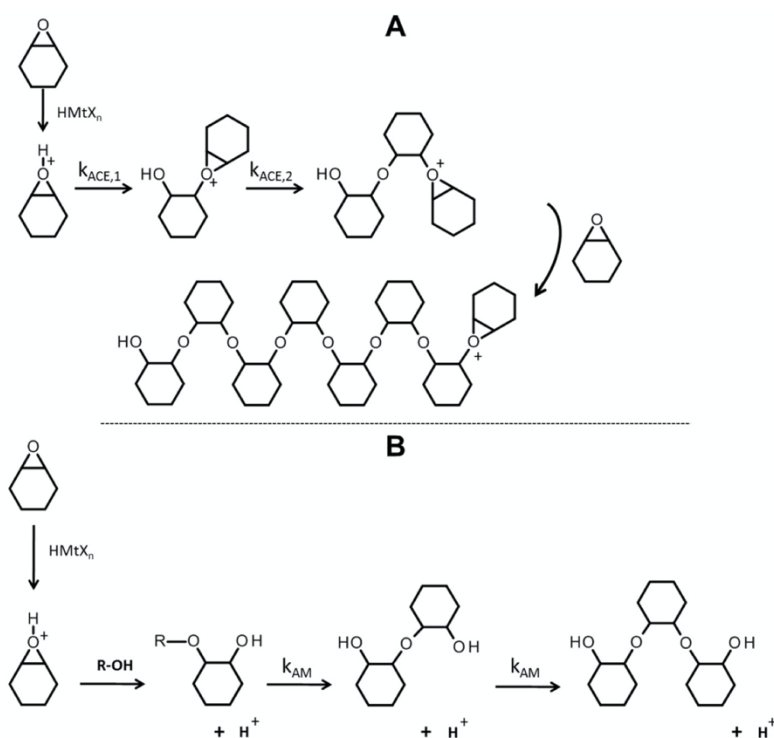


**Figure 2.13:** Normal chain growth mechanism (ACE) of cationic photopolymerization (A) and chain transfer (AM) reaction in presence of hydroxyl group (B) [7].

An organic alcohol reacts with the cationic active centre (charged epoxy ring) that should propagate reacting with another epoxy ring, but due to the alcohol attack there is still a ring opening and a proton is ejected. This proton can bond with other nucleophilic species, which, for example, could be neutral monomers that start a new propagation of the polymer in a different chain: this reaction behaviour is called active monomer (AM) mechanism, which is different from the active chain end (ACE) one that characterized the cationic photopolymerization, and it becomes predominant in presence of polyols and similar compounds. Thanks to AM reaction mechanism the CTA changes its structure/network, kinetics of its formation and thermo-mechanical properties: in literatures the main effects of CTA presence are the decreasing of the glass transition temperature ( $T_g$ ), the higher conversion rate, regulated network and more flexibilization of the structure [4, 7, 8, 9, 19, 22, 33, 34].

The correct choice of CTA could give the possibility of selecting the property of the polymer network with modulation of its weight percentage in the formulation: in fact the first section of the work, the main task is the selection of the proper chain transfer agent that could enhance the reactivity of the BADGE resin and could modify the thermo-mechanical behaviour, acting on the crosslinked network regulation.

### 2.2.3 Other additives

The main properties linked with the epoxy thermoset, like from BADGE resin polymerization, are high  $T_g$ , high modulus, excellent corrosion resistance, high hardness and abrasion resistance, although the ductility and toughness of this polymer are rather low if it's compared to other polymer, like thermoplastics; as mentioned before this is a problem that afflicts the most of photopolymers employed in stereolithography applications. Starting from different studies in literatures [15, 16, 17, 18, 19, 20, 21, 22, 23, 24, 25, 31] which are focusing

particularly on the toughening of the epoxy matrix in composites, the improvement of properties is achievable considering nanoparticles: from carbon nanotubes, graphene and graphene oxide, different type of nanorubber particles (like core-shell particles for example) and nanosilica. It had to be mentioned that all these additives are tested and studied in epoxy thermoset obtained by amine or anhydride curing, when considering the cationic photopolymer the cross-linked network is different and maybe the reaction with this additives could be not achieve the same expected outcome. Although some studies [19, 20], which are related with the UV coatings development, underline the efficiency of nanosilica as reinforcement in cationic cured epoxy thermoset: thanks to presence of distributed hydroxy groups on the silica surface chain transfer effects (see figure 2.14) is active in the reaction, in this way there is the creation of good interfacial adhesion between matrix and silica particles. In addition the dimension of particles in the nanoscale leads to less interference with UV curing technique (if agglomeration is correctly prevented), in fact the conversion increased thanks also to the chain transfer effect. Nanosilica particles enhance the mechanical properties of the epoxy resin, changing Tg and storage module. Another additives, frequently used release coatings, are polysiloxane which improves the mechanical performances of the epoxy matrix: they could be functionalized adding epoxy groups or, in the case of UV curing, the presence of hydroxy groups in the siloxane could provide the bonds with the epoxy resin. Every addition in weight percentage increases the viscosity of the formulation, for some application this effect must be controlled otherwise the processing problems could occur.

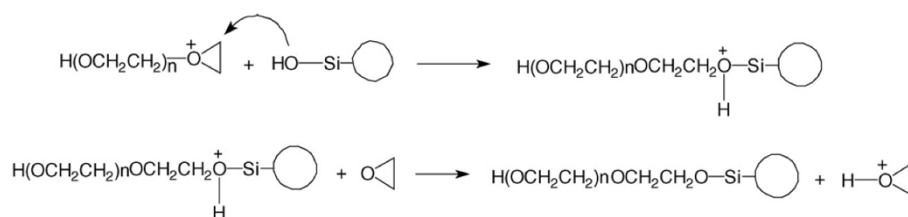


**Figure 2.14:** CTA effect because of the surface hydroxyl group of silica nanoparticles [19].

In the third part of the work an analysis will be provided in order to show how different additives added to the resin change the final properties of the thermoset: in particular nanosilica particles, core-shell rubber particles and different polysiloxane will be taking into account for material modification.

#### 2.2.4 Cationic photoinitiators

The photoinitiator is responsible of the start of the cationic photopolymerization, as mentioned before is composed by an anionic part, responsible for the polymer chemistry, and a cationic part, which determines the photochemistry. The most representatives salts among all cationic photoinitiators are the diaryliodonium and triarylsulfonium salts; thanks to their efficiency and stability the importance of cationic curing has grown: the structure of this salts is shown in figure 2.15.

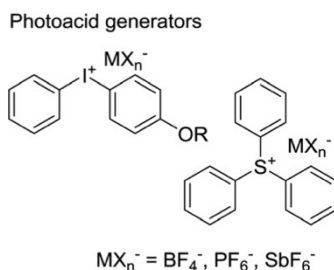
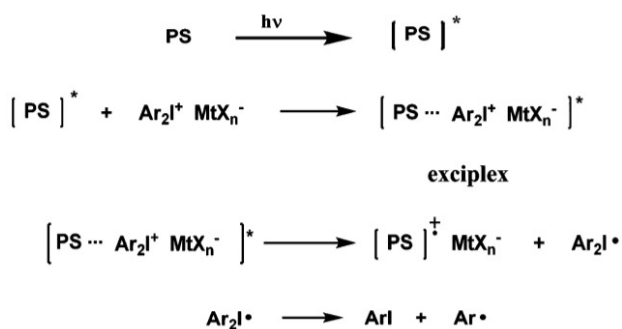


**Figure 2.15:** Examples of Cationic photoinitiators [23].

After irradiation the chromophore cation is excited to a singlet state, from this state it occurs a photochemical decomposition (homolytically and heterolytically) which leads to formation of radical-cations, radicals, cations and arylhalides. In the end these highly reactive species react with monomer through hydrogen abstraction, from homolytic cleavage species, or through electrophilic attack, from heterolytic path species, to originate a neutral species and the acid of the anionic part (see figure 2.9). The efficiency of the photoinitiator is determined by the quantum yield, which is the ratio between the number of molecules that react and the amount of photons absorbed by the system: this parameter is strongly determined by the photolysis and the formation of photoacid. Diaryliodonium salts were the first discovered by the work of Crivello et al. in 1970: the absorption characteristics are strongly influenced by the substituents, which influences also the solubility and toxicity, and the chromophores and usually the quantum yield of this type of salts are usually high, almost around 0.9. Triarylsulfonium salts were discovered later and they are characterised by a higher thermal and chemical stability: same as diaryliodonium changing the substituents and the chromophores the absorption bands change. Nowadays for reaching higher solubility in organic formulations of these photoinitiators they are mixed in solution with propylene carbonate.

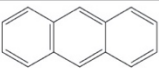
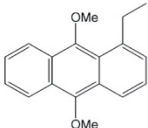
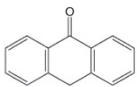
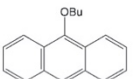
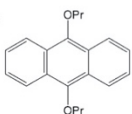
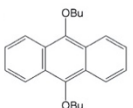
#### 2.2.4.1 Photosensitizers

Usually the absorption range of typical cationic photoinitiator is in the short wavelength UV region between 220 nm and 350 nm: for some practical application, like curing with LEDs, lasers or even sunlight, this range results unsuitable, in order to extend at longer wavelength the sensitivity of the salts photosensitizers are frequently used: the main job done by this type of molecule is the energy transfer from a longer wavelength irradiation absorption to the photoinitiator. The main mechanism which consents the energy transfer is the electron-transfer ones: the figure 2.16 shows the reaction occurring between a photosensitizer (PS) and a diaryliodonium salt, that could be taken as general behaviour of photosensitization of cationic photoinitiators. The photosensitizer absorbs the incident light and now it is in an excited state: then there is the formation of an exciplex, after reaction with the salt, this species is highly unstable and because of this the salt is reduced by electron-transfer leading to the formation of the reactive cation radical and another unstable radical (see figure 2.16).



**Figure 2.16:** Photosensitization mechanism (electron-transfer) of PAG [26].

The most common sensitizers for cationic photoreaction are anthracene (AN), pyrene and perylene: especially anthracene shows high efficiency with every class of diaryliodonium and triarylsulfonium salts, which are photosensitized only by the AN [30]; the absorbance characteristics of anthracene and different derivatives are shown in the figure 2.17. It is important to underline that AN has limited solubility (usually around 0,5% in weight percentage) and modification of his basic structure for obtaining several derivatives increases the solubility in different organic mixtures. The direct advantages of photosensitizers in cationic photocuring higher conversion rates and better reactivity of the systems thanks to the capability of absorbing at higher wavelength [30].

Notation	Structure	mp (°C)	UV spectra	
			$\lambda_{\text{max}}$ (nm)	$\epsilon$
AN		216–218	218	15220
			220	15190
			251	163470
			294	930
			309	1690
			323	3620
			339	6700
			356	9850
			375	9480
EDMA		117–119	220	18240
			253	101260
			261	154130
			361	6450
			380	8860
			401	7360
AR		155–158	258	33990
			269	20140
			308	4520
			367	730
MBA		78–79	218	14640
			248	98410
			255	154540
			334	3180
			350	5650
			368	8580
DPA		93–95	217	19490
			251	99260
			258	152900
			362	7410
			381	11230
			403	9590
DBA		110–112	217	20020
			252	99540
			259	153770
			363	7660
			381	11530
			403	9910

**Figure 2.17:** Anthracene and derivatives peculiar characteristics [30].

Regarding the application of cationic photopolymer in the additive manufacturing sector, which is the aim of this project, using a photosensitizer is fundamental in order to have high absorbance at the emitting wavelength of the laser: in addition to this the photosensitization of the photoinitiator helps in controlling the dimension of the layer formation during irradiation, avoiding overpolymerization of the cationic formulation. Since the photoinitiator choose in this application is the triarylsulfonium hexafluoroantimonate and the laser has an emitting wavelength of 375 nm the best choice as photosensitizer is the anthracene.

### 3. Additive manufacturing process

#### 3.1 Introduction to additive manufacturing technique

The name additive manufacturing (AM) shows directly the opposition of this process method to the traditional process based on subtractive and moulding approaches: the final object is obtained by sequential and continuous layers addition over layers, see figure 3.1.

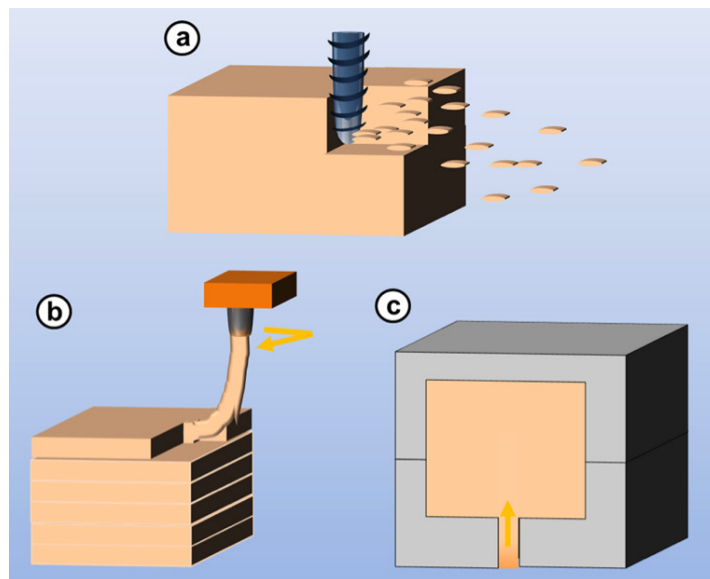


**Figure 3.1:** Difference between subtractive (a), additive (b) and formative (c) production process [3].

The growing demand for rapid fabrication of prototype in the 1980s caused the development of additive techniques: the basic idea, that is still valid today, was that from a CAD/CAM model, which reproduced virtually the object, the prototype could be easily obtained though layer by layer addition. The productive process starts from the design of the virtual model in a CAD software, when it is complete, the file has to be virtually sliced in different layers and if there is the structure collapse risk, also supports are added to the model. Once all this software operations are concluded, the file is ready to be processed in the machine: the coordinates of the CAD/CAM model and the sliced structure are the printing information of every single layers creation that the 3D printer needs for building the final model though layers superimposition. The process exposed is represented in figure 3.2.

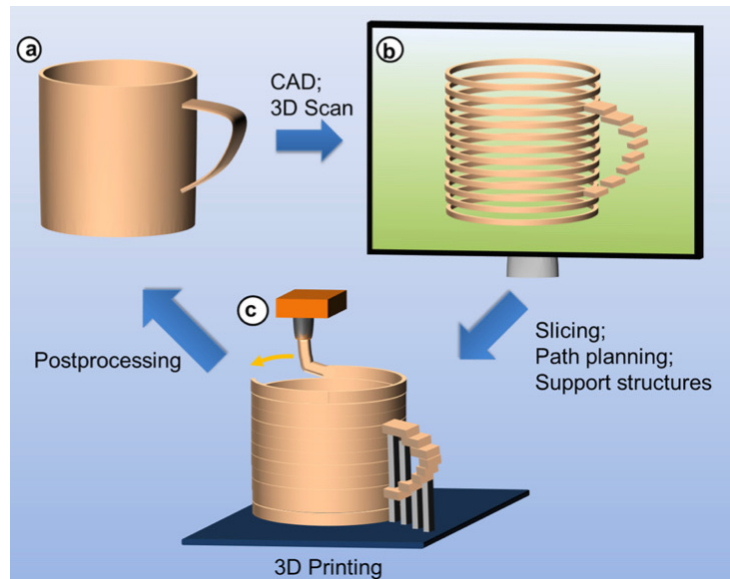


**Figure 3.2:** Additive manufacturing steps, from CAD model (a) to 3D printed part, though previous slicing and support structure creation (b) [3].

The real advantage of rapid prototyping technique, this was the first application of the 3D printing machine, is the maximum freedom design of the part: complexity is not an issue, ideally any shape or surface design is possible thanks to the peculiar method of layers addition. Design of the object and layer thickness, which is decided by the slicing operation, directly determine different process features: build speed, resolution, supporting structure, final material properties and post-processing operations. The presence of supports in the final object and usually a low resolution of surfaces due to the slicing operation demand a post-printing operations: cleaning, support removal, surface finishing and in some case machining of the part. Because of the high stress applied to the material during layers deposition, post-curing and heat treatment are normally applied. The design capability offers by this technique is enormous but it still has its own limits: lower building speed than traditional forming process, inferior spatial resolution, limited working volumes and long post-process operations. The material that is processed in this 3D printers has to be post-treated in order to release stress and reach proper mechanical properties, which usually are inferior to the products obtained by traditional process [3].

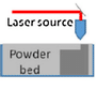
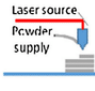
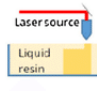
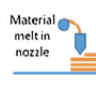
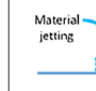
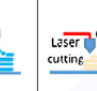
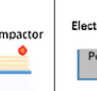

Nevertheless this limitations, which essentially derive from the fact that initially the additive manufacturing was thought for rapid prototyping, the research and development in the 3D printing is growing continuously: the unique ductility and innovation in the part design offer new possibilities of innovative applications in several sector, like automotive, aeronautics, electronics, biomedicine, tissue engineering, drug delivery and food industries. It remains, anyway, mandatory in the additive manufacturing future development to overcome some main issues:

- Building speed, which is high for the creation of functional prototype but results slow when it is compared with traditional production process of specific class of material. For example in the production of part made from thermoplastic polymer, the injection moulding is more reliable in terms of speed rather than powder or filament based additive techniques.
- Materials and their properties are still very limited: usually the lack of mechanical characteristics of an AM product are not always linked with the type of additive process itself but also with the restricted choice of printable materials. Anisotropy is a critical feature that more or less afflicted every AM techniques. For limiting the stress

accumulation and restore the correct material properties post-treatments are always applied to printed parts. In addition multimaterials structures are still an issue because of contamination, thermal reactivity and rheological difference between printable materials, only some modified AM techniques can mix materials but only between one layer and the other and not inside the same layer. Composites are nowadays employed in order to reach higher properties of the actual printable materials.

- Resolution is another major issue: layer by layer construction has intrinsic problem of lower resolution because of the stair case surfaces derived from the slicing operation. Because of this surface finishing is needed but sometimes is not enough because the surface quality of printed parts is insufficient for potential applications. In order to reaching higher resolution and quality the layer thickness can be reduced but there are physical limits linked with materials and type of AM processes: for example in powder bed based additive manufacturing the layer height is determined by the dimension of the particles, which have a minimum diameter settled for safety reason and for processability issues. The higher resolution among the additive manufacturing processes can be obtained by using vat photopolymerization based approaches in which the quality of the final product is strictly linked with the photopolymer rheological and absorbing properties.

Today the additive manufacturing techniques are various and, thanks to them, essentially metals and polymers can be processed, even though new class of materials are becoming processable like ceramics, composites, biomaterials and hydrogels but with limitations. A rough distinction between AM processes can be made considering the type of raw material for starting the printing job: three major categories of techniques are solid based, liquid based and powder based. Inside of every categories there are different types of process: the liquid based AM category, which is valid only for photopolymers, includes inkjet printing process and photopolymerization processes based on lasers or UV lamps. The powder based AM category consists of powder bed fusion, direct energy deposition (only metals) and binder jetting processes; finally the solid based AM category includes material extrusion processes. For a better overview of additive manufacturing techniques, the figure 3.3 shows schematically every cited processes, underlining the difference between them.

Additive Manufacturing (AM) Processes										
Process	Laser Based AM Processes				Extrusion Thermal	Material Jetting	Material Adhesion	Electron Beam		
	Laser Melting		Laser Polymerization							
Process Schematic										
Name Material	SLS	DMD	SLA		FDM	3DP	LOM	EBM		
	SLM	LENS	SGC		Robocasting	IJP	SFP			
	DMLS	SLC	LTP			MJM				
		LPD	BIS			BPM				
			HIS			Thermojet				
Bulk Material Type										
	Powder	Liquid	Solid							

**Figure 3.3:** Additive manufacturing techniques overview [35].

The aim of this project is focusing on cationic photopolymer applied to 3D printing, so in the next section it will be introduced the stereolithography technique which is the starting point for the development of hot lithography approach, that allows the printability of less reactive and high viscous systems.



### 3.2 Stereolithography

Stereolithography (or SLA) is the oldest additive manufacturing technique: initially developed by Dr. Hideo Kodama in 1981, the first patented SLA printer arrived in 1986 thanks to Charles W. Hull. The early application was rapid prototyping of complex and new design polymer models, nowadays the continuous research in AM field opens the way to new method based on the SLA approach: digital light processing (DLP), two-photon polymerization (2PP), continuous liquid interface production (CLIP) and hot lithography [3, 13, 36]. Essentially every SLA based techniques use a coherent light source (usually in the range of UV light wavelength) for inducing the formation of a cross linked network in the liquid resin: after the creation of the first layer, fresh liquid resin covers it and the light induced polymerization leads to a new layer addition. The model is obtained by layers by layers addition, usually, with high spatial resolution and low surface roughness, thanks to the light source (especially the lasers). On the other side, SLA is slower and more expensive than other additive manufacturing setups: the building speed is essentially determined by the time needed by laser scanning of the layer and by the action of fresh liquid resin recoating; the higher cost is depending on the liquid resin components. The light irradiation, in order to get photopolymerization of the resin, can be generated by two different type of source: one is laser, whose wavelength is in the UV range, and the other is projection of the entire image of the layer by an UV lamp or LED and mirrors system. The latter source type is peculiar of DLP and CLIP method which are considered faster and less expensive rather than laser based SLA, but, because of the mirroring system and image pixels creation, the resolution is always lower than the one achievable with laser sources. The incident light in the SLA can be emitted from two different position: the laser can irradiate the liquid resin from above or from below, the first is called free surface approach and the latter is called constrained surface approach; because of these different methods the setting of the whole SLA machine changes as exposed in the scheme in figure 3.4.

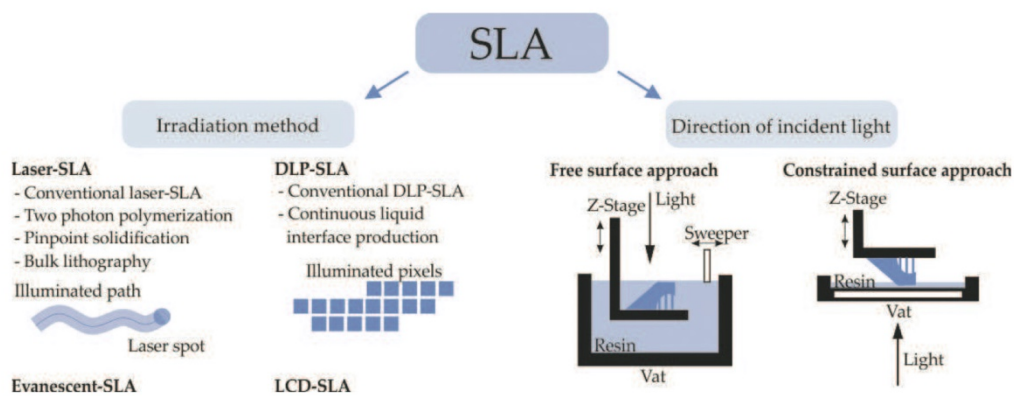


**Figure 3.4:** SLA classification scheme based on irradiation system (left side) and on incident light direction (right side) [36].

The free surface approach was the first setting for SLA developed: the platform, that supports the model during layers addition, is submerged in liquid resin bath; the laser irradiates the new layer from above of the resin bath. After the polymerization of the layer, the platform is lowered by a certain distance and the new resin is coated by a blade (or sweeper in the figure 3.4): the operation is repeated for each layers until the ending of the building job, this action is the most



time consuming one of the overall process [3, 36]. An example of bottom-exposure laser-stereolithography setup shown in figure 3.5 is composed by:

- the light source emitting system, which includes laser module and scanner, mirror system.
- the building platform, which moves in the z-axis direction, where the final object is forming by layers addition.
- the transparent resin vat, which contains the liquid resin before the photocuring starts.

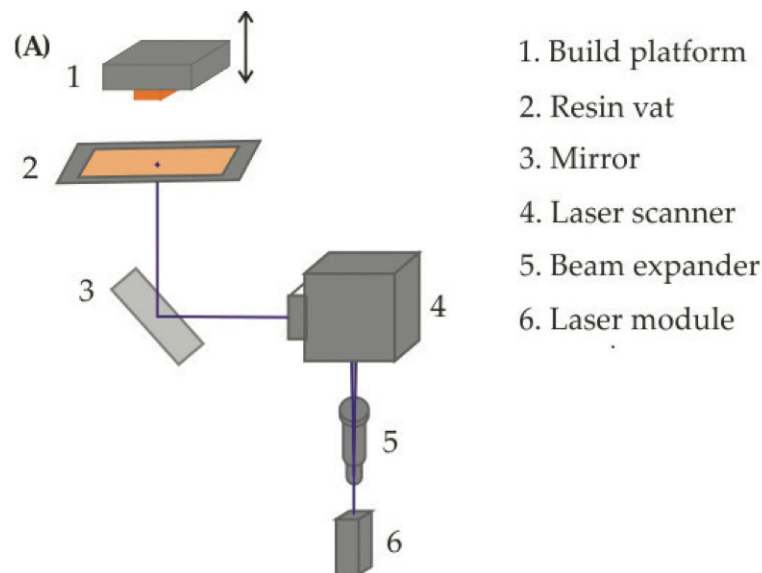


**Figure 3.5:** Example of bottom-exposure laser SLA [36].

The constrained surface method (bottom-exposure system) has irradiation of laser, oriented by a mirrors unit, from the bottom of the transparent resin vat. The building platform goes down when new layer formation starts and it raises when the layer polymerization is completed; because the model is suspended downward, supports or in general lighter structures have to be taken into account for avoiding the fall of the part. The presence of a recoating unit depends essentially on the rheological properties of the liquid resin: ideally after the formation of a layer the submerge platform is raised, and if the resin has low viscosity, the recoating of the vat with uniform film of liquid resin is possible without any mechanical sweeper; on the contrary if the viscosity is high the recoating is incomplete, leading to necessity of a mechanical action before next layer curing [37]. Elimination of mechanical redeposition step of the liquid strongly reduces the cycle time of a printing job. The constrained surface approach in SLA machine is becoming more and more popular because of real advantages compared to the free surface method: first of all the cost is reduced, because the platform is not submerged in the liquid resin, in addition the absence of this aspect leads to a better material utilization during printing, and it cuts the waste of resin. Secondly the z-axis movement of the platform is more precise and accurate, this helps the new surface layer formation, enabling better surface finish. The main issue that is presented by this approach is linked with adhesion force between each printed layer and the vat: it is mandatory that the polymerized layer, while the platform is raising, adheres on the layer above and do not remain stick on the vat. In order to overcome this reaction between vat and the resin anti-adhesion or hydrophobic film are applied on the transparent vat, otherwise mechanical separation methods with shear forces or tilting steps. During SLA processes the resolution in z-axis and in the x-y direction is simultaneously decided by laser parameters, like

speed, intensity and spot diameter, and by photochemical properties of the liquid resin formulations: the curing depth that directly controls the vertical resolution is affected by the presence of sensitizers or absorbers in the liquid resin and by the scanning speed and intensity of laser source [3, 36, 37]. The lateral resolution depends on the laser spot dimension, on the accuracy of the laser in scanning the surface, decided by mirrors movements, and again on the composition of the liquid resin. Resin viscosity plays a central role in the SLA process, in fact if it exceeds a certain value, that directly depends on the printer specific and on the rheology of the photopolymer, the resin results difficult, or even impossible, to process in SLA machine [37]. The figure 3.6 resumes the important characteristics of laser SLA.

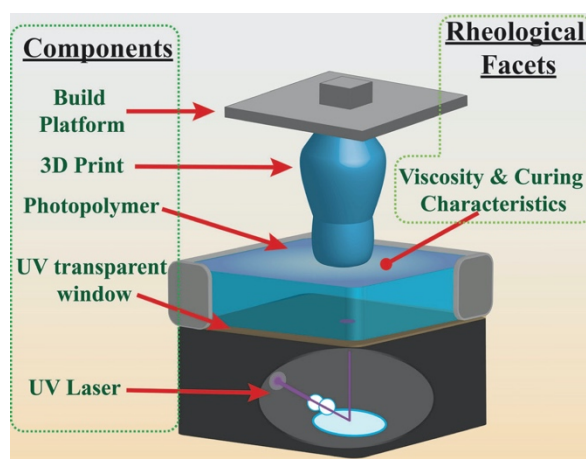


**Figure 3.6:** Scheme of laser SLA printer [37]

Reducing the viscosity in some cases is essential and the way for achieving this result is using diluents or solvents that can systematically lower the viscosity of the formulations; the other way of diminishing the high viscosity associated to some filled or pure liquid photopolymer is using high temperature [3]. From this assumption a new method based on SLA approach has been developed and it is called hot lithography[11, 12].

### 3.2.1 Hot lithography approach

The development of this new kind of SLA process is an answer to the, so called, dilemma of the 3D printing [11], shown in figure 3.7.

	GEOMETRY	MATERIAL	ECONOMICS
SELECTIVE LASER SINTERING	~	✓	✗
FUSED DEPOSITION MODELING	✗	✓	~
INKJET PHOTOPOLYMERS	✓	✗	✓
STEREOLITHOGRAPHY	✓	✗	✓

**Figure 3.7:** Additive manufacturing of polymers dilemma [11].

This dilemma afflicts the field of the polymer additive manufacturing: low viscosity photopolymers, which usually are processed in liquid based AM machines, present poor mechanical properties and brittle behaviour, which make them unsuitable for real industrial application. On the other hand FDM or SLS methods can process high performance polymer for wider application sectors, but the printed products obtained have very low surface qualities and inadequate resolution; on the contrary SLA process guarantees accurate and exceptionally finished model and prototypes. To sum up, the dilemma of polymer AM is the absence of an appropriate technique that can combine high quality printed part with suitable mechanical properties.

Basically since the photopolymers employed in the conventional SLA must show low viscosity in order to be processed: usually this property dramatically affects the final mechanical properties of the cross-linked network, because of the low molecular weight and limited molecular dimensions of the chemical components. Better performances of polymers are linked with higher molecular weight and longer chain backbone monomers, but the viscosity will increase and at the same time the reactivity of the system will be lower at room temperature: hot lithography method, developed by Cubicure [11, 12], proposed the creation of bottom-exposure SLA setup (shown in figure 3.8) that can be heated up in all of its components: the vat, the building platform and the coating unit can reach processing temperature up to 150 °C.

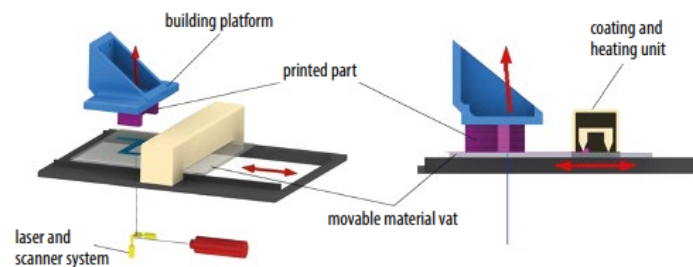


**Figure 3.8:** Scheme of hot lithography process [11].

The first commercial machine made by Cubicure is Caligma 200 (figure 3.9): ideally the machine can process any photocurable resins with high viscosity, but it is mandatory that the systems remain thermally stable at operating temperature [11, 12]. The control in this machine must assure the maintenance of a constant temperature without any peaks or overheating phenomena: the coating unit is realized in order to guarantee a regular deposition of resin film every new layer preparation and at same time operates as a hot container for the resin. The machine prints objects following the layer by layer addition method same as a normal bottom-exposure SLA: this allows to obtain high resolution and accurate printed parts, which is the peculiarity of the stereolithography approach; in addition high precision laser unit and low power absorption make this machines very interesting for future applications [11]. Although the working volume is limited, only 300 mm × 100 mm, and because of this only high precision and micro parts can be produced in series, maintaining high accuracy and precision [11, 12].



**Figure 3.9:** Caligma 200 from Cubicure [11].

Working at high temperatures influences positively the process speed: the blade can go faster in the liquid resin deposition steps and the scanning speed can be higher because of the reactivity of the heated systems. This is valid for high viscous radical photopolymers based on acrylates: the high temperatures strongly reduce the scanning speed for obtaining a green part and enhance the mechanical properties of the thermoset, this is obtained thanks to modified DLP system operating as hot lithography machine, this has been obtained at TU Wien [13].

The innovative exploitation of the temperature in SLA process opens to future development of newly resin formulations: since high viscosity do not results an issue for processing the resin, which can be chemically functionalised or modified with additives, in order to improve thermoset properties, operations that usually raised the overall systems viscosity [14]. In addition resins or photopolymers that are even solid at room temperature can be easily printed with this new method: studying totally new formulations new properties and features could be reachable for SLA printed parts without losing spatial resolution and high accuracy. Finally an important consequence that coming from the hot lithography approach is the possibility to try to process new type of resins which are too low reactive at room temperature and potentially it could be possible to expand the printable material portfolio, which is one the limit of all additive manufacturing processes and especially of stereolithography.

## 4. Materials and methods

This chapter is dedicated to the description of the materials involved in the project and of the analysis methods for giving a characterization of the polymer. In the first sections the chemical components, selected in order to obtain the cationic photopolymer, are taken into account. The other sections are dedicated to the introduction of the test performed on the polymers and to the machine employed for material samples preparation. Finally the hot lithography printer, located in the TU Wien lab, will be described, since it represents a new method for processing photopolymers.

### 4.1 Materials

Essentially the basic material is a thermosetting polymer obtained by the cationic photopolymerization of an epoxy resin. In the first part of the work, as already said, the pure resin with the photoinitiator is modified by addition of chain transfer agents, that should change the propagation reactions of the polymerization (see paragraph 2.2.2). Other additions, that will help to modify the mechanical properties or the photochemical behaviour, are photosensitizers, fumed silica, core-shell rubber particles and different types of poly-siloxane based additives. In the following sections every chemical component will be introduced and it will recapitulate the function associated to them.

#### 4.1.1 BADGE resin

As already mentioned, the epoxy resins are the most important type of cationic photopolymerized monomers: they are characterized by good thermo-mechanical features, high thermal stability, great adhesion and chemical resistance. The presence of the three-ring member rings allow the final thermoset polymers to reach very low shrinkage after cationic photocuring. Among the epoxy resins, in this work, the BADGE resin represents the most used and well known epoxy resin: mainly it is applied in composites, coatings and adhesives field. The backbone structure of BADGE/DEGBA is shown in figure 4.1: the reaction between epichlorohydrin, in excess, and bisphenol-A leads to formation of BADGE, which is characterized by high viscosity and good thermal stability.

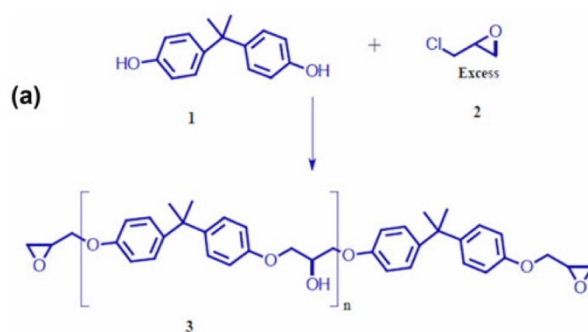


**Figure 4.1:** BADGE (3) structure obtained by reaction between bisphenol-A (1) and epichlorohydrin (2) [31].

The molar mass of BADGE is around 340 g/mol and the resin is characterized by high number of equivalent epoxy groups for 1 kg of formulation. In this work the BADGE resin and the cationic photoinitiator (described below) represent the common components in every formulations and the pure mixing of them is called Reference in the exposition and discussion of the analysis done in this project.

#### 4.1.2 Cationic Photoinitiator

The cationic photoinitiator is the component that generates the propagating species of the reaction: it is mainly composed of the cationic part, which defines the photochemistry, and the anionic part, which is responsible of the chemistry of the initiator and the reaction. As described before (see paragraph 2.2.4), the salt used in combination with the BADGE resin is the triarylsulfonium hexafluoroantimonate (see figure 4.2 for the structure): this cationic photoinitiator is characterized by very high thermal stability, which is an important factor in this work since the resin will be processed at high temperature (not at room temperature). The anionic part determines, thanks to its negatively charge, the strength of the acid generated and the propagation rate of the polymerization: among all possible perfluorometallates the one that shows high reactivity of the cation photocuring is the  $\text{SbF}_6^-$ , despite its toxicity. In order to overcome the poor solubility of the salt, it is rather common to use the triarylsulfonium in solution with 50% weight percentage of propylene carbonate. In figure 4.2 is shown the chemical structure of the photoinitiator and the absorption spectrum, which has its maximum at 230 nm; the quantum yield is around 0.7.

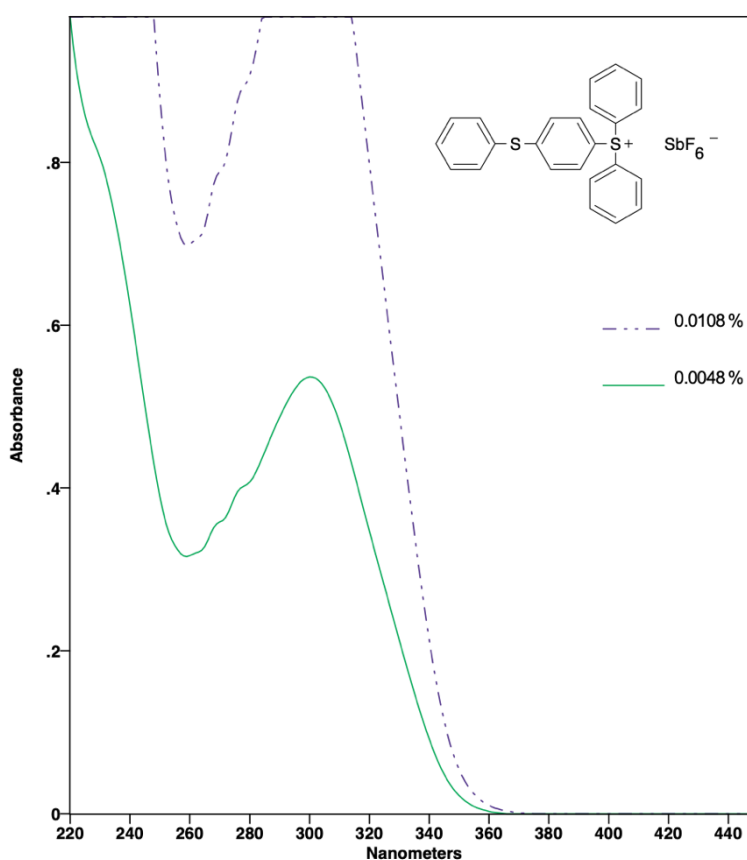


**Figure 4.2:** Triarylsulfonium hexafluoroantimonate structure and absorption spectrum[38].

#### 4.1.3 Chain transfer agents

The chain transfer agent (CTA) is a chemical compound mainly used for obtaining modification of the cationic photopolymer: especially alcohols show high reactivity in epoxy resin based cationic systems. The kinetics and the rate of the polymerization change thanks to the presence of polyalcohols as reported in several articles [3, 4, 7, 8, 9, 19, 20, 23, 26, 33, 34]: the cationic photocured polymers show substantial modification of cross-linked network, which directly influenced the storage modules and the glass transition temperature curves, obtained by DMTA measurements. In addition it is reported that the conversion of epoxy groups is higher in the presence of chain transfer agents.

In this project several CTAs are taken into account in order to study the difference influence on the pure BADGE resin: the expected result is the achievement of a well-regulated network thanks to the presence of CTA, which modify the cross-linking formation during the cationic photocuring. The cationic systems with CTAs inside should behave differently from the pure photocured BADGE and this behaviour will be analysed through mechanical, thermal and rheological tests. The selected CTAs for starting the study are: trimethylolpropane, polypropylenglycole, polytetrahydrofuran (polyTHF) and Boltorn H20 (hyperbranched polymer). The figure 4.3 contains the chemical structures of these compounds.

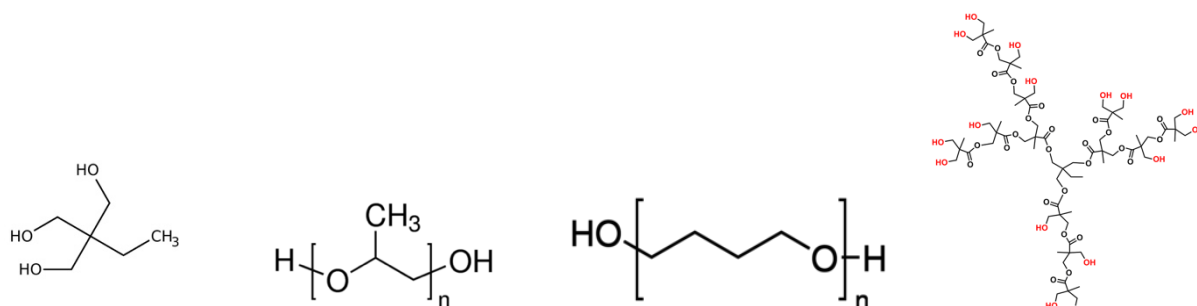


**Figure 4.3:** trimethylolpropane [39], polypropylenglycole [40], PolyTHF [41] and Boltorn H20 [42] (from left to right).

They will add in different molar percentage to the basic formulation which is made of BADGE resin and cationic photoinitiator, taking into consideration the proportion between equivalent hydroxyl groups and epoxides rings. The figures below show the chemical structures of involved CTAs.

#### 4.1.4 Photosensitizer

The main function related to the use of a photosensitizer is absorption at higher wavelengths in order to pass this energy to the photoinitiator. This is mostly common used in pigmented formulations, where reaching absorption over UV region is fundamental. In this work the choice of anthracene as photosensitizer for the sulfonium salt is dictated by the idea of having a better control in the spatial resolution and in the curing depth during the printing process: in the presence of the photosensitizer, the layer formation reaction results more controlled and the final printed object shows better resolution. The anthracene, in addition, has the maximum absorption at 375 nm (see figure 2.17), which the wavelength of laser emission of the 3D



printer, and it shows very good photosensitization of triarylsulfonium, which is chemically stable. The UV spectra of anthracene and its derivatives (see figure 2.17) are shown in figure 4.4. One problem linked with anthracene is the solubility in BADGE resin: the maximum weight percentage reachable is 0.5% which, anyway, is enough for obtaining the desired effects. The article [30] explains that the derivatives of anthracene shows better solubility than anthracene, maintaining the same efficiency with different cationic photocurable monomers.

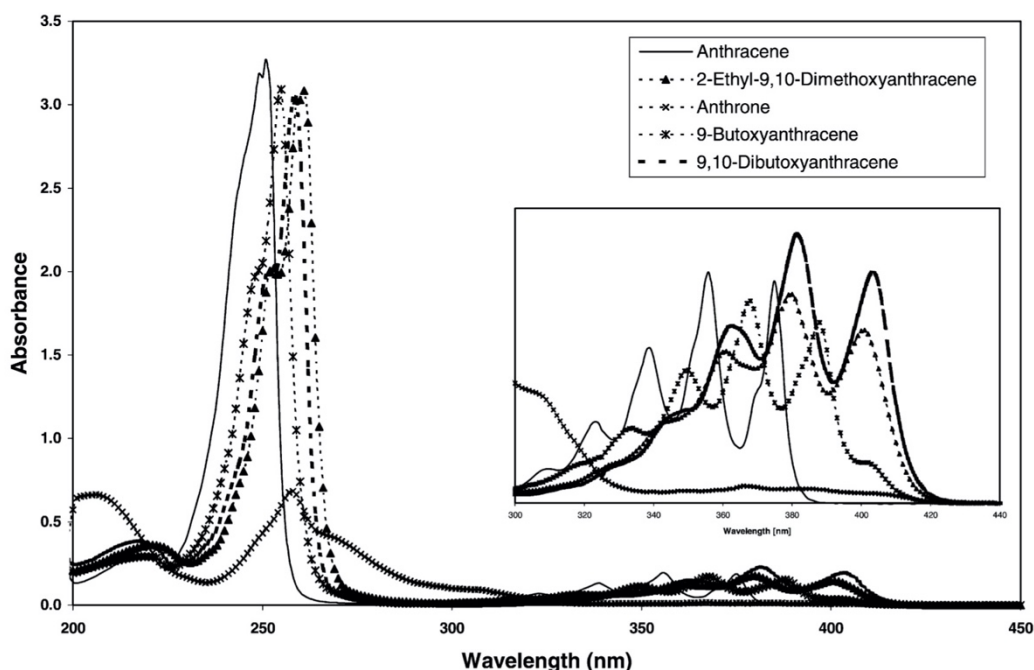


**Figure 4.4:** Anthracene and its derivatives UV spectra in methanol [30].

#### 4.1.5 Additives for thermoset modification

Despite the good properties for a thermoset and the multitude of industrial applications, the epoxy resins, which include also BADGE, are still inferior in term of elongation at break and toughness to the majority of thermoplastic polymer. Their behaviour is essentially similar to a brittle material because of the highly cross-linked network: in order to improve their mechanical behaviour, during the years different additives has been proposed [15, 16, 17, 18, 19, 20, 21, 22, 23, 24, 25, 31]. The studies has been conducted especially on epoxy resin cured with amines: the selected additives are nanosilica particles, different type of core-shell rubber particles and reactive liquid rubber, in addition combination of these has been analysed. Another modifier, already citated, is polysiloxane, which are usually mixed with epoxy resins in the field of release coatings and adhesives: the desired functions of these additives are toughening and mechanical improvement in general of the polymer network, despite solubility issues in the liquid resin.

Regarding the improvement of the overall mechanical behaviour of cationic cured epoxy resins the studies are more focused on the effects linked with the addition of nanosilica particles, which directly are directly involved in the cation reaction as CTA because of the presence of hydroxyl groups on the surface (see figure 2.14) [19, 20]. This influence is directly visible because the filled thermoset shows higher epoxy conversion, different Tg and storage module behaviour, that are effects strongly dependent on CTA traces in cationic photopolymerization.



In general exceeding with this additives leads to problem of solubility, in case of liquid rubber and siloxane, of agglomeration, especially for the particles, and overall viscosity, which becomes prohibitive for some applications.

In this work the changes of the epoxy resin caused by the addition of nanosilica, polysiloxane, core-shell rubber will be analysed through DMA, tensile test, RSA and photo-DSC.

## 4.2 Analysis methods and machines

In this chapter an overview of the test methods and machines will be presented: the information come from the datasheet of the machines.

### 4.2.1 Thermal dynamic mechanical analysis

DMA or DMTA is the analysis commonly used for investigating the viscoelastic properties of the polymer. During this analysis an oscillating load is applied on the samples at certain frequency and at the same a temperature ramp is settled. Since a polymer is a viscoelastic material, his response to this type of stress depends on the temperature and on the frequency applied: the polymer could behave like an elastic solid at low temperature (under  $T_g$  usually) and this behaviour changes when the temperature gets higher or the frequency goes down, looking alike a viscous liquid. The stress of the polymer is described by the equation 4.1:

$$\sigma(t) = \sigma_0 \sin(\omega t + \delta) \quad (4.1)$$

Where:

- $\sigma(t)$  is the stress in function of the time
- $\sigma_0$  is the maximum stress
- $\omega$  is the frequency of the oscillation
- $t$  is time
- $\delta$  is the phase angle between stress and strain

If the polymer behaves as pure elastic material the response is pure elastic and it is in phase with the applied stress:  $\delta$  is zero in this case. On the contrary the response of pure viscous liquid is shifted of  $90^\circ$  respect to the applied stress. Because of this double nature of the polymer it is possible to define two modules that explained the polymer behaviour: one is the storage module ( $E'$ ) which represents the elastic part of the material and the other is the loss module ( $E''$ ) that represents the viscous part of the material. The equation 4.2 shows that the ratio between the two modules is called  $\tan \delta$  and it is important because the temperature at which the curve shows its maximum is referred as the glass transition temperature ( $T_g$ ).

$$\tan(\delta) = \frac{E''}{E'} \quad (4.2)$$

The output of a typical DMA analysis is the graph containing all three curves:  $E'$ ,  $E''$  and  $\tan(\delta)$ . The DMA is more sensitive and accurate than the DSC for obtaining the value of the glass transition temperature ( $T_g$ ) of the material.

The instrument used for the analysis, in this case, is DMA-2980 shown in figure 4.5: the measurement configuration is three-point bending type. The software for the data analysis obtained is the TA Analysis software, developed by the same producer of the machine.



**Figure 4.5:** DMA-2980 machine in three-point bending configuration.

#### *4.2.2 Tensile test*

The tensile test gives the main information about mechanical properties of the tested samples: the machine is designed in order to apply to the samples a force for deforming it and the final results is the stress-strain curve of the material. From this graph it is possible to determine the Young module, which the slope of the linear part of the curve, the maximum stress of the material, the yield stress, which marks the transition from elastic to plastic behaviour of the material, and finally the elongation at break. The sample is fixed between two clamps that apply the force and the software linked to the machine calculates the movement of the clamps; the figure 4.6 shows the setting used.

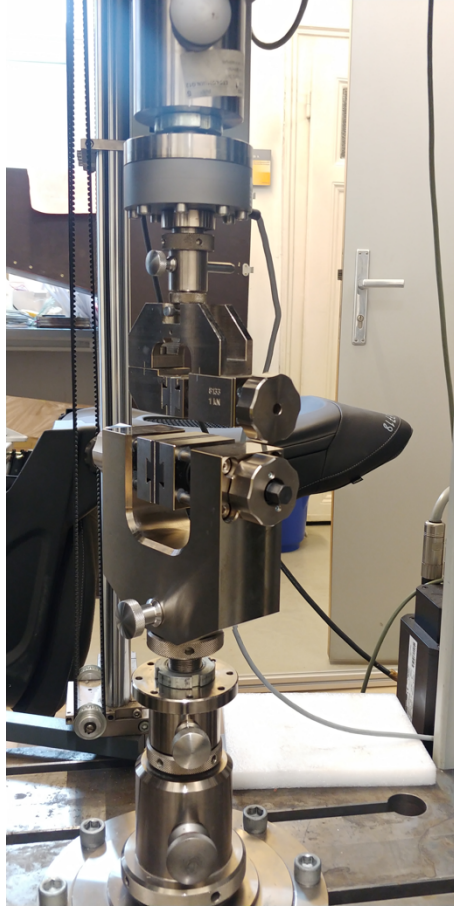


**Figure 4.6:** Tensile test configuration.

From considering the force applied to the sample and the total shift of the clamps from the original position, the software shows the stress-strain graph, which is valid because the dimensions of the sample are requested by the software before starting the test. Important parameters in order to obtain the correct results are the speed of the clamps movement which is 5 mm/min and the force applied by the load cell which is 1kN. The basic equations 4.3, 4.4, 4.5 for determining the mechanical data of the samples are written below:

$$\sigma = \frac{F}{A} \quad (4.3), \quad \varepsilon = \frac{\Delta l}{l_0} \quad (4.4), \quad E = \frac{\sigma}{\varepsilon} \quad (4.5)$$

Where:

- $\sigma$  is the stress of the sample
- $\varepsilon$  is the strain or elongation of the sample
- $E$  is the elastic module of the material measured in the elastic region
- $F$  is the force applied by the load cell
- $A$  is the cross section of the sample
- $\Delta l$  is the difference between the initial length and instant deformation of the sample
- $l_0$  is initial length of the sample

#### 4.2.3 Stress relaxation analysis

Since a polymer is a viscoelastic material, typical behaviour that can be observed is the so called stress relaxation: when a constant deformation is applied to a polymer, first of all it will reply with an initial stress, that, if it is measured for long time, will decrease. The way of how this stress decreases in the material is linked with his inner structure: initially there is a rapid rearrangement of the structure which cause a high speed in stress decreasing, then the material starts to stabilize his response and the stress reaches an almost constant value. This last statement is valid for a thermoset which thanks to its cross-linked network shows higher rigidity, on the other way a thermoplastic polymer can reach total relaxation, of course after a very long time or for high temperatures. The machine RSA-G2, used for performing this test, is shown in figure 4.7: essentially the configuration of the test is three-point bending type, but as additional feature the test is performed in water at 37 °C. A metal cylinder, shown in figure 4.7, surrounds the samples and the clamps, this object ones is sealed with screws allows the immersion of the system in water for starting the measurement.



**Figure 4.7:** RSA-G2 machine during calibration with metal cylinder for measuring stress relaxation in water.

#### 4.2.4 Photo differential scanning calorimetry analysis

Differential scanning calorimetry analysis is a common thermal test in order to understand the evolution of the systems through temperature variations. The sample is placed in an aluminium crucible inside an heating chamber, where at the same time an empty crucible is present. The two crucibles are heating separately and the machine will automatically detect the difference of heat between the two in order to have the same temperature in both crucible. The final curve will show the thermal flux variation, that could be exothermal or endothermal. Since the study of the cationic photopolymerization rate is very important for the final application of 3D printing, the cationic photocuring of epoxy resin will be directly detected thanks to the photo-DSC method: it means that a DSC analysis will be done at the same time that the photoreaction occurs, triggered by an UV lamp. Photo-Differential Scanning Calorimetry experiments will be done on a Netzsch Photo-DSC 204 F1 Phoenix equipment with an autosampler. The light sources for UV respectively LED curing will be used in combination with a glassfiber filled double-core light guide (3 mm fibre diameter). All measurements will be conducted under inert atmosphere ( $N_2$  flow of 20 mL/min). The power of the UV lamp is calibrated at 1 W. The heat flow of the polymerization reaction will be recorded over time, the temperature will be maintained at constant value. The software Proteus-Thermal Analysis from Netzsch was used for data analysis. The Exfo OmniCure™ 2000 with a broadband Hg-lamp (320-500 nm, 3 W  $cm^{-2}$  at the tip of the light guide) is the UV source coupled with the DSC. In figure 4.8 the photo-DSC is settled for the measurements.

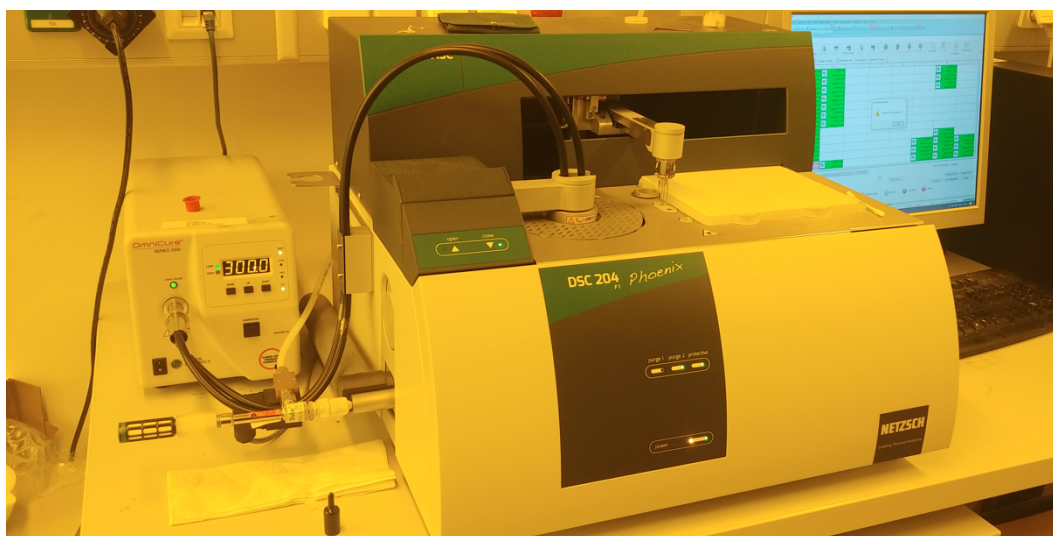


**Figure 4.8:** Photo-DSC machine.

#### 4.2.5 Photo-rheology

Photo-rheology coupled with real time IR analysis (NIR or MIR) is a powerful in situ instrument for obtaining complete characterization of photocurable thermoset: the conversion rate and the evolution of rheological features of the material are the main outputs given by the experiment. The setup of such instruments is reported in this article [10]: the measurements of different resins have been carried out, showing the capability of this machine in detecting all important parameters. For the sector of stereolithography the study of resin photocuring is



relevant because, since the measurement is conducted on samples with thickness in 50-500  $\mu\text{m}$  interval, direct characterization of layer formation can be made. The information from IR is final conversion of functional groups (double bond in radical photopolymerization and epoxy groups in cationic photopolymerization) and the rheological data are time to gel point ( $t_g$ ), storage module ( $G'$ ) and loss module ( $G''$ ), shrinkage force ( $F_N$ ). In addition this type of analysis can be done at higher temperatures, which are interesting when hot lithography approach is involved. The data obtained by this instrument are considered highly reproducible, although errors come from friction and adhesion problems between rheometer plate and sample, also IR adsorption issues could be present if the samples is too thin (50  $\mu\text{m}$ ) and incomplete curing when the samples is too thick (500  $\mu\text{m}$ ). RT-NIR-photorheology measurements will be performed on an Anton Paar MCR 302 WESP with a P-PTD 200/GL Peltier, borosilicate glass plate (60 mm diameter, 6 mm thickness) and a PP25 measuring system. Additionally the rheometer is coupled with a Bruker Vertex 80 FTIR spectrometer with external mirrors to guide the IR beam through the sample during the rheology measurement. The IR beam passes through the glass plate and is reflected by the PP25 measuring system before returning to the MCT-detector. For UV curing an Exfo OmniCure™ 2000 with a broadband Hg-lamp (320-500 nm, 3 W  $\text{cm}^{-2}$  at the tip of the light guide) is used. The IR chamber will be continuously purged with dry air. Spectra were recorded from 7000-4000  $\text{cm}^{-1}$  at a resolution of 8  $\text{cm}^{-1}$  and a frequency of 4 Hz. The configuration of the machine is reported in figure 4.9.

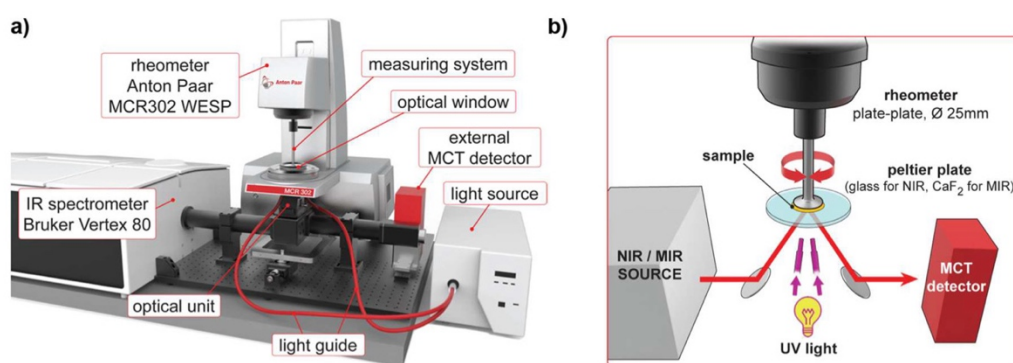


**Figure 4.9:** Photo-rheometer setup (a) and schematic representation of analysis process (b) [10].

Rheology measurements will be analysed with the Software Rheoplus by Anton Paar. IR spectra will be analysed with the software Opus 7 by Bruker. The photo-rheology test will be executed at 80 °C with sample thickness of 200  $\mu\text{m}$ .

### 4.3 Formulations and samples preparation

In this section the description of liquid formulations and samples preparation will be presented: a brief presentation of machines and methods involved is also included.

As already specified the BADGE resin has to be mixed with different components: in every formulations 3% in weight percentage cationic photoinitiator (triarylsulfonium hexafluoroantimonate) is added, since it is in solution with 50% in weight of propylene carbonate the solubility is not an issue. Since all the formulations prepared are light sensitive, the lab where they have been mixed is illuminated by an orange or yellow light for avoid premature photocuring of the liquid photopolymer.

For mixing the formulations, the SpeedMixer machines, located in the lab, are used at maximum rpm (2350 or 3500 rpm) for several minutes until the formulations reach a stable and homogenous appearance. This machine, see figure 4.10, is designed for mixing all kind of components thanks to the generation of complex centrifuge forces which are generated by the motion of the mixing chamber. In addition magnetic stirring of the heated formulations could be performed if the mixing is not homogenous. In order to enhance the solubility of solid chemicals, a cryomill (Retsch Cryomill) is used for grinding the substances to fine powders. The precooling-time at 5 Hz was set to automatic, so that the apparatus determinates the necessary cooling time itself, when it is connected to the liquid nitrogen tank. The precooling was followed by three mill-cycles of two minutes with 25 Hz, with intermediate cooling of 30 seconds at 5 Hz.



**Figure 4.10:** SpeedMixer machines.

The chain transfer agents is added to the resin considering the equivalent hydroxy groups presence: for this reason the CTA percentage addition is calculated in equivalent molar percentage, taking in consideration the ratio between equivalent hydroxy and epoxy groups. For starting the studies of the different CTAs in epoxy resin, the molar percentages of each CTAs will be 5%, 10% and 20%, with an additional exception of 30% formulation for the trimethylolpropane.

The trimethylolpropane is characterized by the presence in its structure of three hydroxy groups: this chemical is solid at room temperature (melting point around 60 °C and molar mass of 134 g/mol) and, for having a better solubilization in the resin, it is grinded in the cryomill. Once obtained finer powders, the trimethylolpropane is been added to the resin and the photoinitiator formulations: in order to facilitate the addition using the scale the right amount in grams of the CTA is been calculated from the molar percentage. In order to homogenize all the formulations with different amount of trimethylpropane (5%, 10%, 20% and 30%), the formulations are heated up to 80 °C for 30 minutes in oven and after that it is mixed in the SpeedMixer for 10 minutes at 350 rpm. The final result is a white stable colloidal suspension that turns transparent at higher temperature (from 70 °C). All four different formulations, containing trimethylolpropane, is been prepared following the same steps.

The polypropylene glycol, selected as CTA for the BADGE resin, is a viscous liquid at room temperature (molar mass of 425 g/mol) and it is characterized by two hydroxy groups: it is added in 5%, 10% and 20% molar percentages respect the functional groups. The mixing of this substance is easier than the trimethylolpropane, in fact only 5 minutes at 3500 rpm are

sufficient to reach an homogenous formulation for all percentages. In this case the final formulations are transparent.

The polytetrahydrofuran (polyTHF 2000), used in this work, is a solid at room temperature (molar mass of 2000 g/mol and melting point around 35 °C) and it is characterized by the presence of two hydroxy groups in its chemical structure. Same as for the previous CTAs, the polyTHF is added to the resin in the three same molar percentages and, for enhancing the solubility in the resin, it is grinded in the cryomill. The formulations are, then, mixed in the SpeedMixer at 3500 rpm for 10 minutes: the final result is similar to the one obtained from the trimethylolpropane mixing.

The Boltorn H20 is a dendrimer with sixteen hydroxy group in its structure and it is solid at room temperature (molar mass of 2100 g/mol and melting point around 120 °C): ideally the mixing with the epoxy is possible and it is very efficient as CTA in cationic photopolymerization, as reported by different articles [9, 33, 34]. Although during the preparation of the formulations containing this hyperbranched polymer, the insolubility of the Boltorn in the resin has resulted impossible to overcome: grinding the solid with cryomill and magnetic stirring of the heated formulations have been insufficient, the Boltorn always precipitates as solid. Another strategy adopted is mixing all the components with a solvent, methanol, styrene and ethanol have been the best choices, but after the removing of the selected solvent with Rotavapor and high vacuum system, afterwards, the Boltorn did not dissolve in the BADGE resin. One reason for this insolubility could be linked with crystallization of the product over the years, but even heated up the Boltorn over the melting point (ideally melting of the crystals), avoiding degradation for overheating, and rapidly cooled down with liquid nitrogen the insolubility still remains. Because of this, the formulations containing the Boltorn have resulted impossible to prepare.

The photosensitizer which is the anthracene for the scopes of the project is solid at room temperature (molar mass of 178 g/mol and melting point around 215 °C) and highly thermally stable: as already mentioned its solubility is limited in epoxy resin, the maximum in weight percent is 0.5% in the BADGE resin. In order to dissolve the sensitizer in the formulation selected for the 3D-printing needs to stay in the liquid resin for almost 12 hours at 80°C in oven (until all crystals are dissolved).

The other additives like fumed silica, epoxy-functionalized core-shell rubber particles and different polysiloxanes have been mixed following the same steps exposed before: using the SpeedMixer for long time (most of the case for about 30 minutes at 3500 rpm) and the oven for heating the formulations, all additives have been dissolved.

The samples for the DMA, tensile and RSA analysis are been prepared by photopolymerization of the liquid formulation in UV chamber (see figure 4.11): which is a ventilated IntelliRay 600 UV curing unit from the company Uvitron with a metal halide UV lamp under air (irradiation power 600 W, UV-A: 125 mW cm<sup>-2</sup>, and vis: 125 mW·cm<sup>-2</sup>). First of all the formulations are heated in the oven and then, for removing possible bubbles incorporated during the mixing, the formulation is placed in a vacuum chamber for complete degassing. The formulation is poured in a silicon mould, shown in figure 4.11, that permits to obtain 6 samples for tensile (dogbone samples 35 mm long and 2 mm thick) test and 4 samples for DMA test (board like shape 2 mm thick and 40 mm long), that are similar to the samples for the RSA, which requires thinner (1 mm) and shorter samples (between 15 and 25 mm). If, after the pouring of the formulation, the liquid presents bubbles, it is possible to remove them in the vacuum chamber. The UV photocuring of the resin in the UV chamber is carried out exposing the silicon mould with the liquid formulation for 300 seconds, each side of the samples, at maximum intensity.



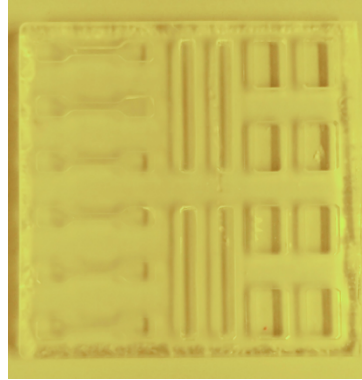
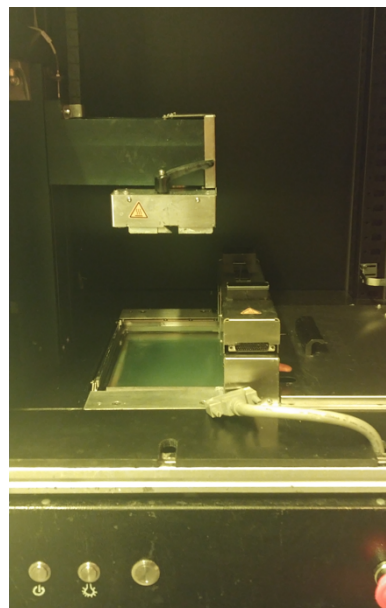


**Figure 4.11:** UV chamber (left) and silicone mould (right).

In order to obtain the correct samples thickness for each tests, each samples is polished with proper abrasive paper placed on a rotating disc with water: the tensile and RSA samples should have thickness around 1 mm, DMA samples should be 2 mm thick. The photo-DSC and photo-rheology analysis work with liquid sample of formulation, in these cases for better handling of the formulation it is heated up around 50 °C.

#### ***4.4 Hot lithography machine***

The idea behind the hot lithography has been already explained, in this section an overview of the machine involved in this project is presented. The 3D printer located in the TU Wien lab is very similar to the one sold by Cubicure: the figure 4.12 shows the machine inside the yellow lab of TU.



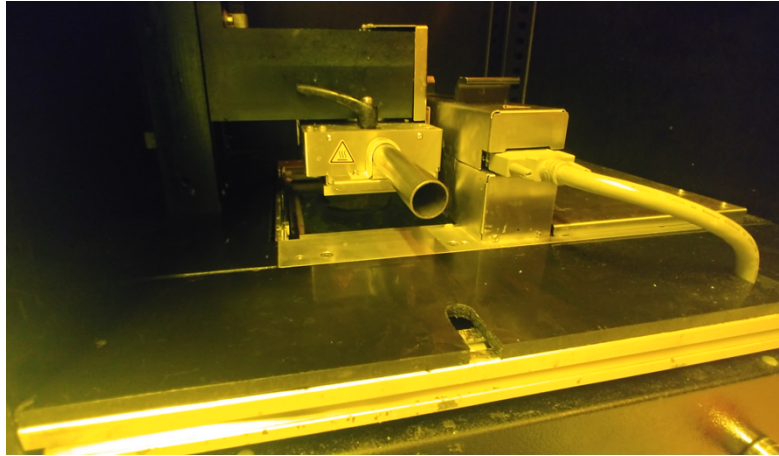


**Figure 4.12:** Hot lithography machine in TU lab (up-left photo), interior of printing machine before starting a printing job (up-right photo) and the setup of hot lithography for 3D printing (down photo).

The maximum operative temperature is 100 °C for the vat and the coating unit, maximum temperature of 80 °C for the building platform. The laser emission wavelength is 375 nm and its power is 70 mW, the laser unit is located under the transparent vat, which is covered with a special foil for avoiding the adhesion of the new layer on it. The laser spot dimension is around 20  $\mu\text{m}$ , the scanning speed and the hatching distance (distance between two consecutive exposure of the laser beam) could be modified by the control software on the computer: the minimum speed is 25 mm/s and the maximum is 10500 mm/s. The hatching distance can be set at 0.3 mm or at 0.02 mm, the laser unit gives the possibility to set two exposures: the orientation of scanning could be vertical (90°) or horizontal (0°) respect to layer building platform. The layer thickness of each layers of the whole part has to be selected in the control program of the machine: the slicing information are already contained in the CLI file uploaded in the machine, this gives to the machine the number of layers for printing the part and the outlines that define the object that has to be drawn by the laser. Other parameters are the speed of the building platform in the z-axis (upward and downward), the force applied by the platform on the vat before laser exposure, the speed of the vat in the x-direction under coating unit and the height of the coating unit respect to the vat. The cycle of new layer formation starts with the vat moving to the right under the coating unit: the heated liquid resin is deposited on the vat thanks to the doctor blade, while the vat is moving backward to the left. The building platform goes down, initially fast and, then, for reaching the correct layer thickness and applying the force on the platform the speed is inferior (ten times or more slower). When the platform stops its motion, the laser starts the scanning of the resin: the laser first scan the outline of the parts and then it begins the filling of the object following the parameters settled in the software. When the laser turns off after fully polymerized the layer, the platform goes up slower: the new layer has to adhere on the previous one or at the metal if it is the first, for this reason the speed of building platform must be slow for avoiding sudden stress on the new layer. From now a new layer can be built and the cycles just described is repeated until the end of the job, when the part is fully printed. The properties of liquid resin and its photoinduced polymerization play a central role in defining the resolution of the final part and all the operation during the printing job. Understanding the behaviour of the resin in the 3D-printer will be the focus of the second part of the work after definition of the proper formulations for starting a printing job.

## **5. First part: selection of chain transfer agent for BADGE cationic photopolymerization**

### ***5.1 Central focus of the first part of the project***

The first part of the work is focused on the selection of the best chain transfer agent in order to allow the BADGE resin printability: the formulation needs to be more reactive than the pure BADGE resin and the cross-linked network of the thermoset needs to be well regulated by the chain transfer agent. In the next sections the results from different tests will be discussed.

### ***5.2 List of formulations***

In this paragraph there is the overall presentation of the formulations tested and, also, the correct nomenclature is described (necessary for understand the tables and the graphs).

The basic formulation is pure BADGE resin with 3% weight percent (%wt) of triarylsulfonium hexafluoroantimonate: the name of this formulation will be “Reference” and it will be its name in all tables and graphs that will be shown in this work. As already explained, four different chain transfer agents will be added to the Reference: the nomenclature for these formulations is explained here for better understanding of the graphs and the tables afterwards. The name for each formulations starts with “CDA” which is followed by an underscore and a number and, again, followed by an underscore and a percentage: the number is associated to the CTA inside the basic formulation and the percentage is the CTA molar one inside. The percentages are 5%, 10% and 20% molar percent and only one of 30% molar. The number connected with the CTA follows this order: the 1 is related to trimethylolpropane, the 2 is referred to the polypropylene glycol 425, the 3 is the polyTHF 2000 and finally the 4 identifies Boltorn H20. To sum up, the all formulations tested are:

- Reference
- CDA\_1\_5%
- CDA\_1\_10%
- CDA\_1\_20%
- CDA\_1\_30%
- CDA\_2\_5%
- CDA\_2\_10%
- CDA\_2\_20%
- CDA\_3\_5%
- CDA\_3\_10%
- CDA\_3\_20%

As previously mentioned, the Boltron H20 was result impossible to dissolve in the BADGE resin, so the CDA\_4\_5%, CDA\_4\_10%, CDA\_4\_20% are not considered in any further experiments presentation and discussion.

### ***5.3 Experimental results and discussions***

In the next paragraphs the results from different tests will be shown and explained in order to select, in the end, a proper formulation for the 3D printing process. Some additional information

about tests are reported in this paragraphs and they remain valid for all time the same analysis is performed again, if it is nothing is specified.

### 5.3.1 DMTA

The DMA tests were performed on three-point bending samples: the figure 5.1 shows the configuration of the machine, the distance between the two bottom supports is 20 mm. The sample thickness should be 1,80 mm (obtained from the polishing with abrasive paper) and the width should be 5 mm (depends on the shrinkage of each formulations): these two values are measured before starting the analysis. The other parameters referred to the test were: the amplitude of 10  $\mu\text{m}$ , preload force of 0,05 N and frequency of 1 Hz. The starting point of the test was  $-50^{\circ}\text{C}$ , then an isothermal at this temperature for 5 minutes was settled and finally a temperature ramp was decided: speed of  $3^{\circ}\text{C}/\text{min}$  and final point around  $180^{\circ}\text{C}$  (stopped before for some formulations because it was too high).

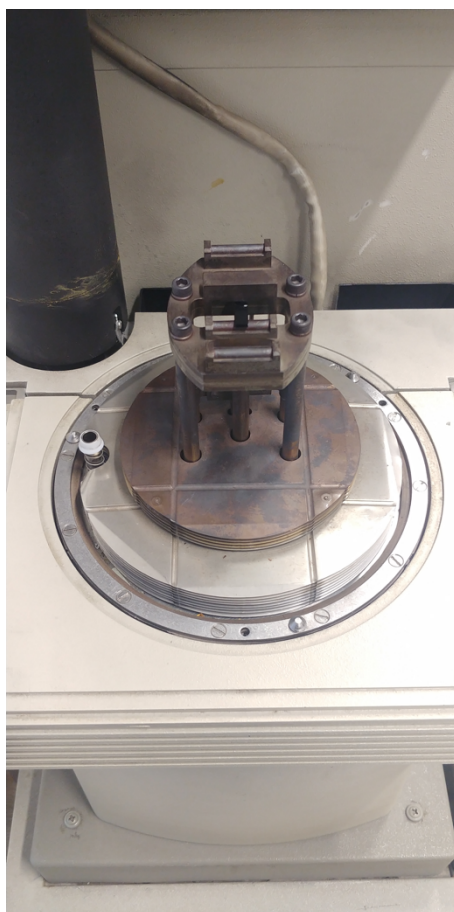


**Figure 5.1:** 3-points bending configuration of DMA machine

The graphs represented in figure 5.2 show the behaviour of storage modulus (a) (reported in logarithmic scale) and  $\tan(\delta)$  (b) plots of CDA\_1 formulations and of the Reference formulation.

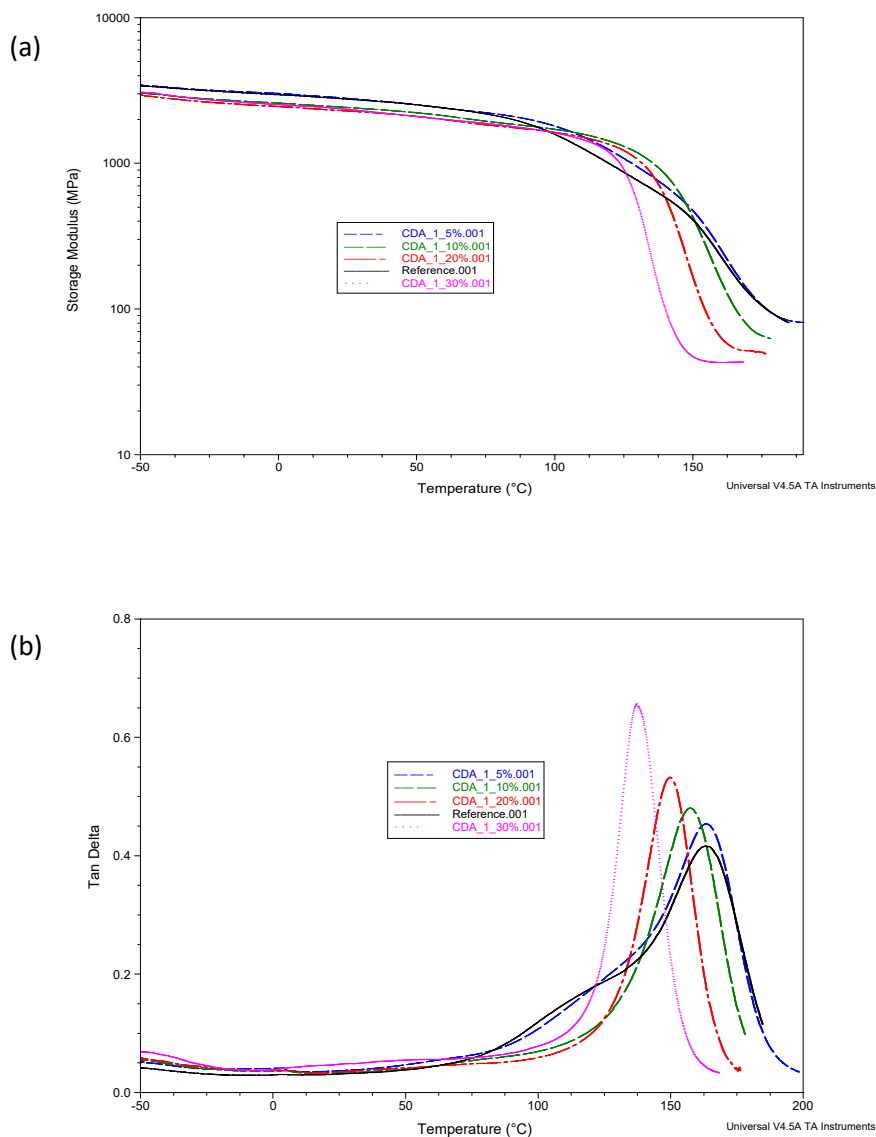


**Figure 5.2:** CDA\_1 group and Reference formulations storage modulus (a) and tan ( $\delta$ ) (b) curves.

The addition of trimethylolpropane changes the cross-linked network of the thermoset and this can be observed in the case of the CDA\_1\_20%, CDA\_1\_10% and CDA\_1\_30%: the regulation of the network changes the storage modulus and the glass transition temperature (lowered) which is calculated considering the maximum of the tan ( $\delta$ ) curve. The effects of the CTA on the network are related to the behaviour of the plots obtained: the glass transition in the storage modulus curve is more sharp in the materials containing 10%, 20% and 30% of the first CTA and the maximum of the tan ( $\delta$ ) curve is more narrow and defined. These changes explain the well-regulated network formation thanks to the presence of the CTA, which it will lead to more homogenous properties of the final material. The CDA\_1\_5% shows an inferior CTA effect on the thermoset network: in fact the CDA\_1\_5% is more similar to the Reference (almost same Tg and similar modulus transition). The important things to report is that the trimethylolpropane strongly change the network of the thermoset (sharp glass transition) avoiding low values of

the  $T_g$ , which remains high and it represents one advantage in employing epoxy based thermoset. Similar consideration will be made for the other groups of formulations.

The graphs in figure 5.3 are the plots obtained from the DMA tests on CDA\_2 formulations: as before they are compared with the Reference. In this case the tests were not performed until reaching 180 °C because the  $T_g$  of these material are lower than the Reference.

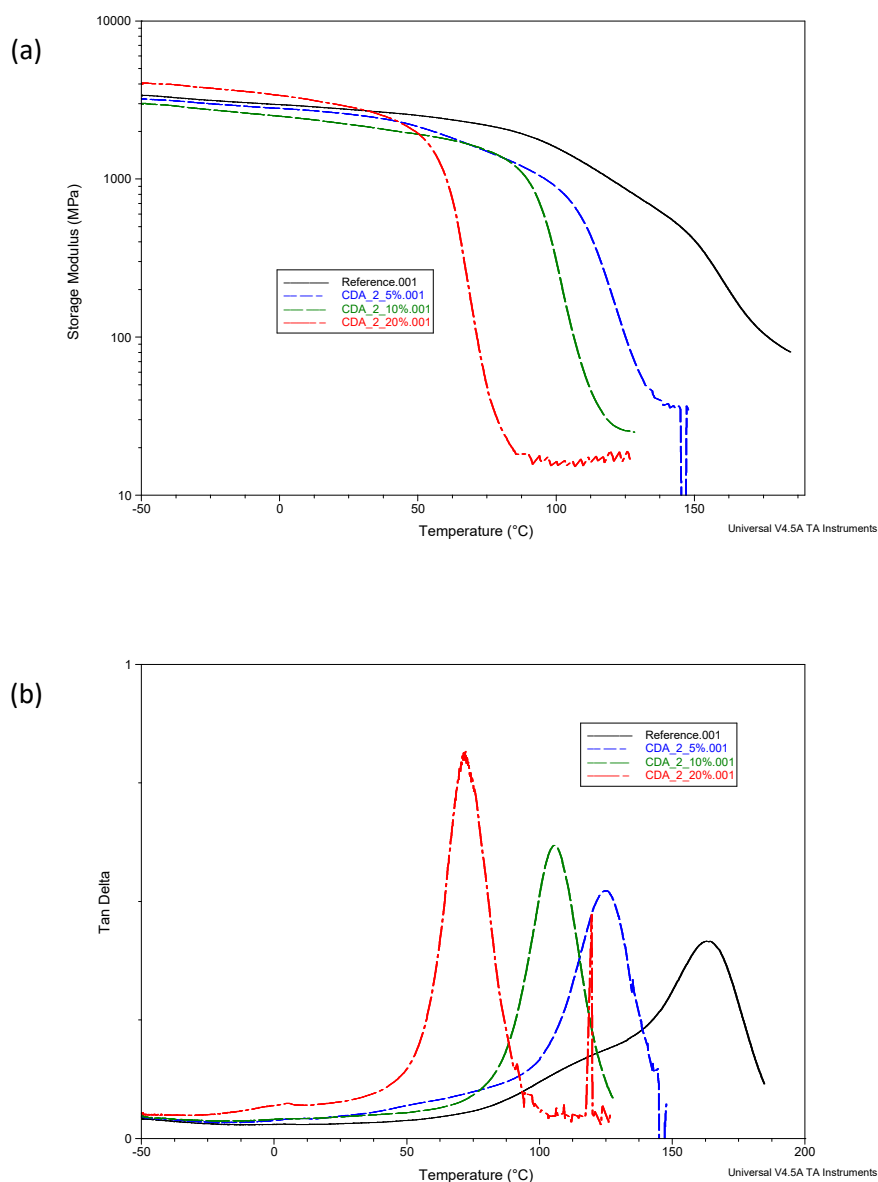


**Figure 5.3:** CDA\_2 group and Reference formulations storage modulus (a) and tan ( $\delta$ ) (b) plots.

In this case the polypropylene glycol as CTA strongly changes the network of thermoset: lowering the  $T_g$  at values below the 120 °C (the Reference has  $T_g$  around 163 °C). The regulation of the network is more evident when observing the CDA\_2\_10% and CDA\_2\_20%,

which shows a strange high modulus at temperature lower than the glass transition one. The CDA\_2\_5% shows a minor regulating effect rather than the others.

The graphs contained in figure 5.4 are referred to the CDA\_3 formulations groups: the material obtained after the photocuring results more soft and fragile, especially the CDA\_3\_20% which makes the photocuring in silicone mould highly difficult because it was very hard to remove (high adhesion to silicone) without breaking the samples. Same as before they are compared with the Reference.

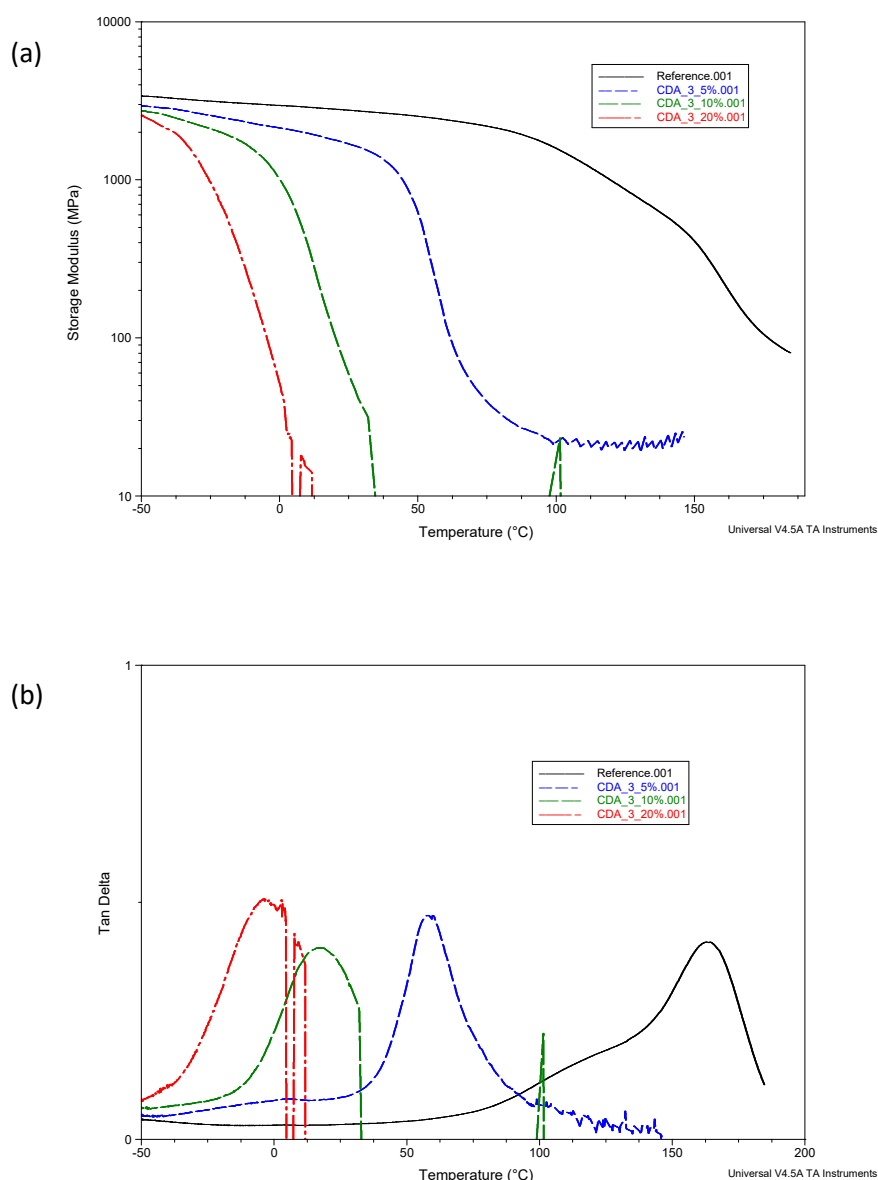


**Figure 5.4:** CDA\_3 group and Reference formulations storage modulus (a) and tan ( $\delta$ ) (b) plots.

The polyTHF dramatically changes the properties of the thermoset, leading to a different material: soft, fragile and with low glass transition temperature. The regulation of network appears also in this case: the sharp transition of the modulus is present although the peak of



$\tan(\delta)$  plot is not so narrow as in the other cases. The plots are not well defined because of the characteristics of the photopolymers which are easily breakable even during the analysis.

Finally in figure 5.6 and figure 5.7 respectively the storage modulus plots (reported in logarithmic scale) and the  $\tan(\delta)$  curves of all formulations tested is represented.

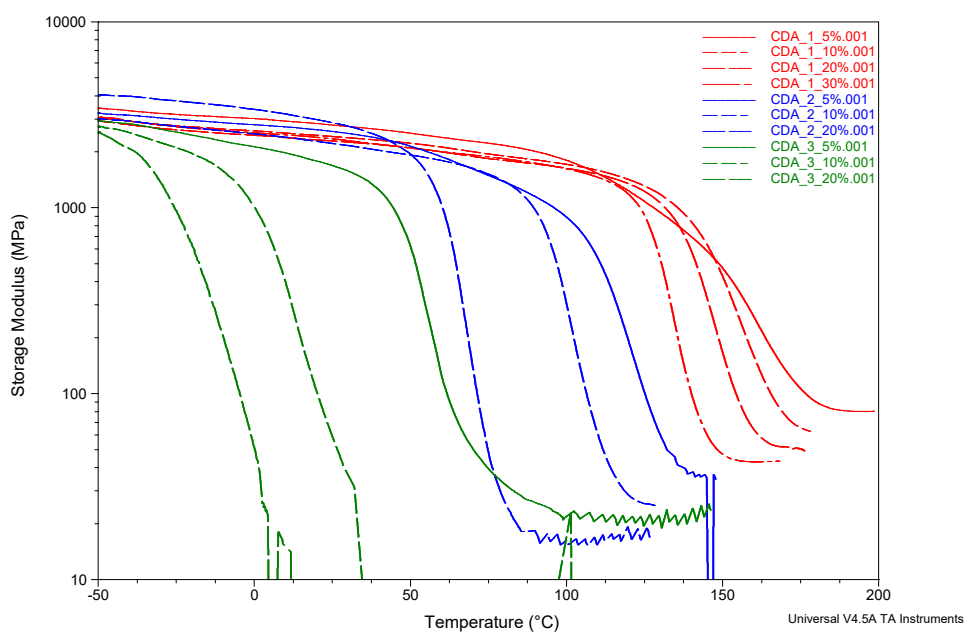


**Figure 5.6:** All CDA formulations storage modulus curves.

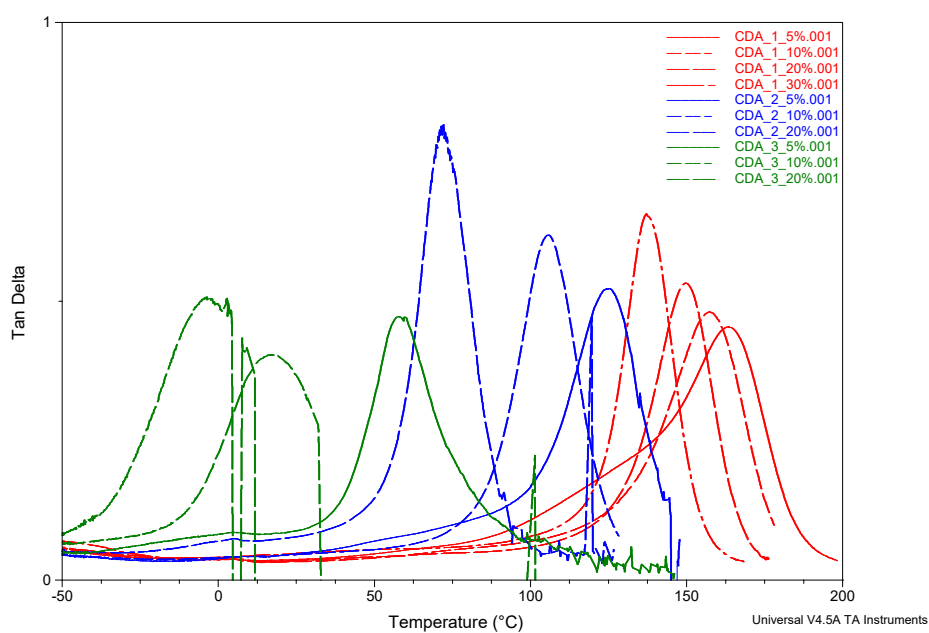


**Figure 5.7:** All CDA formulations  $\tan(\delta)$  curves.



In table 5.1 the results from the DMTA test are summarized for every formulations: the data reported are the storage modulus at 25 °C, the Tg taken as maximum of the tan ( $\delta$ ) plot and also the storage modulus at the end of the curve, which can be related to the crosslinking density [3, 4, 7, 8, 9, 19, 20, 23, 26, 33, 34].

**Table 5.1:** DMTA values of storage modulus ( $G'_{25^{\circ}\text{C}}$ ) at 25 °C, glass transition temperature (Tg) and storage modulus at the end of the curve (plateau zone) ( $G'_{\text{end}}$ ).

Name of formulation	$G'_{25^{\circ}\text{C}}$ [MPa]	Tg [°C]	$G'_{\text{end}}$ [MPa]
CDA_1_5%	2785	163	80,7
CDA_1_10%	2414	157	62,7
CDA_1_20%	2287	149	49,6
CDA_1_30%	2346	137	42,9
CDA_2_5%	2572	120	34,6
CDA_2_10%	2214	105	25,2
CDA_2_20%	2862	72	16,9
CDA_3_5%	1683	58	23,6
CDA_3_10%	58	17	0
CDA_3_20%	0,12	-4	0
Reference	2757	163	81,6

From this first test a preliminary selection can be made considering that the photopolymer have to show sharp glass transition and narrow peak of tan ( $\delta$ ). In addition the maximum of tan ( $\delta$ ), that represents the glass transition temperature, needs to be higher than 120 °C, in order to maintain the thermal and dimensional stability peculiar of the epoxy thermoset. The formulations that result more promising, among all considered, are the CDA\_1\_10%, CDA\_1\_20% and CDA\_1\_30% because they shows good regulation capability of the network and high Tg. The CDA\_2 groups would be considered but the Tg associated to them result are lower or equal 120 °C. The formulations containing the polyTHF are characterized by low mechanical properties, unsuitable for any structural applications. Unfortunately the formulations with Boltorn H20 are resulted impossible to be prepared because of solubility problem: the hyperbranched polyols are reported as very efficient CTA for cationic photopolymerization [9, 33, 34].

To sum up, for the next tests the formulations considered will be the Reference, CDA\_1\_10%, CDA\_1\_20% and the CDA\_1\_30%, which are resulted the best from this first selection and in this way it could be possible to study how the variation of the trimethylolpropane concentration affects the polymer properties. The CDA\_1\_5% shows a behaviour very similar to the Reference so it will not be analysed in the next discussions.

The DMA in general shows that the presence of CTA during the photocuring of the resin reduces the storage modulus and the Tg because of the reduction of crosslinking density in the network: leading to a flexibilization of the overall polymer.

### 5.3.2 Tensile test

The tensile test was performed in order to determine the stress-strain graph which gives the main idea of the overall mechanical properties of the material: young modulus, maximum tensile strength and elongation at break.

The tested formulations were the Reference, the CDA\_1\_10%, the CDA\_1\_20% and the CDA\_1\_30%. The samples thickness of the moulded samples is reduced to 1 mm with polishing operations: the shape is the typical dogbone form used for obtain the proper fracture in the reduced section (in this case 12 mm). The samples were photocured in the silicone mould at 80 °C, which will be considered as the suitable printing temperature (see section 5.3.4). The test were conducted at 5 mm min<sup>-1</sup> speed with 1 kN load cell. For each formulations 6 samples has been tested.

The figure 5.8 shows the stress-strain curves of all resin considered, compared to each other. The curve selected for each formulations is considered the one closer to average of all samples tested.

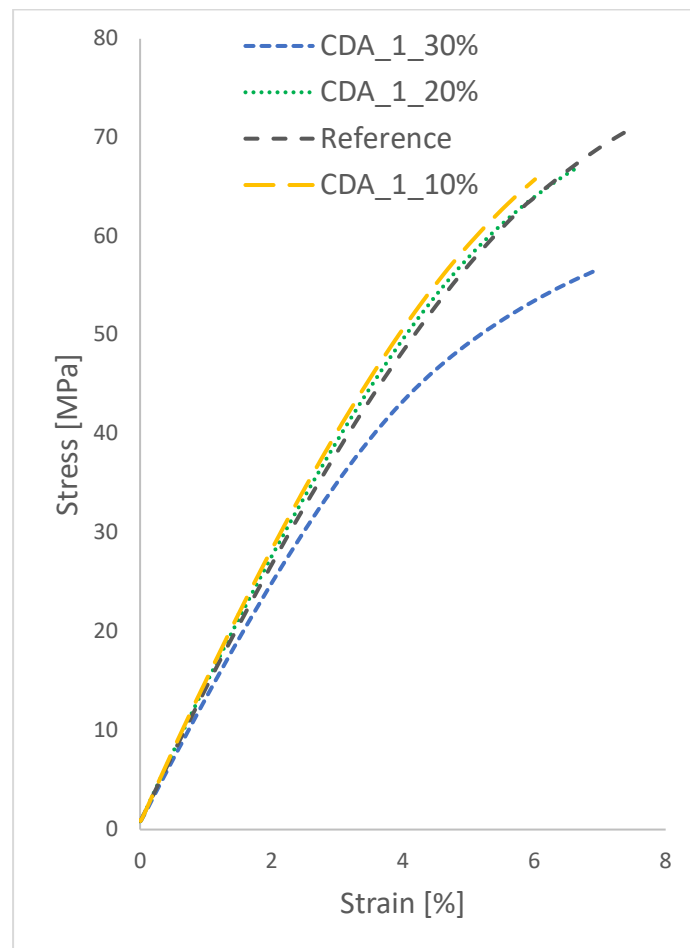


**Figure 5.8:** Stress-strain plots of selected resins, compared to each other.

The table 5.2 recaps all the important mechanical characteristics extracted from the analysis of the curves, the standard deviation for each values is reported. The young modulus has been calculated considering the slope of the curve in the section between 0% and 0,2% strain. The values are the average calculated from the each samples population.

**Table 5.2:** Average values from tensile test of the selected resin formulations.

Name of formulation	Reference	CDA_1_10%	CDA_1_20%	CDA_1_30%
Elastic Modulus [MPa]	1385( $\pm$ 99)	1392( $\pm$ 35)	1398( $\pm$ 24)	1234( $\pm$ 46)
Tensile strength [MPa]	70,66( $\pm$ 10,59)	63,79( $\pm$ 5,41)	67,28( $\pm$ 3,20)	58,56( $\pm$ 4,56)
Elongation at break [%]	6,83( $\pm$ 1,32)	5,95( $\pm$ 0,99)	6,69( $\pm$ 2,43)	7,04( $\pm$ 2,66)

The Reference is essentially a brittle material, typical mechanical behaviour of thermosets: although the presence of the CTA in the formulations, the CDA\_1\_20% and the CDA\_1\_10% do not show big changes respect to the Reference. They are characterized by slightly lower elongation at break and tensile strength. The CDA\_1\_30% is characterized by inferior mechanical properties when compared with the other three material (see figure 5.8).

### 5.3.3 RSA

The stress relaxation analysis were performed in water at 37 °C: this is a standard method for testing thermoset and thermoplastic in the TU Wien laboratories. The 3-point bending configuration was selected and the samples, before were tested, were soaked in water at 37°C for 30 minutes. The figure 5.9 shows how the test has been prepared: the soaked sample is placed on the two support pins and the third pin is lowered a little bit in order to avoid movement when the water is poured in. Then a metallic cylinder surrounds the system and when it is locked with screws the water can be poured inside and the machine is ready to start: see figure 5.9.

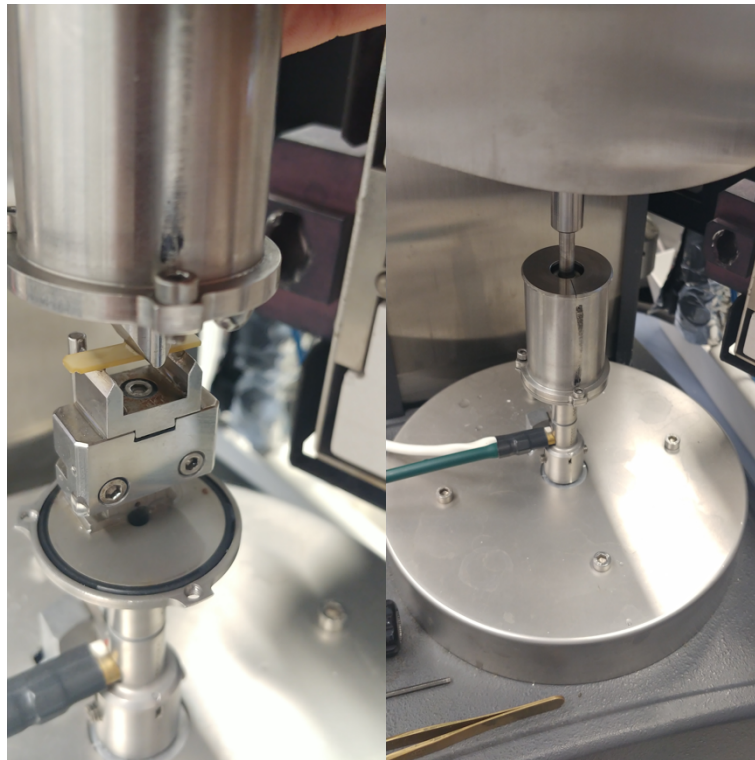


**Figure 5.9:** RSA-G2 machine in 3-point bending configuration on the left and on the right the system ready closed with cylinder and water inside .

The test duration is 2 hours at 37 °C in water, the strain applied to the sample was 2%: the length of the sample should be between 18 and 25 mm, the thickness had to be 1 mm or lower, the shape is the same as the DMA sample.

The photopolymer relaxation curves are compared in the graph in figure 5.10: the time is reported in seconds and the relaxation is expressed in normalized stress which is the ratio between the stress applied to the polymer for maintaining the strain and the initial stress recorded at zero seconds.

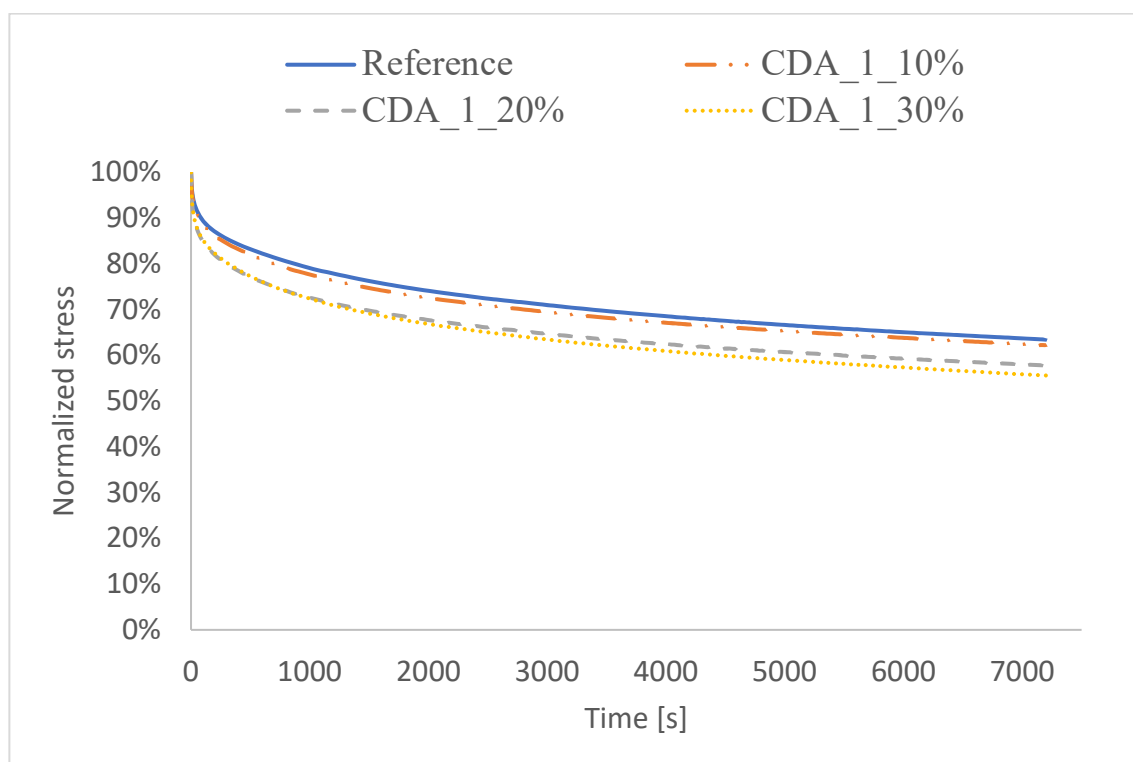


**Figure 5.10:** Stress relaxation curves of the selected formulations, compared to each other.

The table 5.3 shows the exact final relaxation at the end of the test for each samples.

**Table 5.3:** RSA results of the Reference, the selected formulations.

Name of fomulation	Reference	CDA_1_10%	CDA_1_20%	CDA_1_30%
Time [s]	7200	7200	7200	7200
Max relaxation [%]	63,43	62,21	57,79	55,61

The presence of the trimethylolpropane affects the stress relaxation behaviour of the pure photopolymers (the Reference): the CDA\_1\_10% results closer to the Reference, on the other side the CDA\_1\_20% shows higher relaxation than the pure photopolymer and even higher in the case of stress relaxation plot of CDA\_1\_30%.

#### 5.3.4 Photo-DSC

The photo-DSC analysis were performed on liquid resin (around 15 mg) contained in aluminium lid: the measurements permitted to detect the reactivity and the rate of photocured formulation in real time. The tests were conducted at three different temperatures (25 °C, 50°C and 80°C) in order to understand the resins behaviour at higher temperature, which ideally represented the processing condition in the hot lithography machine. The temperature was maintained constant during the test, in fact an isothermal curve for four minutes was settled in order to have constant temperature in the measuring chamber. After this the UV lamp was turned on and the cationic photocuring of the resin started and the system evolution were registered for 600 seconds. After this, another photocuring of 600 seconds were analysed to detect any additional changing in the photopolymer. The latter operation were useful for data analysis: in fact the results had been deducted considering the subtracted curves which is calculated by the confrontation of the two photocuring curves.

The tables 5.4, 5.5 and 5.6 report the results obtained from the analysis of the subtracted curves: the important parameters are the area of the exothermal peak (A), the time at which the curves has the maximum ( $t_{max}$ ), the height of the peak (h) and the time needed for achieve the 95% of the photo reaction ( $t_{95\%}$ ). The comparison are made between formulations tested at the same temperature.

**Table 5.4:** Photo-DSC data at 25 °C of selected formulations; area of the peak (A), the time corresponding to the max ( $t_{max}$ ), the height of the peak (h) and the time needed for complete the 95% of reaction ( $t_{95}$ ).

Name of formulation	Reference	CDA_1_10%	CDA_1_20%	CDA_1_30%
Temp. [°C]	25	25	25	25
A [J/g]	107,1	168,8	200	160,4
$t_{max}$ [s]	27,2	63,3	53,9	36,3
h [mW/mg]	3,282	3,893	3,517	3,207
$t_{95}$ [s]	124,5	99,4	176	218,7

**Table 5.5:** Photo-DSC data at 50 °C of selected formulations; area of the peak (A), the time corresponding to the max ( $t_{max}$ ), the height of the peak (h) and the time needed for complete the 95% of reaction ( $t_{95}$ ).

Name of formulation	Reference	CDA_1_10%	CDA_1_20%	CDA_1_30%
Temp. [°C]	50	50	50	50
Area [J/g]	255,7	269,1	271,6	276,6
$t_{max}$ [s]	16,8	21,2	23	25,4
h [mW/mg]	4,781	11,76	13,5	12,36
$t_{95}$ [s]	250	112,6	72	91,3

**Table 5.6:** Photo-DSC data at 80 °C of selected formulations; area of the peak (A), the time corresponding to the max ( $t_{max}$ ), the height of the peak (h) and the time needed for complete the 95% of reaction ( $t_{95}$ ).

Name of formulation	Reference	CDA_1_10%	CDA_1_20%	CDA_1_30%
Temp. [°C]	80	80	80	80
Area [J/g]	284,3	348,2	354,6	334,9
$t_{max}$ [s]	20,5	15,1	13,7	14,1

h [mW/mg]	10,07	11,29	16,8	14,52
t <sub>95</sub> [s]	81,4	107,9	76,1	78,7

The graphs contained in figure 5.11, in figure 5.12 and in figure 5.13 show the comparison between the four formulations tested at 25 °C, 50 °C and 80 °C respectively.

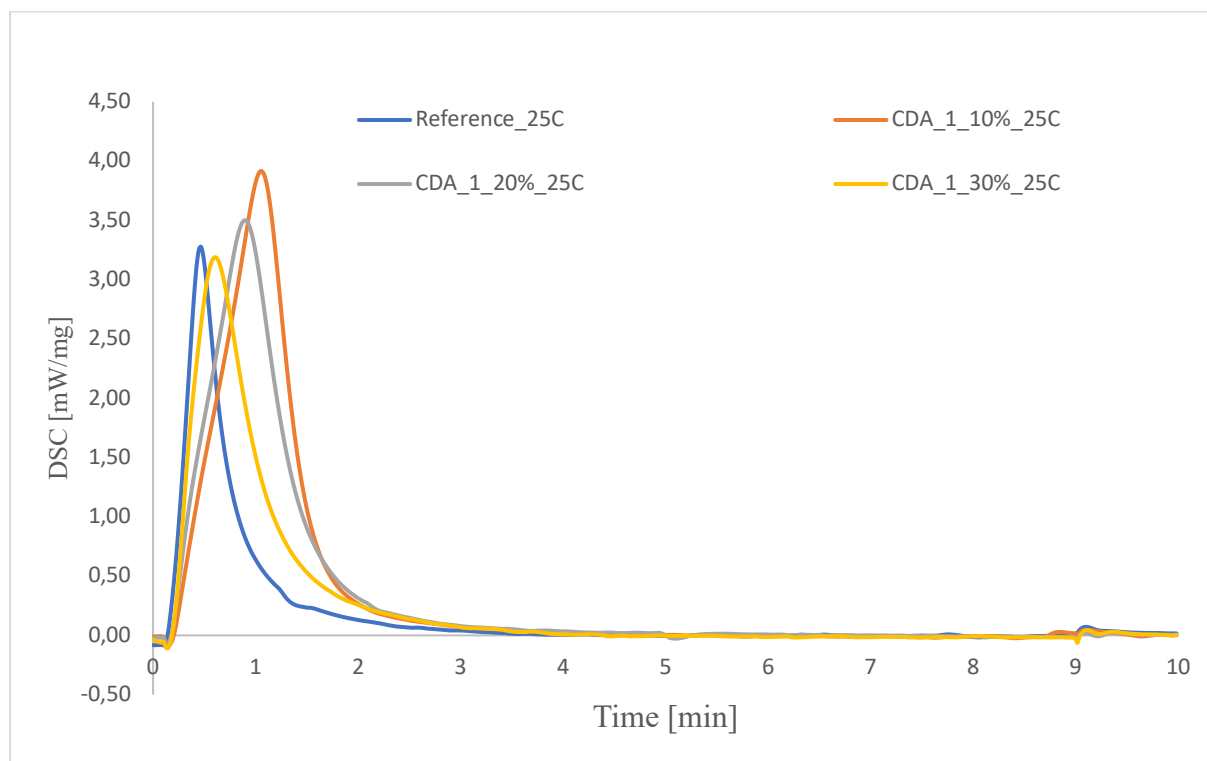


**Figure 5.11:** Photo-DSC (subtractive curve) plots at 25 °C of selected formulations.

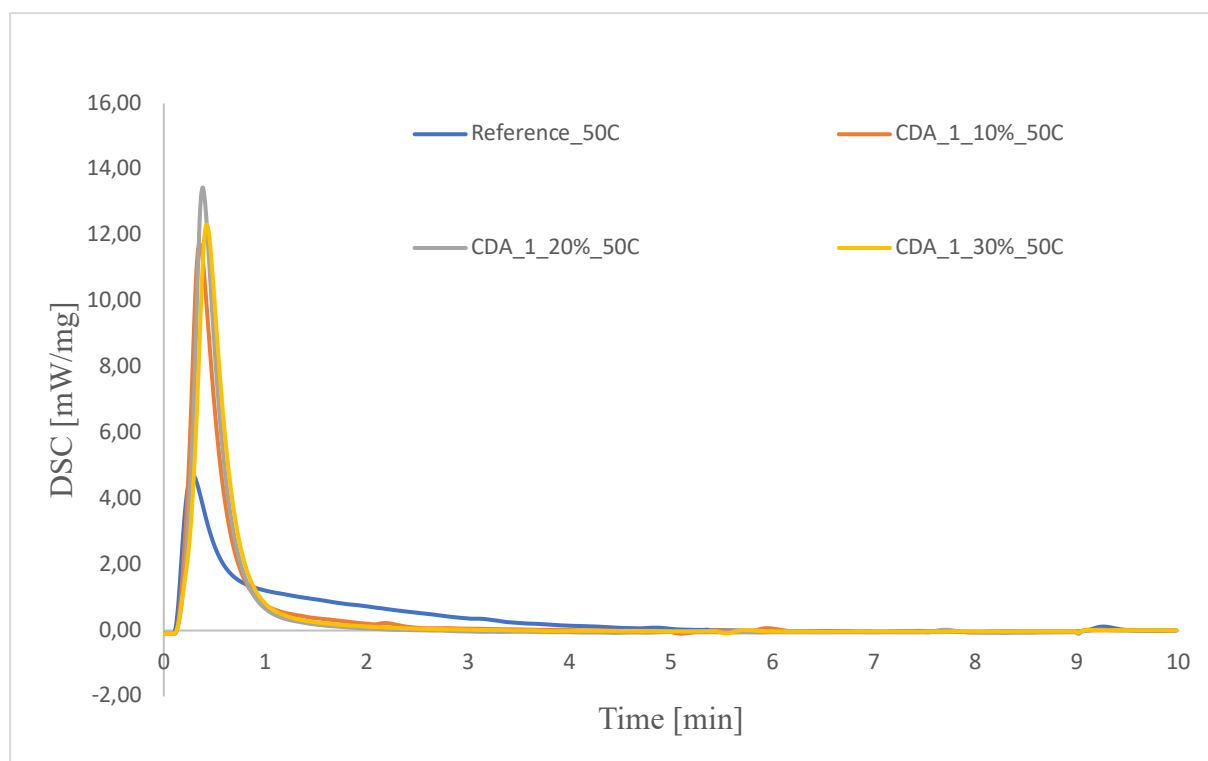


**Figure 5.12:** Photo-DSC (subtractive curve) plots at 50 °C of selected formulations.

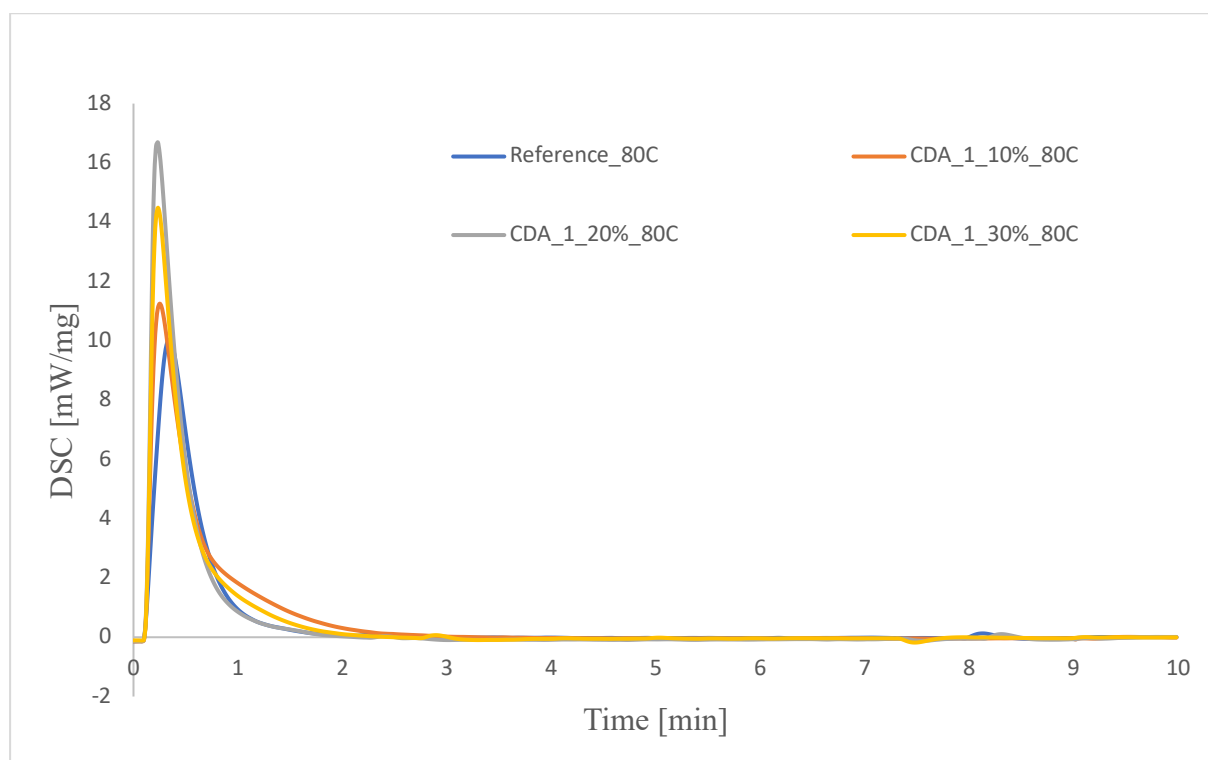


**Figure 5.13:** Photo-DSC (subtractive curve) plots at 80 °C of selected formulations.

At 25 °C the formulations that contains the trimethylolpropane show lower photocuring rate than the Reference, as easily visible from the figure 5.11 and from the value  $t_{95}$  in table 5.4. On the contrary the reactivity in presence of CTA is higher as can be noticed observing the figure



5.11 and the table 5.4, higher is the concentration of the CTA lower is the overall reactivity. At 50 °C the rate of polymerization is similar for all formulations, but the reactivity (higher values of A and h in table 5.5) increases in the presence of trimethylolpropane as shown in the figure 5.12. At 80 °C the CDA\_1\_20% shows superior reactivity and higher polymerization rate (lower  $t_{\max}$  and  $t_{95}$ ) respect to Reference and also to the CDA\_1\_10% and CDA\_1\_30%, this can be observed in figure 5.13. Observing the different values inside the tables, the difference between them is not so big but if it is considered that the additive manufacturing process allows the creation of a layer in very few seconds, even small changes in reactivity and polymerization rate become important for the material.

The cationic photopolymerization is strongly enhanced in efficiency at higher temperature: the presence of the trimethylolpropane the cationic photocuring of the BADGE resin results better in term of time and reactivity, especially the CDA\_1\_20% at 80 °C above all formulations with trimethylolpropane. Since the hot lithography machine can process resin at temperature above room temperature and considering the results from photo-DSC, a possible temperature for processing the resin could be 80 °C.

### 5.3.5 Photo-rheology

As already described, a powerful instrument for studying directly the evolution of photopolymers, from liquid to solid state, is represented by the photo-rheometer coupled with IR signal scanning apparatus. The photo-rheometer is represented in figure 5.14: the rheometer plate-plate is connected directly with the IR source and detector on the bottom and the UV light source is on the left.

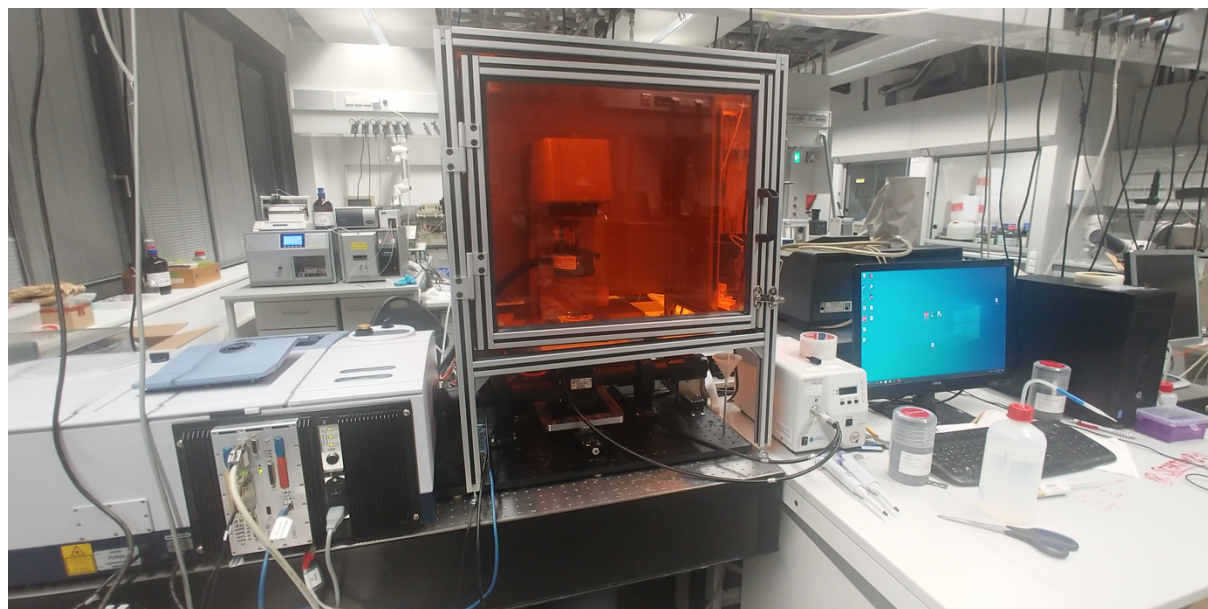


**Figure 5.14:** Photo-rheometer setup in the TU Wien laboratory.

The test was performed on the Reference, the CDA\_1\_10% and the CDA\_1\_20%, the CDA\_1\_30% was considered not interested for this analysis. The temperature was settled at 80 °C, ideally the same that would be chosen in the future 3D printing process; the sample thickness to analyse was fixed at 200  $\mu\text{m}$  and the UV lamp power was calibrated at 3W. The first step was the measurement of the initial rheology parameters (storage modulus  $G'$  and loss



modulus  $G''$ , normal force  $F_n$ ) and the IR spectrum of the liquid resin, which contained the relevant epoxy peak for studying the conversion during photopolymerization. The UV lamp was turned on after 65 seconds this preliminary measured was made: from that moment the photocuring of the polymer started and all the mechanical properties and the conversion spectra were recorded by the photo-rheometer apparatus until the end of test. The oscillation settings for starting the analysis consider frequency of 1 Hz and amplitude around 1%, these are reported also in [10].

The table 5.7 shows the important values related to this analysis: the time  $t_g$  (the value includes 65 seconds before the lamp is turned on) to reach gelation, which is defined as the crossover point between  $G'$  and  $G''$  curves, the maximum of the storage modulus  $G'_{max}$ , the minimum of normal force  $F_n$ , the final conversion  $C_{final}$  of epoxy groups and the conversion at gelation point  $C_g$ . All this data have been selected following the previous studies reported in this article [10].

**Table 5.7:** Results from the photo-rheology of the selected formulations.

Formulation	$t_g$ [s]	$C_g$ [%]	$C_{final}$ [%]	$G'_{max}$ [kPa]	$F_n$ [N]
Reference	89,6	27	88,86	139,91	-5,03
CDA_1_10%	81,8	34	87,85	150,14	-2,52
CDA_1_20%	82,4	37	91,82	213,53	-3,44

The figures 5.15, 5.16 and 5.17 contains respectively the evolution of the  $G'$  and  $G''$  of the Reference, the CDA\_1\_10% and the CDA\_1\_20%, focusing also on the crossover points. The graphs start at 65 seconds when the UV lamp is turned on.

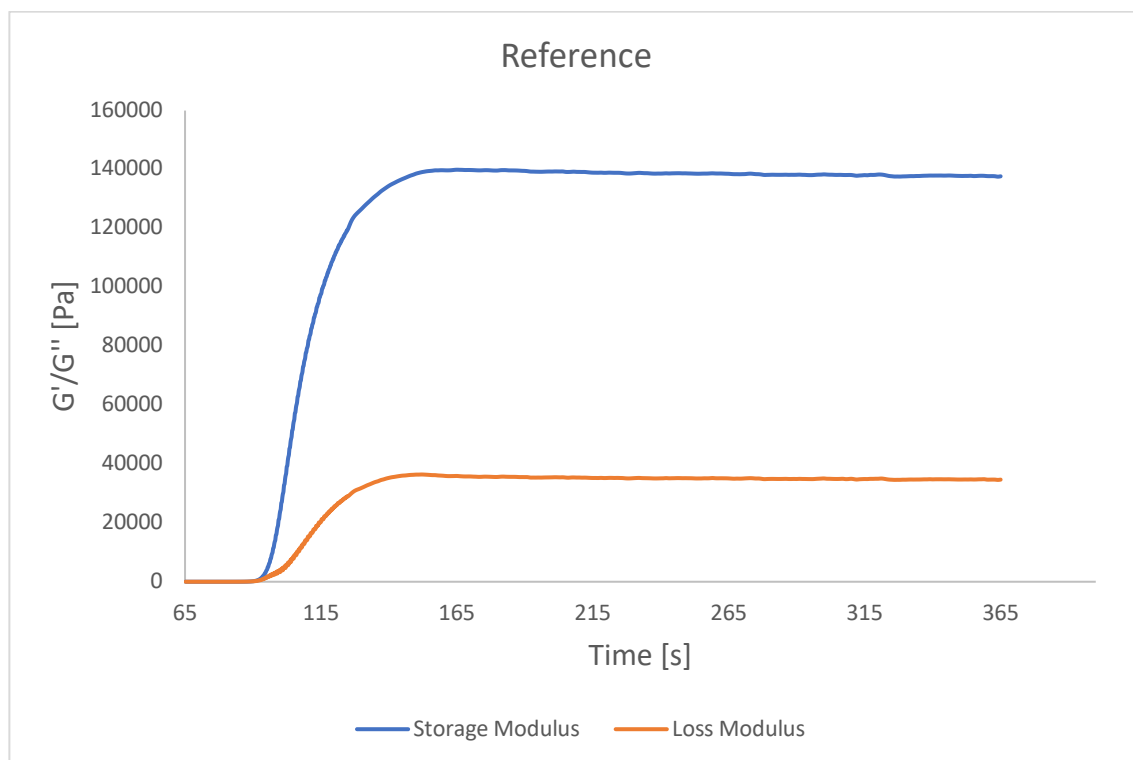


**Figure 5.15:** Photo-rheology study of the Reference formulation.

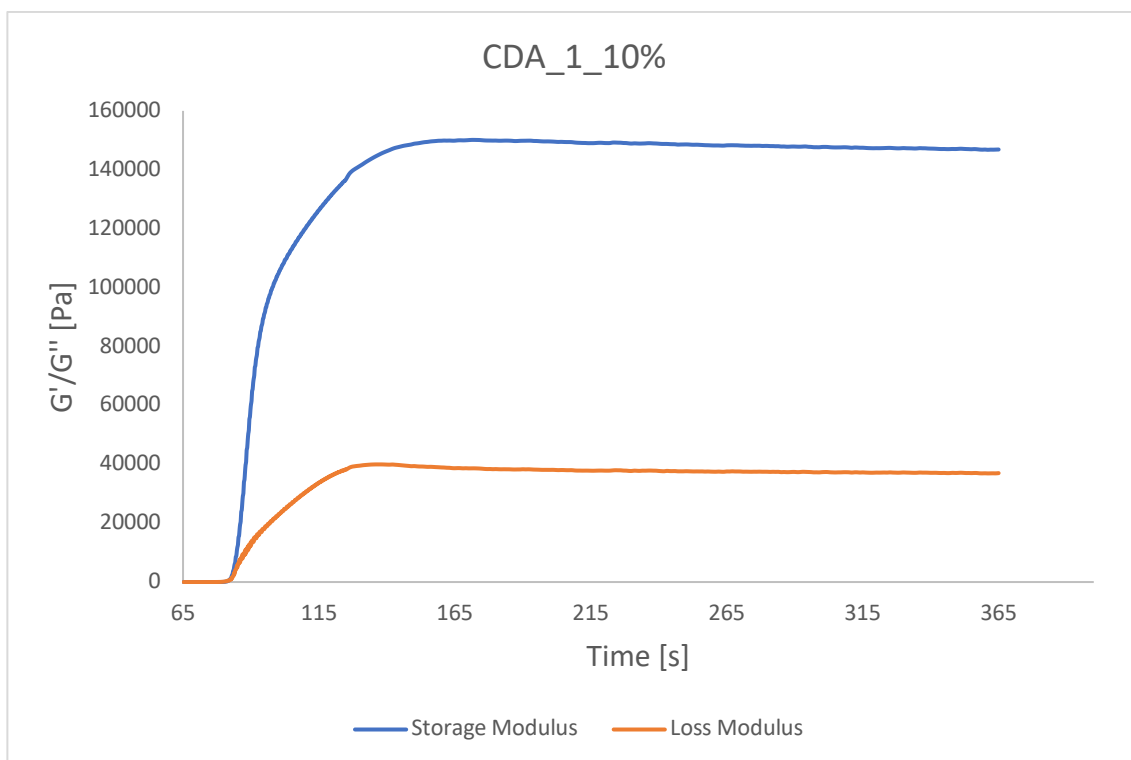


**Figure 5.16:** Photo-rheology study of the CDA\_1\_10% formulation.

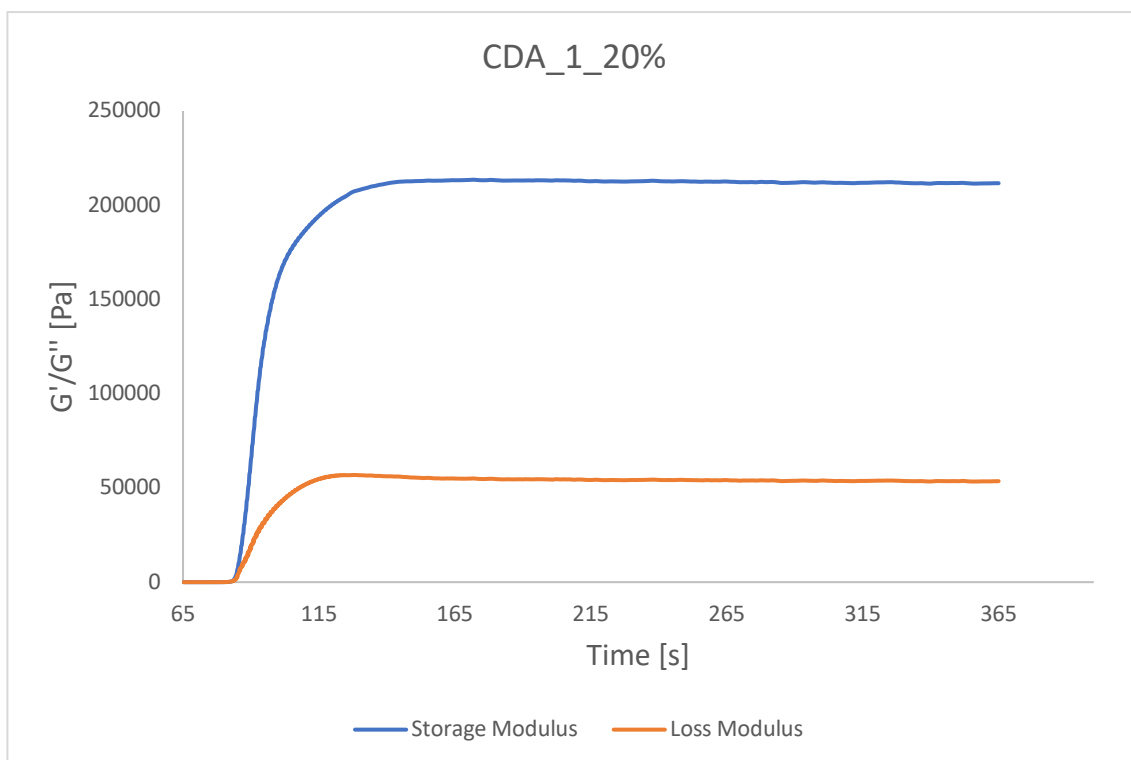


**Figure 5.17:** Photo-rheology study of the CDA\_1\_20% formulation.

The figure 5.18 represents the epoxy ring conversion comparison between the tested formulations. The conversion is considered when the UV lamp is turned on.

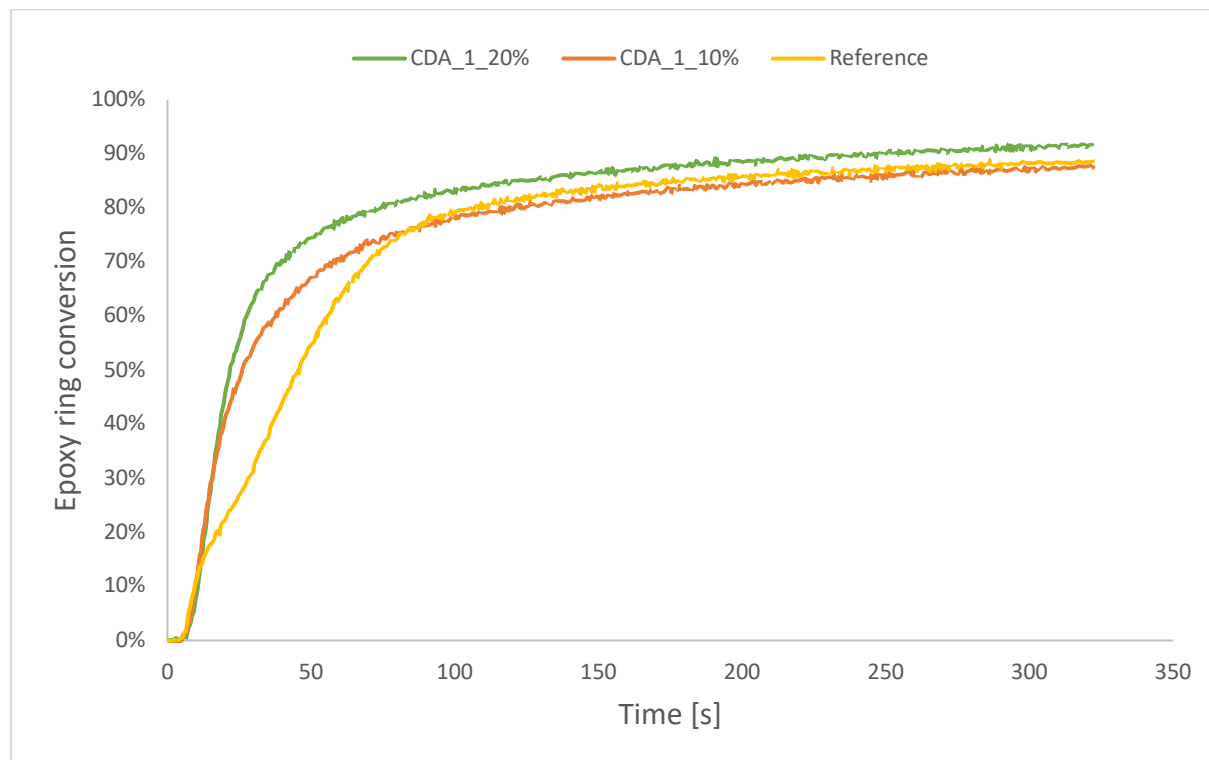


**Figure 5.18:** The epoxy ring conversion plots of the selected formulations, compared to each other.

These parameters are essential for understanding the photocuring of the resin: the conversion of the epoxy groups ( $C_g$  and  $C_{final}$ ) during analysis recorded thanks to the IR detector apparatus gives the idea of chemical evolution of the systems (the ring-opening reaction makes disappear the IR signal of the epoxy ring). The conversion influences the shrinkage directly: from the gelation point the system is becoming solid and the normal force applied, which could be related to the shrinkage stress, is recorded by the instruments. The minimum value of  $F_n$  is just an indication of the real shrinkage occurring during the photopolymerization, because other physical (like adhesion) and thermal changes in the polymer influences the overall shrinkage[10]; after reaching a minimum the force start to increase because of the complete transformation from liquid to solid. The time needed to reach gelation explains the reactivity of the formulations, lower values mean higher reactivity of the resin. The mechanical behaviour of the photopolymer is related to the value of  $G'_{max}$ , which reaches a plateau at high conversion of resin. The Reference resin is slower than the CDA\_1\_10% and the CDA\_1\_20%: these two has very similar  $t_g$ . The final conversion and the conversion at gel point increase for the CDA\_1\_20%, and for this reason the maximum  $G'$  is the highest of the all formulations. The shrinkage stress of CDA\_1\_20% expressed by the value of  $F_n$  is lower than the Reference, but higher than the CDA\_1\_10%. In general the CTA presence enhances the reactivity and the speed of the reaction, leading to lower shrinkage due to the network regulation, which affects also the mechanical performance in terms of higher storage modulus.

Final considerations that can be made observing this results are related to the additive manufacturing application: lower values of  $t_g$  of the modified formulations are crucial for 3D

printing at a proper speed, high conversion at gel point and high  $G'$  gives ideally a good green strength to the resin that will form the layer. In the end lower shrinkage means better resolution and dimensional control over the layer formation: in fact ring-opening reaction due to cationic photopolymerization of epoxy resin leads to higher dimensional stability of products than the radical photocured materials.

#### ***5.4 Preliminary conclusions***

At the end of this first part of the project the selected formulations for starting a 3D printing process study is the CDA\_1\_20%: it shows high reactivity both considering the photo-DSC and the photo-rheology results. This higher efficiency is given by the presence of trimethylolpropane which works as chain transfer agent in the cationic photopolymerization: this enables higher epoxy conversion and polymerization rate. The main positive effect is the regulation of the crosslinked network of the final material, underlined by the narrowing of the  $\tan(\delta)$  curve and the correlated sharp glass transition of the storage modulus from DMA measurements. Higher is the concentration of the CTA in the Reference higher is the regulation of the network, related to the storage modulus and  $\tan(\delta)$  variations. The tensile properties do not change significantly even though the trimethylolpropane presence in the CDA\_1\_20%, on the other way the regulation of the crosslinked network affects the stress relaxation behaviour where the CDA\_1\_20% shows higher relaxation respect to the Reference (from 63,44% to 57,79%), because of the lower crosslinking density. The  $T_g$  of the modified formulation anyway remains quite closer to pure one, which is an important feature of the epoxy resin. The analysis made at 80 °C underlines better efficiency of the overall cationic photocuring process, as consequence of this the printability studies on the CDA\_1\_20% were conducted at 80 °C as the process temperature.

## **6. Second part: 3D printing of cationic photopolymer using hot lithography approach**

### ***6.1 Central focus of the second part of the project***

In this second part the CDA\_1\_20% formulation will be printed using the hot lithography machine of TU Wien in order to prove the real printability of it and to study the influence of the additive manufacturing process on the material. The goal is to obtain the printed samples that will be tested and they will be directly compared to the one obtained by photocuring in the UV chamber. In the next sections the path followed for printing parts will be explained.

### ***6.2 Formulations preparation for printing***

The formulation containing the 20% molar of trimethylolpropane were prepared following the same procedure explained in the paragraph 4.3: a complete degassing was necessary in the vacuum chamber and then it was heated up to 80 °C before printing. In the first irradiation tests the CDA\_1\_20% was compared to the Reference for showing that the presence of the CTA in the formulations effectively raised the reactivity and the rate of polymerization; in the next printing jobs 0,5%wt of anthracene was dissolved in the formulations, in order to have better spatial resolution and to enhance the absorption at the wavelength emitted by the laser.

### ***6.3 3D printing of the resin***

The hot lithography machine, shown in figure 4.12, can process viscous and poorly reactive resins at room temperature: the possibility of working at higher temperature overcomes the limit of processing new material in normal stereolithography machine. The SLA machine could process resins that shows at maximum viscosity of 5 Pa s at 30 s<sup>-1</sup>, or in other cases 10 Pa s at 100 s<sup>-1</sup>[37]. The advantage of using hot lithography process is represented by higher maximum resin viscosity limit for the 3D printing at defined process temperature (maximum 100 °C for the vat), this limit is imposed at 20 Pa s for the machine [11, 12].

The Reference shows a viscosity of 10,4 Pa s at 100 s<sup>-1</sup> at room temperature, the viscosity of the CDA\_1\_20% is around 9.2 Pa s at 100 s<sup>-1</sup> at room temperature (measured by Anthon Paar MCR300 rheometer in plate-plate configuration): they would be difficult to process in normal SLA machine because of high viscosity, nevertheless low reactivity at 25 °C (see curves in section 5.3.4). At 80 °C the viscosities of the Reference and of the CDA\_1\_20% reach values of 0,072 Pa s and of 0,065 to Pa s (at 100 s<sup>-1</sup>): this values are ideal for correct processing of this type of resins in hot lithography machine. But the real reason for using this particular approach on this epoxy based formulations is that at higher temperature the efficiency of the cationic photocuring is strongly enhanced: the photopolymerization rate and the reactivity are higher and they become even better thanks to the presence of the CTA.

In the next paragraphs the study of process parameters in order to print the CDA\_1\_20% will be analysed: first simple laser irradiation tests were performed on the Reference and on the CDA\_1\_20%, after the process parameters setting for printing mechanical samples and objects was determined.

#### ***6.3.1 Irradiation tests***

The irradiation tests essentially was made for determining the formation of a single layer of photopolymer: the laser drew the profile and the filling of a circle, the speed of the laser were different in order to see which one could create a layer with enough strength for sustaining the whole 3D printing cycle. In these test the layer thickness was not important, the main parameters controlled in the machine software were laser speed, hatch style direction and distance.

First of all the Reference and the CDA\_1\_20% were compared for showing the higher processability of the second than the first: the filling of the disc was made in two direction (90° and then 0° respect to x-axis) with hatch distance of 0,02 mm in both cases, the speed of the laser was 200 mm/s and the temperature of the transparent vat was 80 °C. The figure 6.1 shows the results from this first test: the disc obtained from the laser irradiation of the Reference is softer and easily breakable respect to the one obtained from the photopolymerization of the CDA\_1\_20% at the same speed, which is still transparent but more strong and suitable for a printing job. In order to obtain a suitable layer from the Reference formulation, the speed of the laser has to be lowered at 50 mm/s: the result is shown in figure 6.2.

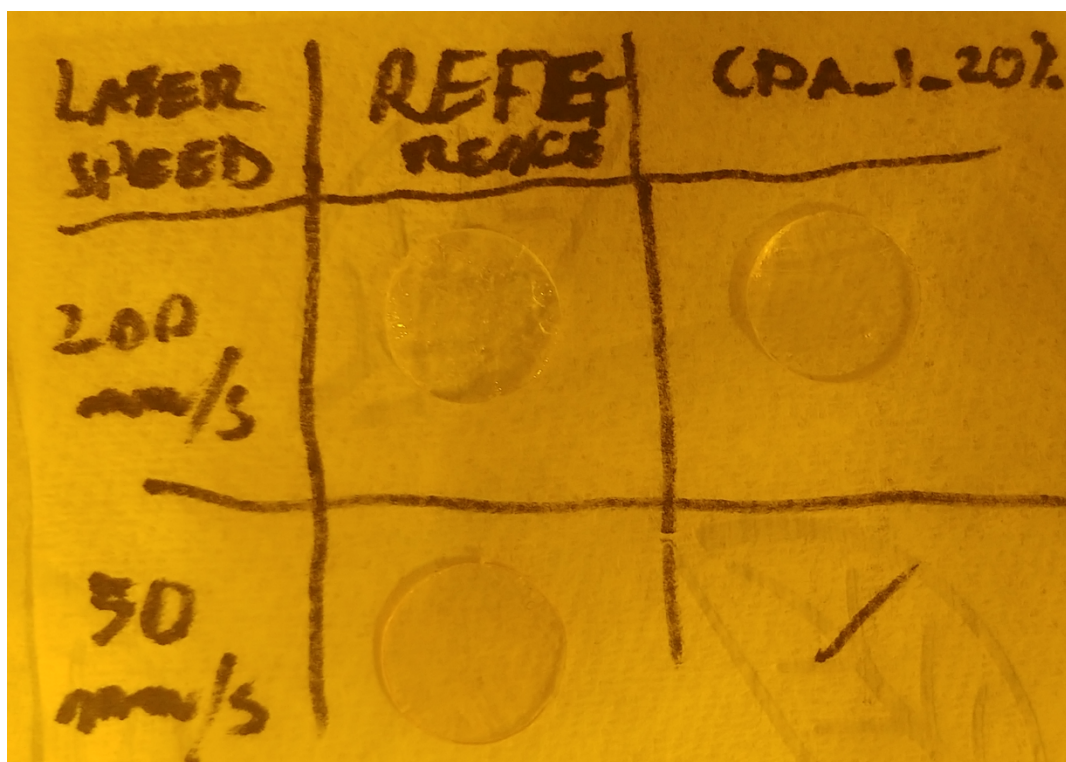


**Figure 6.1:** Discs obtained by irradiation of the CDA\_1\_20% and the Reference formulations compared, at the same laser speed of 200 mm/s the CDA\_1\_20% looks more solid than the Reference one obtain at same laser speed.

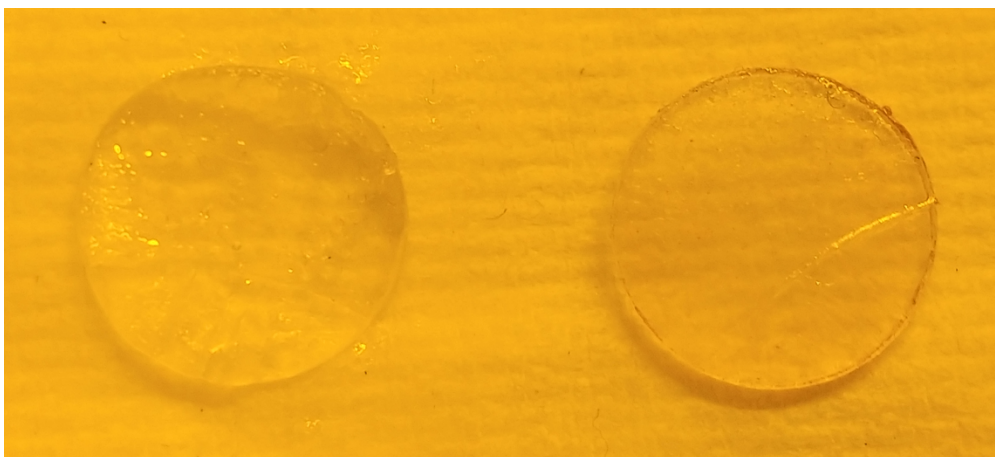


**Figure 6.2:** Two Reference resin discs, one obtained by laser irradiation at 200 mm/s on the left and on the right a disc obtained by laser irradiation at 50 mm/s .

The laser irradiation tests were then performed only on the CDA\_1\_20% that showed good printability of a single layer at 80°C with laser speed of 350 mm/s and 500 mm/s. At higher laser speeds the resin did not react enough after one exposure: the layer was similar to a gel-like material. These laser speeds were the starting point of the definition of process parameters. The figure 6.3 reports the results obtained from these laser irradiations.

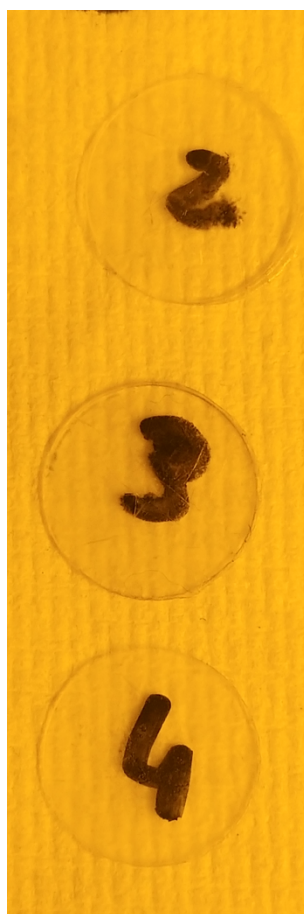


**Figure 6.3:** Discs of CDA\_1\_20% obtained by laser irradiation test at different speeds, 200 (number 2), 350 (number 3) and 500 (number 4) mm/s.

### *6.3.2 Definition of process parameters*

After laser irradiation tests, the next stage was the definition of process parameters: the process temperatures of the building platform and of the coating unit were settled at 80 °C. The speed in the z-axis of the building platform had to be regulated in relation of the distance from the transparent vat: when it got closer (few centimetres) to the vat, the speed of the platform was considerably reduced (10 mm/min) for avoiding excessive stresses on the liquid resin and on the vat, otherwise the speed could be higher for the rest of the process (500 mm/min). The force applied by the platform on the vat was controlled by a sensor and it had to be limited around 100 N: same as before for avoiding high pressure on the resin and on the vat. The laser emission started when the platform reached the correct distance necessary for starting the new layer formation, the limit of force applied and the speed defined controlled this process step. The movement of the vat under the coating unit was defined by a certain speed, settled by the user into the control software of the machine, who decided automatically the height of the building platform after the creation of one layer. The interaction of the vat with the doctor blade, that should work also as material container, could be more than one and also deactivated if necessary. Usually thanks to the low viscosity achieved at high temperatures, this recoating step is reduced in terms of time in the whole printing process, because the resin is characterized by a spontaneous recoating of the cured area [13, 37].

The thickness of the each layers and also their numbers are defined by the job selected in the software of the machine: the printing job can be created and modified in the software Autodesk Netfabb, in which the user can define the position and the dimension of the objects (previously designed in any CAD software like Solidwork or Autodesk Inventor). Then the file saved in this software must be converted in CLI type file in order to be correctly processed by the control software of the machine. As already said, the filling operated by the laser can be settled in the machine control software knowing the contour lines of the object from the CLI file: the laser filling for all printing jobs was realized in the two orientation (0° and 90°) with hatch distance of 0.02 mm in both directions.

The post-curing process for this epoxy-based resin was defined as a thermal treatment in oven for 4 hours at 250 °C: in this way the total conversion of epoxy could be achieved without degradation of the polymer.

### *6.3.3 Printing of parts*

In this paragraph details and results related to different 3D printing experiments are reported: first mechanical samples were printed for studying the properties of the printed material and then compared with the photopolymer tested previously. At last a small object was printed to show the real printability of the resin. Two main problems faced during the printing of the resin have to be underlined here.

The first was related to the use of the coating unit for preparing new liquid resin film in order to start next layer formation. The hot liquid resin formulation, after the vat moved backward from underneath of the blade, did not settle homogeneously on the vat but it tended to return back to the centre of the vat, that represented the usual printing position. Because of this behaviour (maybe linked to the liquid surface effects) the coating unit was impossible to involve in the process, because of this it was deactivated. During the printing job, when the building platform was at the maximum height before went down again for starting a new layer formation, the control software gave the possibility to pause the job: thanks to this it was possible to check if there was enough resin for printing new layer, otherwise manual resins addition or manual recoating was operated. The interruption operation of the printing job represented a



fundamental step for knowing how the part creation was going: the building platform could be removed during this break of the process for observing the layer just realized.

The second issue regarded the heat generated by the cationic photopolymerization: during the 3D printing, the photocuring of the layer generated big amount of heat that was very localized on the printing zone of the vat. This concentration of heat on the vat during the layer by layer addition raised and, after some printing jobs, bubbles started to arise on the vat, leading to problems of adhesion between layers and new layers creation. The transparent vat is composed by different parts: the closest to the laser is made of transparent glass, the next is made of silicone and then a Teflon film for avoid adhesion of the new layer to the vat. The bubble were generated between the antiadhesion foil and the silicone part and after several cycles of printing these bubbles broke the Teflon foil, requiring the substitution of the vat. The failure of the Teflon foil, which was unusual in such short time, could be related to the multiple effects derived from the pressure applied by the platform during the printing, from the process temperature and in this case from the cationic photopolymerization. In particular the heat generated from multiple photocuring of layers would accelerate the bubbles formation because of the rapid evaporation of the solvents inside the glue used for sticking the Teflon foil on the silicone part of the vat. This problem was particularly visible during the printing of one small object: after 40 layers the bubbles generated were considered too invasive for finishing the objects, see figure 6.4. In fact for the next printing jobs the foil was removed from the printing area and the resin was processed on the silicone part of the vat, as represented in figures 6.5.

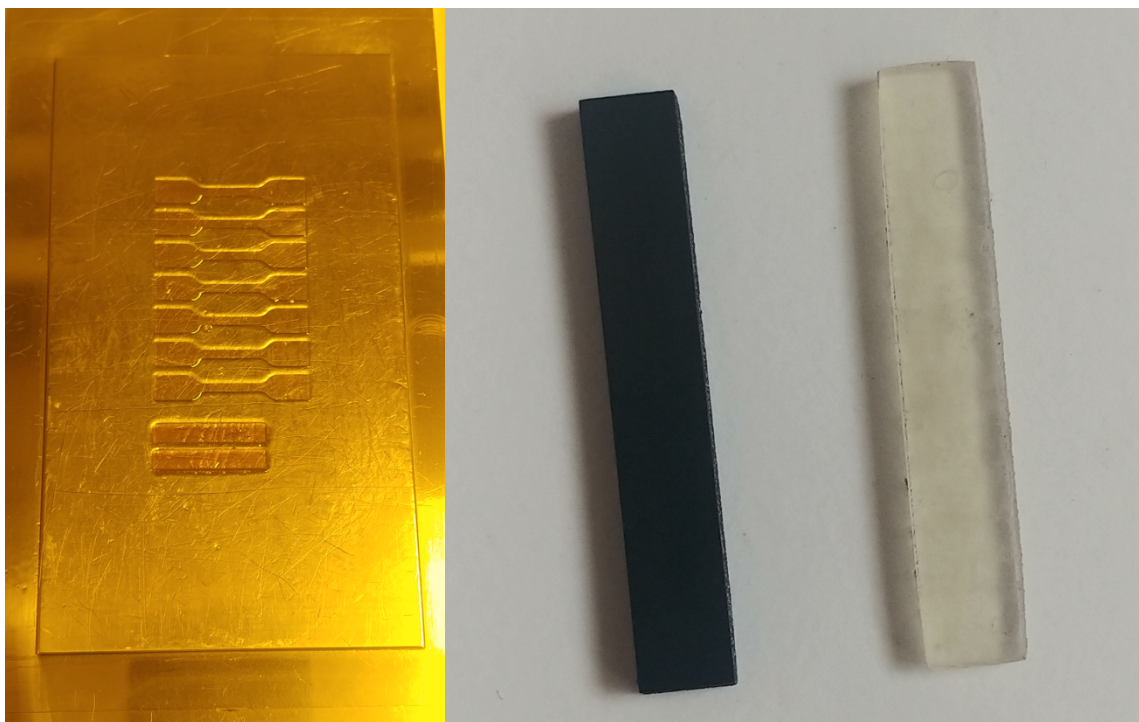


**Figure 6.4:** Bubbles formation during the printing job on the transparent vat.



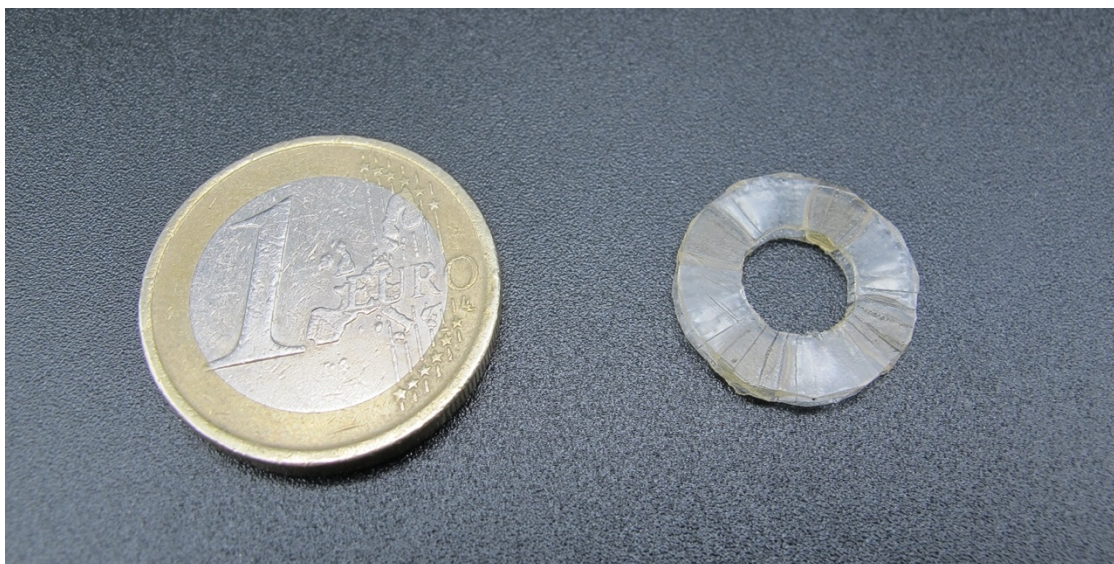
**Figure 6.5:** Silicone part of the vat after removal of the broken foil.

The realization of mechanical samples were less stressful in terms of heat generated for the machine because since their thickness should be the same as the one tested before, the number of layers involved was limited. The samples realized were RSA samples, tensile test samples and DMA samples: the best laser speed for obtaining them was 350 mm/s and the layer thickness selected was 100  $\mu\text{m}$ . The samples were printed in the xyz direction[citazione articolo]: this means the major surface section of the samples lays on the xy plane, which is represented by the vat. When properly printed and removed from the platform, the samples were washed in isopropanol for removing the unpolymerized parts and then they were post-treated in oven at 250 °C for 4 hours. In figure 6.6 some examples of printed and post-treated samples are presented. The test results will be explained in the 6.4 paragraph.



**Figure 6.6:** Example of printed samples on the building platform (on the left), on the right DMA samples before (light/transparent yellow) and after (black) thermal treatment.

The small object, shown in figure 6.7, was printed as a prove for underling the printability of the epoxy-based formulation: the layer thickness is 100  $\mu\text{m}$  and the laser speed selected is 200 mm/s.





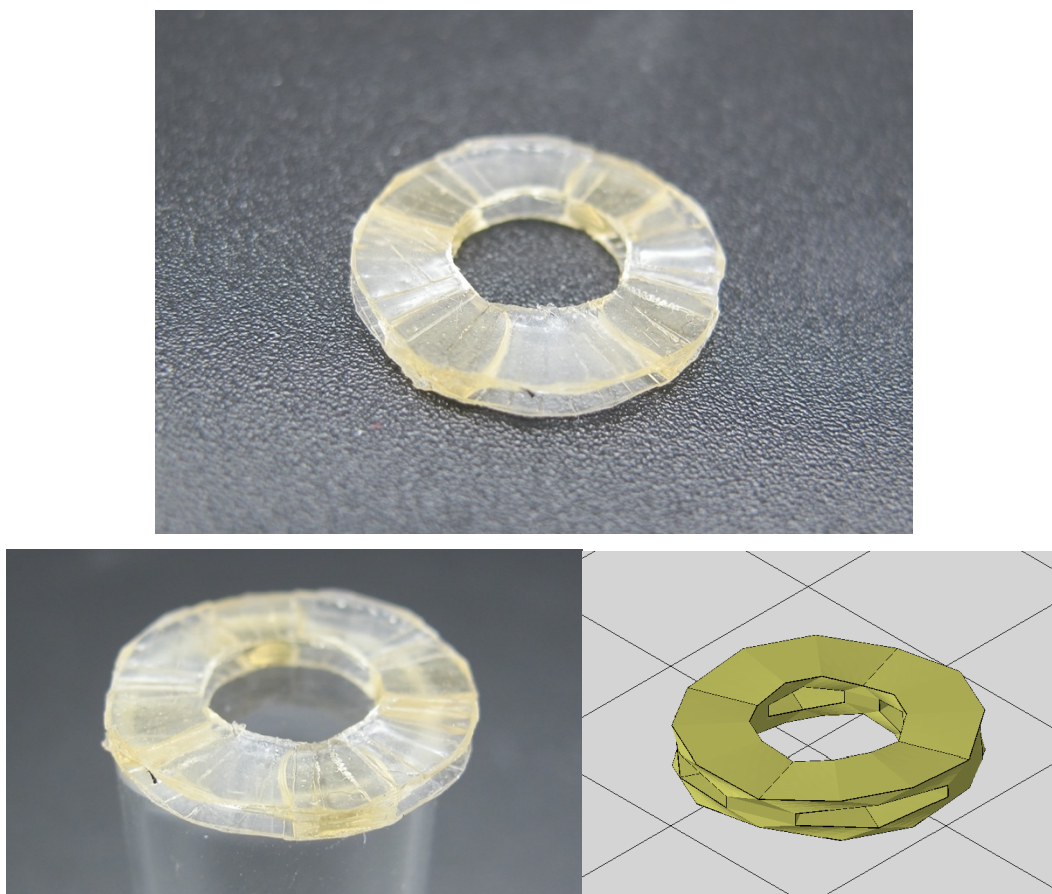


**Figure 6.7:** Small part with particular structure printed by hot lithography approach.

The effect of the anthracene inside the formulation, mentioned previously (paragraph 2.4.1), is visible in figure 6.8: in the absence of this component, the formulation tends to lose resolution because of the presence of extra-polymerized zone around the section of the object printed.

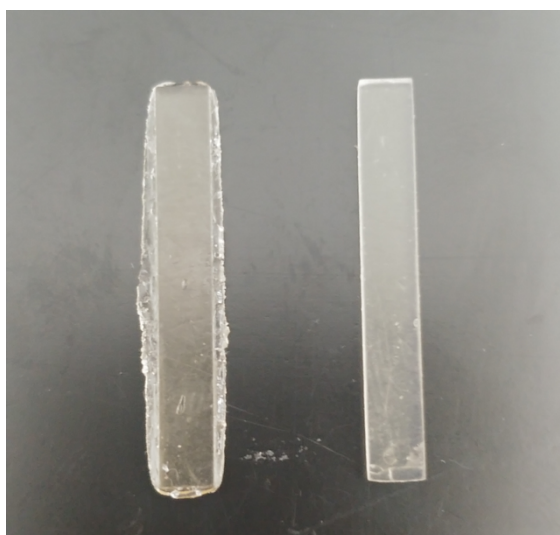


**Figure 6.8:** DMA samples printed without (on the left) and with (on the right) anthracene inside the CDA\_1\_20% formulation.

## 6.4 Test results and discussions

As mentioned before, the samples, printed and thermally post-cured (4 hours at 250 °C), were tested and compared to the CDA\_1\_20% and the Reference photopolymers previously studied. The condition of every tests was the same as previously mentioned.

### 6.4.1 DMTA

The figure 6.9 shows the storage modulus plot of the CDA\_1\_20% printed and post-cured directly compared to the CDA\_1\_20% and the Reference. The figure 6.10 shows the same three  $\tan(\delta)$  plots compared.

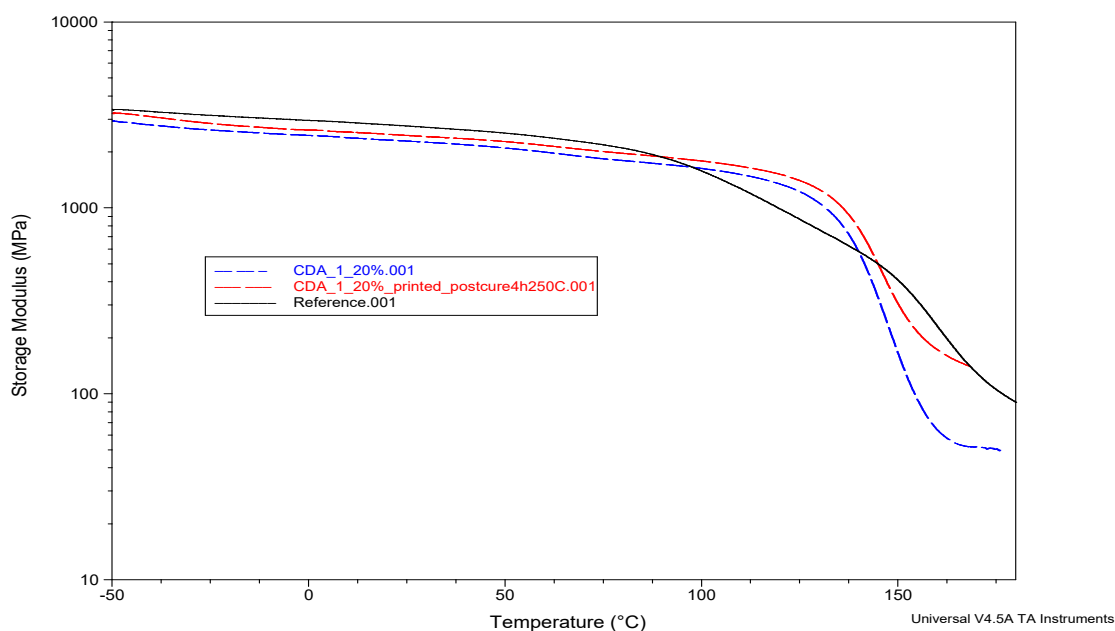


**Figure 6.9:** Storage modulus curve of the CDA\_1\_20% printed and post-cured, compared with the curves of the CDA\_1\_20% and the Reference moulded.

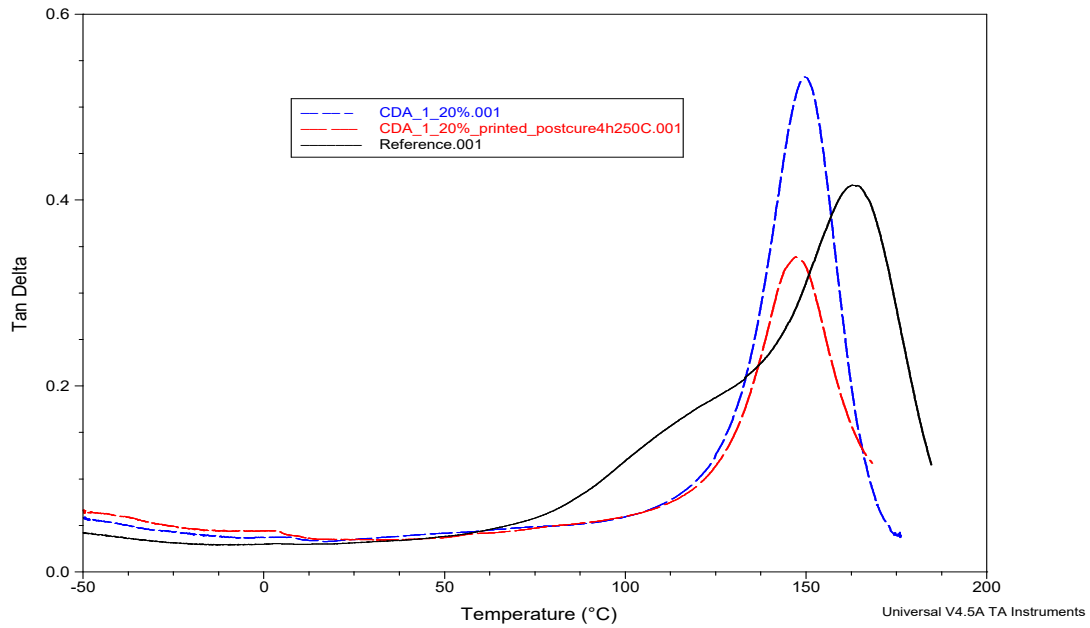


**Figure 6.9:** Tan( $\delta$ ) curve of the CDA\_1\_20% printed and post-cured, compared with the curves of the CDA\_1\_20% and the Reference moulded.

From DMTA analysis is easily visible that the properties of the photopolymers are the same described before: the slightly higher modulus of the printed CDA\_1\_20% photopolymer can be explained by the higher conversion and crosslinking density (visible from the storage modulus plot) achieved thanks to hot lithography at 80 °C and the thermal post-treatment. The glass transition temperature remains the same in the printed samples, the network regulation effects of the trimethylolpropane are still visible in the printed sample. The table 6.1 shows the main values obtained from this test.

**Table 6.1:** Results from DMA test

Name of formulation	G'25°C [MPa]	Tg [°C]	G'end [MPa]
Reference	2757	163	81,6
CDA_1_20%	2287	149	49,6
CDA_1_20%-printed	2453	147	140

From this test, the overall properties of the CDA\_1\_20% are maintained when the formulations is processed through hot lithography machine.

#### 6.4.2 Tensile test

In the figure 6.10 the stress-strain curve of the CDA\_1\_20% printed and post-cured is presented and it is compared with the CDA\_1\_20% and the Reference photopolymerized in the silicone mould. The table 6.2 recaps the main results from this test.

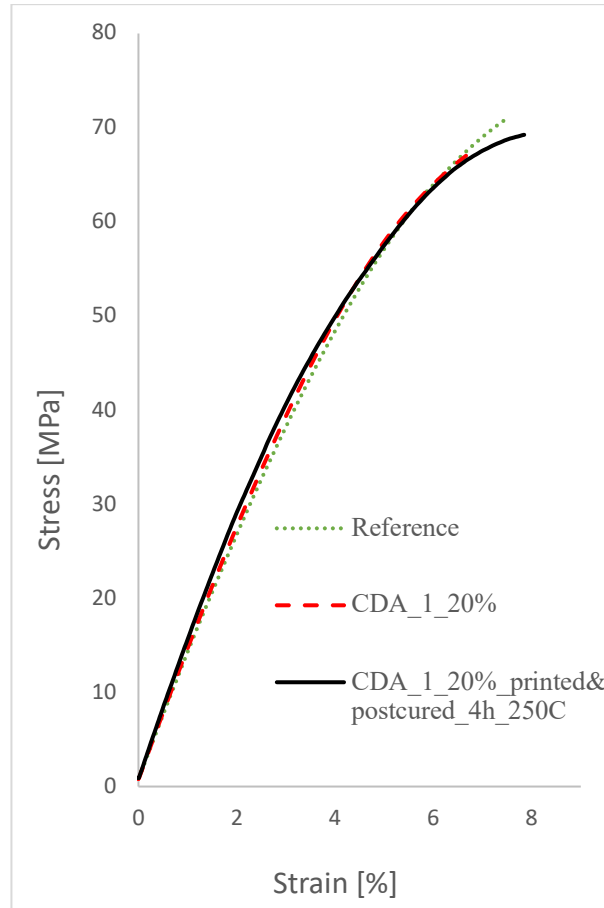


**Figure 6.10:** Stress-strain curve of the CDA\_1\_20% printed and thermal post-cured sample, compared with the Reference and the CDA\_1\_20%.

**Table 6.2:** Tensile test results of the printed samples, compared with the previous tensile results of photocured resins.

Name of formulation	Elastic modulus [MPa]	Tensile strength [Mpa]	Elongation at break [%]
Reference	1385(±99)	70,66(±10,59)	6,83(±1,32)
CDA_1_20%	1398(±24)	67,28(±3,20)	6,69(±2,43)
CDA_1_20%_printed and postcured_4h_250C	1514(±48)	69,26(±2,40)	7,57(±0,83)

From this tensile test, the properties of the photopolymer processed in the printer result very similar to the Reference, so slightly improved respect to the CDA\_1\_20% photopolymerized in the UV oven. The elastic modulus results higher than the Reference because of the higher crosslinking density reached after thermal post-curing, visible from DMTA results. The effect of post-treatment is visible in figure 6.11: stress-strain curve of simply printed sample is compared to the tensile behaviour of printed and post-cured sample, which shows higher elastic modulus and tensile strength. Both samples were printed at the same condition.

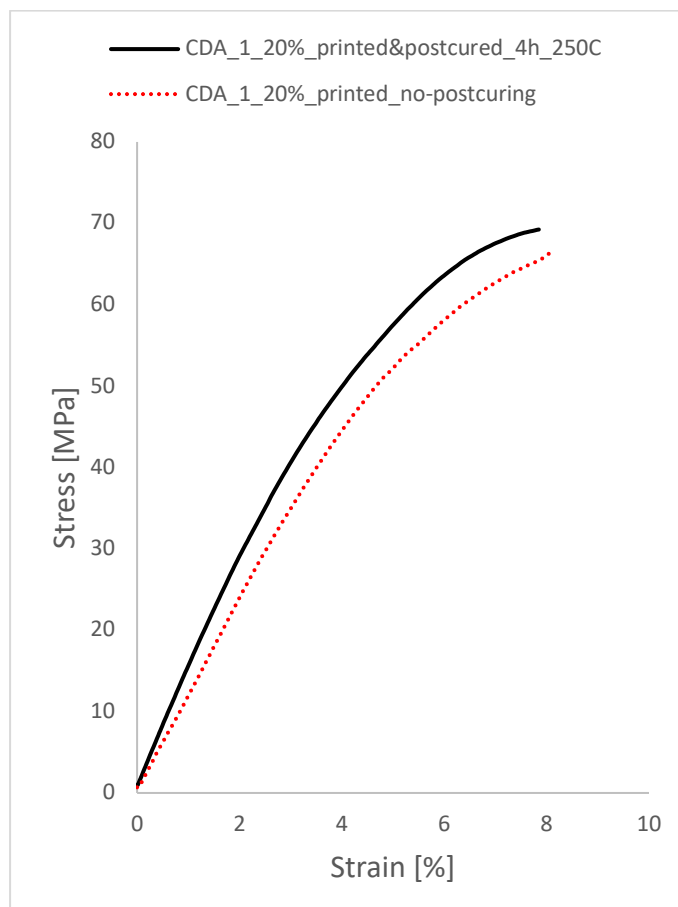


**Figure 6.11:** Stress-strain curves for showing the effects of the thermal post-treatment on printed parts.

#### 6.4.3 RSA

The stress relaxation plot of the printed CDA\_1\_20% thermoset is contained in figure 6.12, and it is compared with the relaxation curves of the CDA\_1\_20% and the Reference.



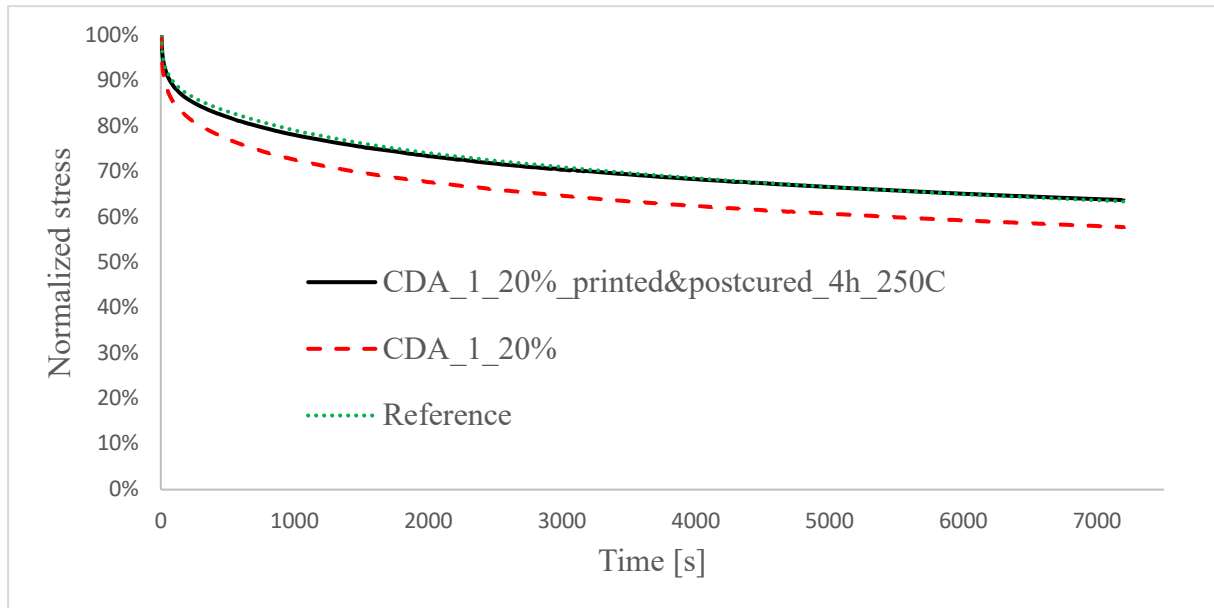


**Figure 6.12:** Stress relaxation curves of the CDA\_1\_20% printed and post-cured, the CDA\_1\_20% and the Reference.

The printed photopolymers is characterized by a lower stress relaxation than the CDA\_1\_20% photocured by UV and, also in this case, the printed photopolymer shows a relaxation of stress similar to the Reference because of the higher crosslink density achieved.

### 6.5 Preliminary conclusions

The printing process in general has positive effects on the mechanical characteristics of the polymer, thanks also to the thermal post-process that increases the conversion of epoxy groups. The photopolymers still remains essentially characterized by a brittle behaviour but it has been proven its 3D printability using the hot lithography approach, nevertheless the existence of process issues, described in the section 6.3.3. For avoiding bubble formation the main solution is the use of different glue that could resist at higher localized thermal stress, because in absence of the antiadhesion foil the risk that new layers do not adhere to each other is elevated. For processing this type of resins, a redesign of the vat and the coating unit could be done: instead of having this type of vat, that cannot be filled entirely with the material, the presence of a closed delimitation at the border of the vat could help in the creation of a little pool of liquid resin, that at high temperature could easily cover the printing zone with liquid film, and the problem faced with the coating unit could be limited. This setting could be built very similar to the DLP based printers, which are present inside the lab of TU Wien. Otherwise an intense study of liquid resin surface properties has to be done in order to modify the behaviour of the liquid resin with the coating unit of the hot lithography machine.

## 7. Third part: properties modification of the thermoset through different additives addition

## 7.1 Central focus of the third part of the project

The third part of this project is focused on the addition of different additives in order to obtain more interesting mechanical behaviour of the epoxy based photopolymers. To achieve this goal, several modifiers has been added to the Reference and to the CDA\_1\_20% formulations and they have been tested by tensile test, DMTA and RSA. The photo-DSC analysis has been done for studying the reactivity of the new formulations in order to see if they could be printable same as the CDA\_1\_20%. In the end a short printability study is described.

## 7.2 List of formulations

Two main groups of formulations were prepared: the CDA\_1\_20% was modified adding 1% and 2% in weight percent of nanosilica particles (provided dy sigma Aldrich, 0,007  $\mu\text{m}$ ), adding 1%, 2%, 3%, 5% and 10% in weight percent of core-shell rubber particles miscible in epoxy resin (provided by Evonik). Different poly-siloxanes with hydroxyl groups in the backbone were added to the Reference formulation: the aim was to study the improvement of the epoxy-based thermoset network derived by the use of siloxane modifier and the presence of hydroxyl groups, that should works as CTA during cationic photocuring. In order to understand this behaviour three main type of poly-siloxanes were selected: Tegomer H-Si 2311 (viscous liquid) and Tegomer H-Si 6440P (solid pellets) provided by Evonik and also Wax OH 350D (solid flakes) provided by Wacker. For every chemicals the weight percentages inside the Reference were 1%, 3% and 5%, once selected the best additive, it were added also to the CDA\_1\_20%. The backbone structures of the poly-siloxane are represented in figure 7.1 (the Wax OH 350D should have a chemical structure similar to Tegomer H-Si 6440P, it was impossible to know the exact one because of the lack of data sheet about this substance).

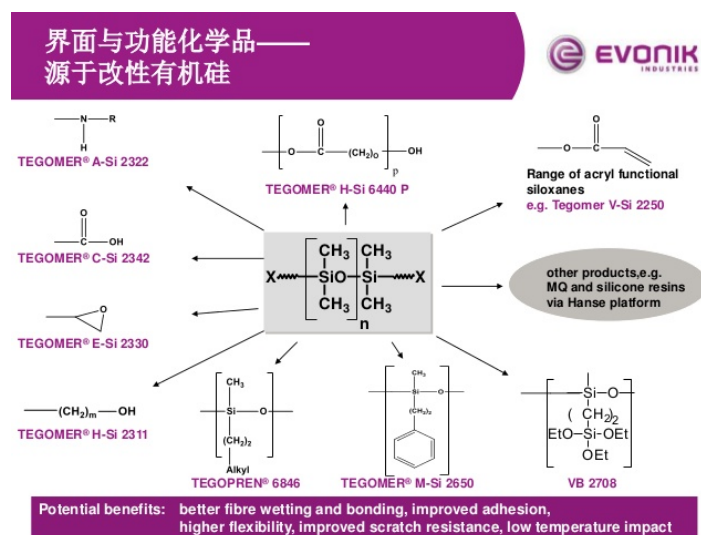


Figure 7.1: Poly-siloxanes backbone structures [43].

For dissolving in the formulations these products, the Speedmixer were used for mixing after the formulation containing the additive was heated up at 90 °C: the dissolution of poly-siloxanes needed 20 minutes of mixing operation in total after being heated in the oven, the particles requested 40 minutes for complete mixing at 90 °C. The formulations were considered homogeneous when any macroscopic aggregation of particles or phase separation were not visible.

The viscosity of all formulations increases because of the presence of this additives: for example the nanosilica after 2% in weight percent generates highly viscous formulation even at 90 °C (difficult to be processed even in the hot lithography printer of TU Wien). The polysiloxanes raises the viscosity of the liquid resin and also their addition in weight percentage is limited by their miscibility in the epoxy resins.

### 7.3 Test results and discussions

In the next sections the results from tensile test, DMTA, RSA and photo-DSC will be explained, the methods and the procedures used for the different analysis are the same described in the previous chapters. In this case all the samples were photopolymerized in the UV oven, using the same silicone mould for obtaining the correct sample shapes.

#### 7.3.1 Tensile test

The tensile tests were conducted on the samples of the CDA\_1\_20% modified with core-shell rubber particles and fumed silica. The results of this analysis is reported in figure 7.2 for silica modified formulations and in figure 7.3 for core-shell particles formulations, in both graphs the CDA\_1\_20% unmodified is added for comparison. The table 7.1 recaps the mechanical properties of all additions to the CDA\_1\_20% formulation.

**Table 7.1:** Tensile test results of all modified CDA\_1\_20% formulations.

Name of formulation	Elastic modulus [MPa]	Tensile strenght [Mpa]	Elongation at break [%]
CDA_1_20%	1398(±24)	67,28(±3,20)	6,69(±2,43)
1% Silica	1412(±23)	75,12(±3,89)	11,22(±1,84)
2% Silica	1404(±42)	75,59(±2,44)	12,97(±1,47)
1% Rubber	1415(±96)	62,49(±6,04)	5,95(±0,61)
2% Rubber	1310(±25)	62,9(±5,35)	8,02(±2,10)
3% Rubber	1294(±27)	63,51(±3,39)	7,58(±0,81)
5% Rubber	1261(±92)	63,41(±4,53)	9,48(±2,83)
10% Rubber	1265(±30)	58,94(±2,17)	8,41(±1,45)
1% Wax OH 350D	1537(±42)	75,59(±2,72)	9,53(±0,86)
5% Tegomer H-Si 2311	1479(±14)	69,53(±6,64)	7,72(±1,35)

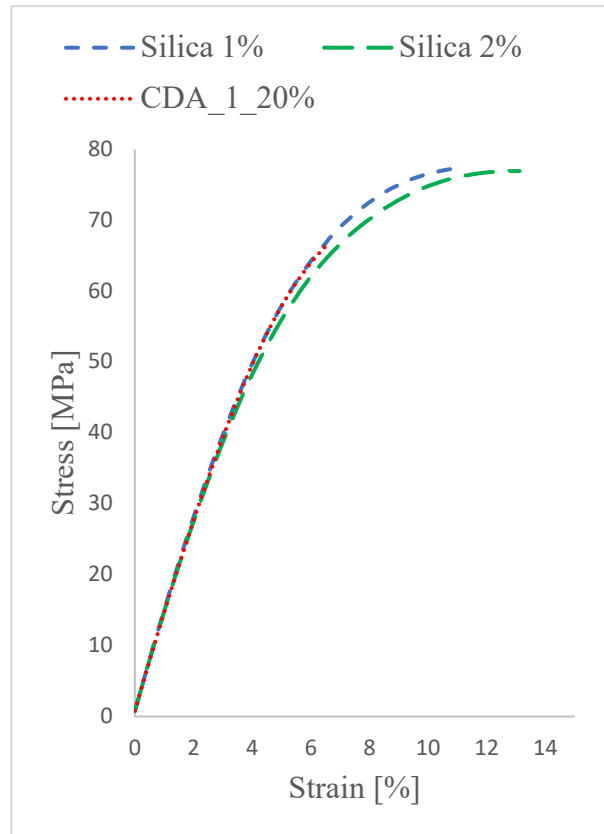


**Figure 7.1:** Stress strain curves of the CDA\_1\_20% with fumed silica formulations.

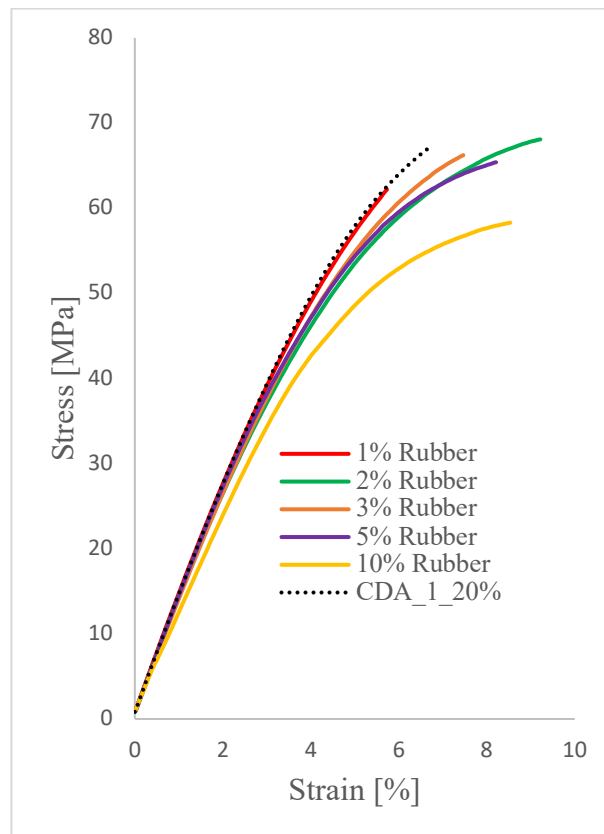


**Figure 7.2:** Stress strain curves of the CDA\_1\_20% with core-shell rubber particles formulations.

The main advantage of using core-shell rubber particles should be the toughening of the thermoset network: the elongation at break should be higher and the elastic modulus should decrease because of softening of the matrix, same behaviour should follow by the tensile strength. In figure 7.3 it is noticeable that the presence of the core-shell particles change the mechanical behaviour of the CDA\_1\_20% but with very little improvement in terms of the elongation at break of the material. The elastic modulus decreases with the higher concentration of rubber particles. Anyway the expected and pronounced toughening effect of the rubber particles remains limited in the CDA\_1\_20% resin at high concentration and, even, inefficient and negative at low concentration. The tensile test results of these formulations are difficult to represent and understand, maybe because the distribution of this type of additives is not homogenous inside the matrix (it will be more clear after DMTA results presentation).

The fumed silica addition, on the other side, leads to good improvement of the mechanical behaviour of the photopolymer: from figure 7.2 it is visible that with the presence of 2% in weight of silica the mechanical behaviour of the CDA\_1\_20% totally gets better, the elongation at breaks reaches the 13% and also the tensile strength of the material improves. The elastic modulus, measured as the slope in the linear sector of the stress-strain curve, is slightly higher in the presence of silica, because of the hydroxyl groups presence on the silica particles surface that acts like CTA during cationic photocuring[19, 20].

The results of the tensile tests performed on the Reference modified with different poly-siloxanes are resumed in table 7.2.

**Table 7.2:** Tensile test results of all modified Reference formulations.

Name of formulation	Elastic modulus [MPa]	Tensile strength [Mpa]	Elongation at break [%]
Reference	1385(±99)	70,66(±10,59)	6,83(±1,32)
1% Tegomer H-Si 6440P	1664(±50)	72,22(±9,65)	6,14(±1,34)
3% Tegomer H-Si 6440P	1617(±34)	71,47(±6,28)	6,80(±1,56)
5% Tegomer H-Si 6440P	1518(±40)	69,33(±6,21)	6,68(±1,41)
1% Tegomer H-Si 2311	1609(±50)	74,14(±6,23)	7,42(±1,78)
3% Tegomer H-Si 2311	1699(±61)	77,33(±5,57)	6,86(±0,94)
5% Tegomer H-Si 2311	1723(±70)	79,72(±4,59)	6,86(±0,64)
1% Wax OH 350D	1763(±144)	83,11(±2,50)	7,18(±0,99)
3% Wax OH 350D	1654(±51)	72,60(±7,54)	6,74(±1,16)
5% Wax OH 350D	1567(±68)	71,51(±3,88)	7,37(±0,94)

The graphs represented in figure 7.4, 7.5, 7.6 show the stress-strain curves of the three difference classes of poly-siloxane added to the Reference in the same three weight percentages (1%, 3% and 5%), they are compared to the unmodified Reference.

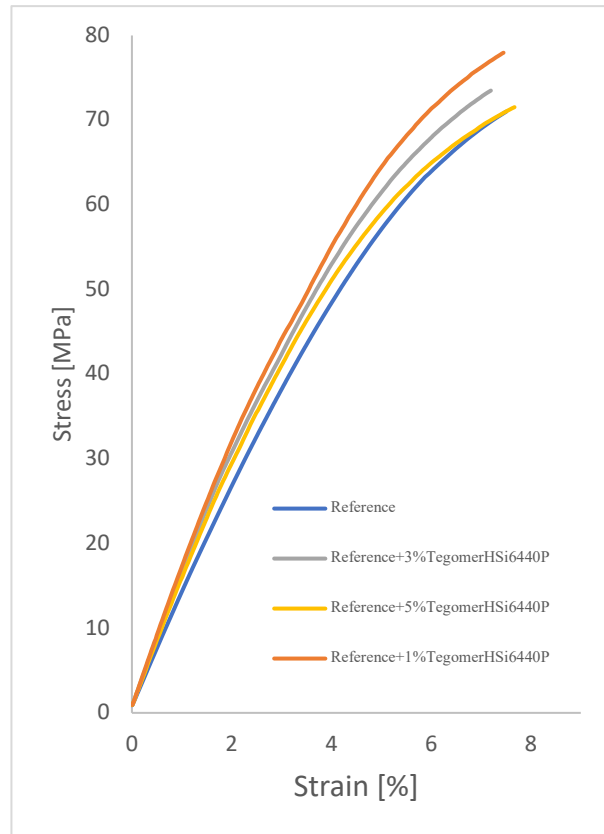


**Figure 7.4:** Stress-strain curves of the Reference formulations with Tegomer H-Si 6440P.

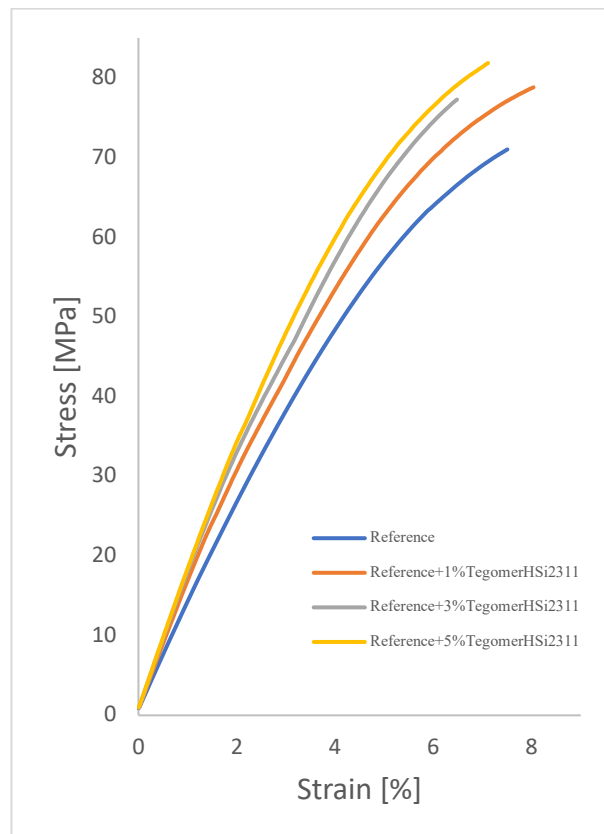


**Figure 7.5:** Stress-strain curves of the Reference formulations with Tegomer H-Si 2311.

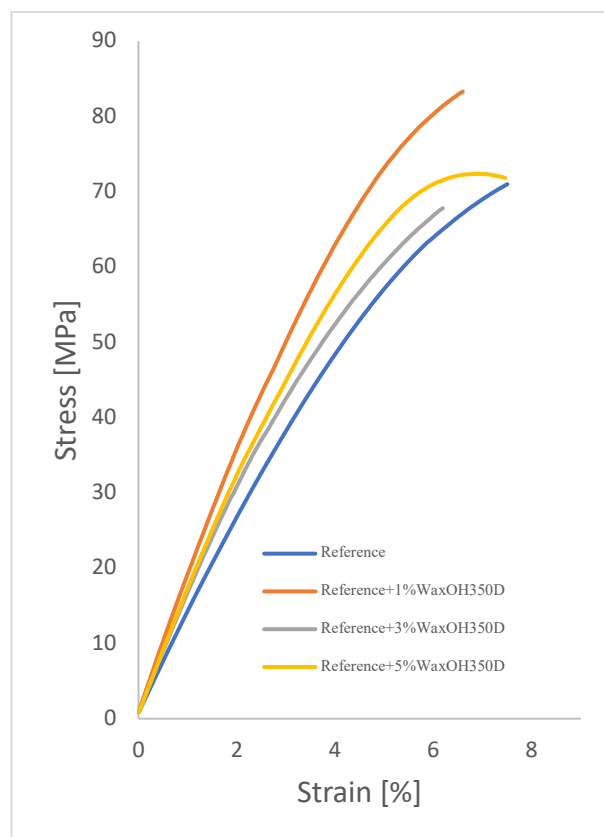


**Figure 7.6:** Stress-strain curves of the Reference formulations with Wax OH 350D.

In general the addition to the Reference of the poly-siloxane tends to enhance the rigidity of the systems: in fact the slope of the linear part of the stress strain-strain presents higher coefficient. The presence of the poly-siloxane does not lead to improvement in the elongation at break, that it has been considered one main reason of the addition of siloxane: other noticeable effect is the higher tensile strength reached thanks to specific addition of products, as in the cases of 1% in weight of Wax OH 350D and of 5% in weight of Tegomer H-Si 2311.

These poly-siloxanes are chosen as further possible modification of CDA\_1\_20% in the same weight percentages. The stress-strain curves are represented in figure 7.7.

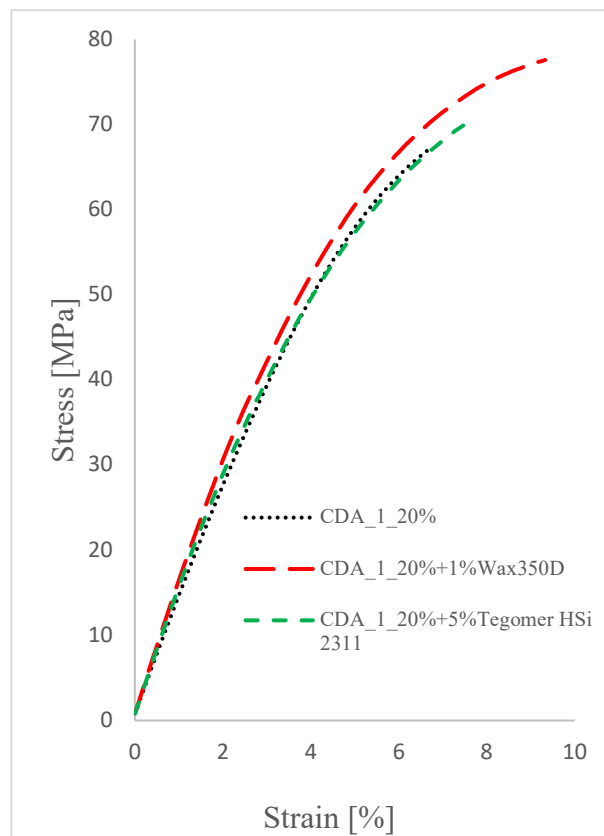


**Figure 7.7:** Stress-strain curve of the unmodified CDA\_1\_20% compared to curves of the CDA\_1\_20% with poly-siloxane.

The effects of poly-siloxane on the CDA\_1\_20% are less interesting respect to the addition of the nanosilica particles (see table 7.1 for values) which work better as a reinforcement for the selected photopolymer.

### 7.3.2 DMTA

The DMTA was conducted on the photocured CDA\_1\_20% formulations modified with core-shell particles, nanosilica particles and siloxane. The photopolymers obtained by the curing of the Reference formulations with different siloxane were also tested.

The table 7.3 contains the analysis results of the different modifications done on CDA\_1\_20%, they are compared to the pure Reference and CDA\_1\_20%. For the polymers containing the rubber particles, two different possible values of T<sub>g</sub> are reported: one is the temperature of the maximum of  $\tan(\delta)$  plot, the other is the temperature at which the storage modulus (not in the logarithm scale) curve shows an inflection point (T<sub>inf</sub>).

**Table 7.3:** DMTA results of modified CDA\_1\_20% formulations.

Name of formulation	G'25°C [MPa]	T <sub>g</sub> [°C]	T <sub>inf</sub> [°C]
Reference	2757	163	/
CDA_1_20%	2287	149	/
1% Silica	2467	148	/
2% Silica	2708	147	/



1% Rubber	2940	162	86
2% Rubber	2306	145	84
3% Rubber	2827	150	65
5% Rubber	2092	156	34
10% Rubber	1475	148	18
1% Wax OH 350D	2857	148	/
5% Tegomer H-Si 2311	2475	147	/

The graphs in figure 7.8 are the storage modulus (a) curves of the unmodified CDA\_1\_20%, the pure Reference and the CDA\_1\_20% filled with 1% and 2% in weight of fumed silica, compared to each other. The  $\tan(\delta)$  plots (b) are also shown in figure 7.8.

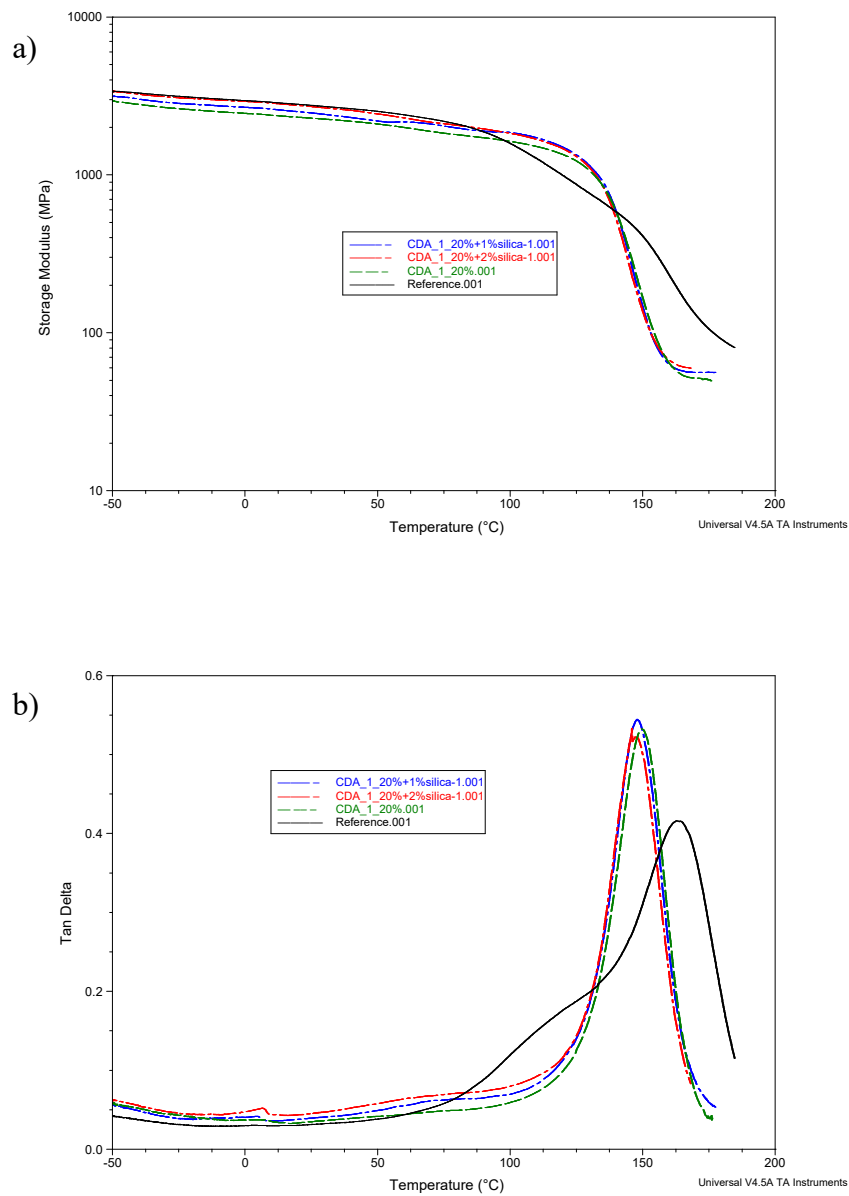


**Figure 7.8:** Storage modulus (a) and  $\tan(\delta)$  (b) plots of silica modified CDA\_1\_20% formulations, compared to pure CDA\_1\_20% and Reference.

The graphs in figure 7.9 represent the storage modulus (a) curves of CDA\_1\_20% modified with 1% in weight of Wax OH 350D and 5% in weight of Tegomer H-Si 2311, compared to the Reference and the pure CDA\_1\_20% plots. The  $\tan(\delta)$  curves (b) are shown in figure 7.9.

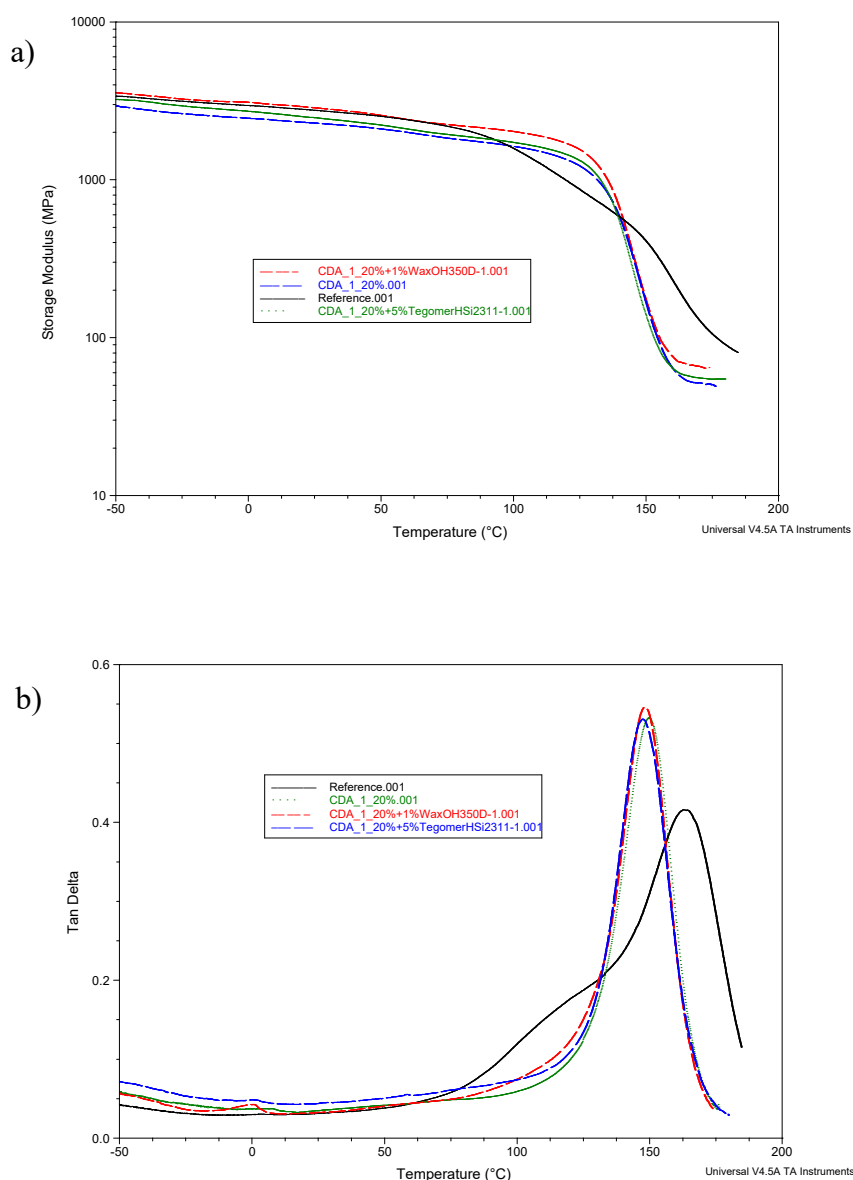


**Figure 7.9:** Storage modulus (a) and  $\tan(\delta)$  (b) plots of poly-siloxanes modified CDA\_1\_20% formulations, compared to pure CDA\_1\_20% and Reference.

In figure 7.10 the  $\tan(\delta)$  (b) and storage modulus (a) curves (not in the logarithm scale) of the CDA\_1\_20% with the addition of 1%, 2%, 3%, 5% and 10% in weight of core-shell rubber particles.

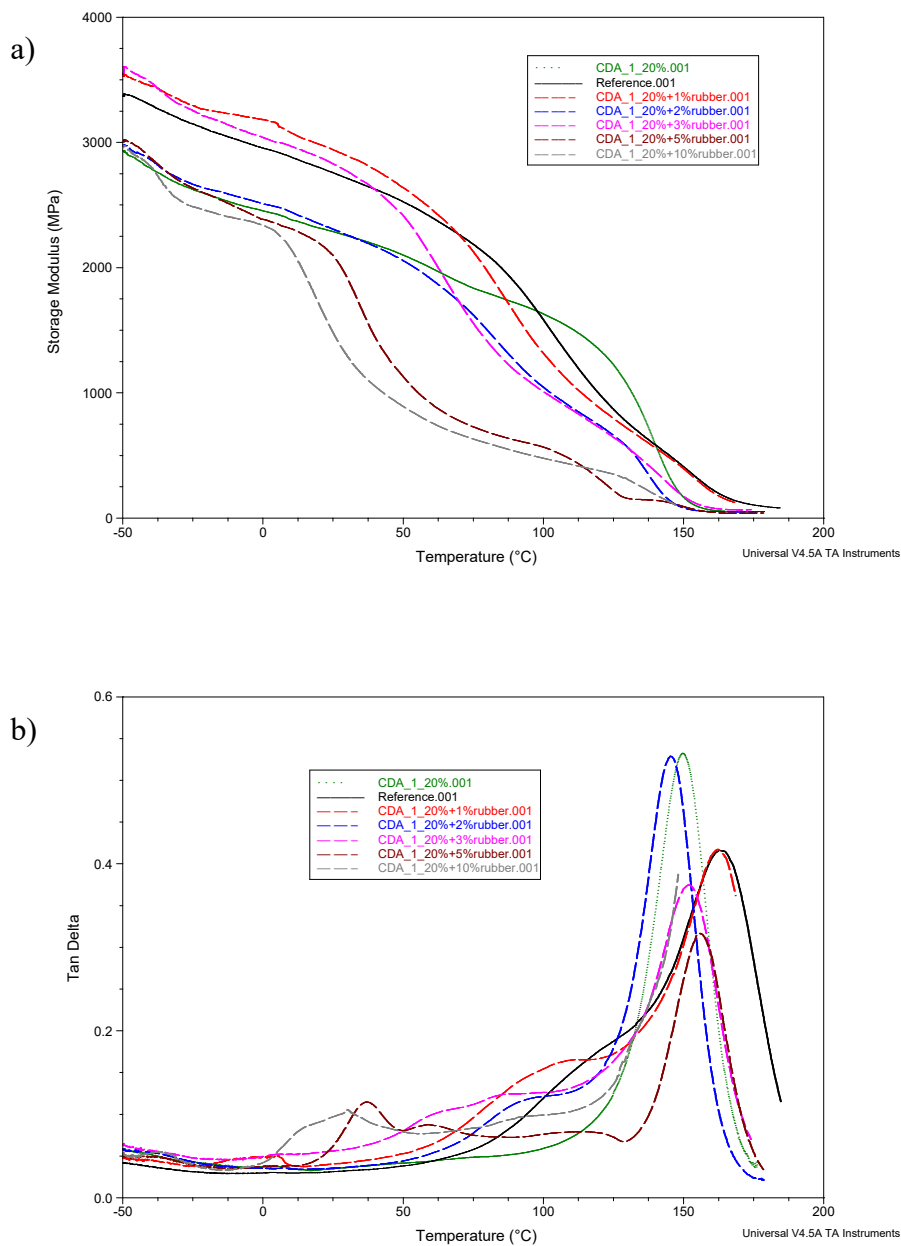


**Figure 7.10:** Storage modulus (a) and  $\tan(\delta)$  (b) plots of rubber modified CDA\_1\_20% formulations, compared to pure CDA\_1\_20% and Reference.

The DMTA confirms the benefits derived from the addition of the fumed silica to the CDA\_1\_20%: better storage modulus than the pure formulations, almost any changes of the glass transition temperature (1 or 2 °C difference) and also the sharp glass transition visible in the storage modulus is still present. The siloxane addition reveals similar effects on the CDA\_1\_20%, in particular the addition of 1% Wax OH 350D. The rubber particles seems to transform the behaviour of the storage modulus of the photopolymers: the sharp glass transition is shifted at low values of storage modulus, the peak of  $\tan(\delta)$  plot does not change according to the change of particles concentration, in some it is shifted at higher temperature (more similar to the resin). The glass transition temperature measured taking into account the presence of

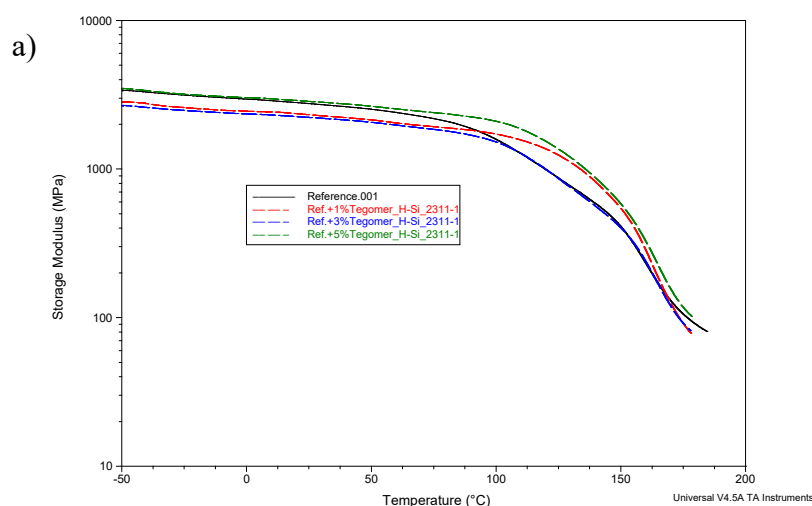
pronounced inflection in the storage modulus curve decreases when the concentration of the additive increases: anyway the effects of the trimethylolpropane as chain transfer agent are somehow limited by the presence of the rubber particles, and also because of incorrect distribution inside the matrix. After these tests results observations, this type of core-shell rubber particles is considered not suitable as toughening agents for this photopolymer.

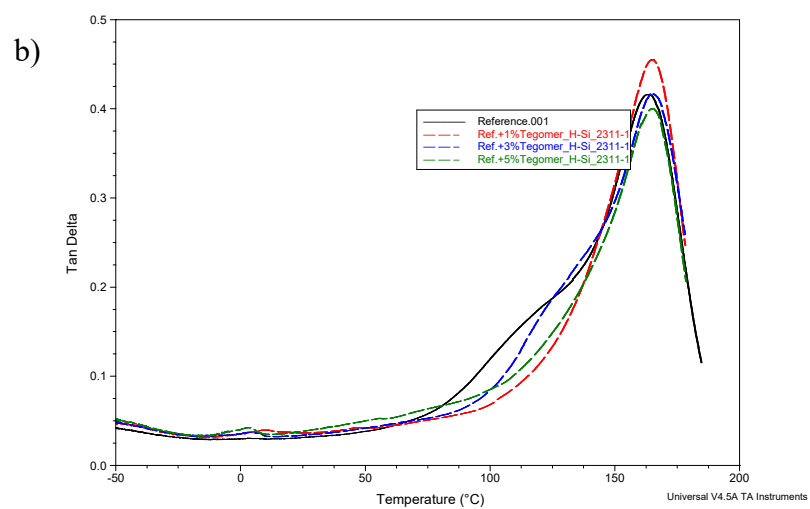
The DMTA results of the Reference formulations modified by the presence of poly-siloxane with hydroxyl groups are inserted in table 7.4.

**Table 7.4:** DMTA results of modified Reference formulations.

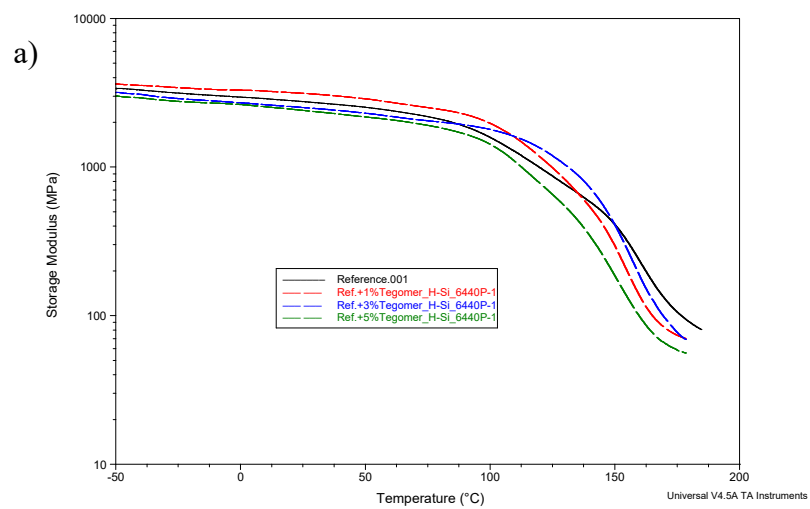
Name of formulation	G' <sub>25°C</sub> [MPa]	Tg [°C]
Reference	2757	163
CDA_1_20%	2287	149
1% Tegomer H-Si 6440P	3134	156
3% Tegomer H-Si 6440P	2513	158
5% Tegomer H-Si 6440P	2404	151
1% Tegomer H-Si 2311	2319	164
3% Tegomer H-Si 2311	2224	164
5% Tegomer H-Si 2311	2848	164
1% Wax OH 350D	3266	155
3% Wax OH 350D	2919	160
5% Wax OH 350D	2758	155

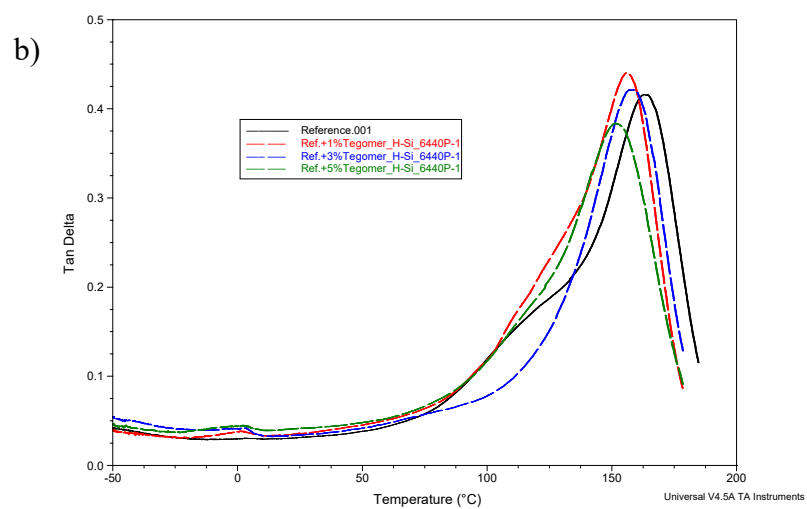
The storage modulus and  $\tan(\delta)$  curves of the three different groups of siloxanes formulations are reported in reported in figure 7.11, 7.12, 7.13; each group is compared to the pure Reference formulation.



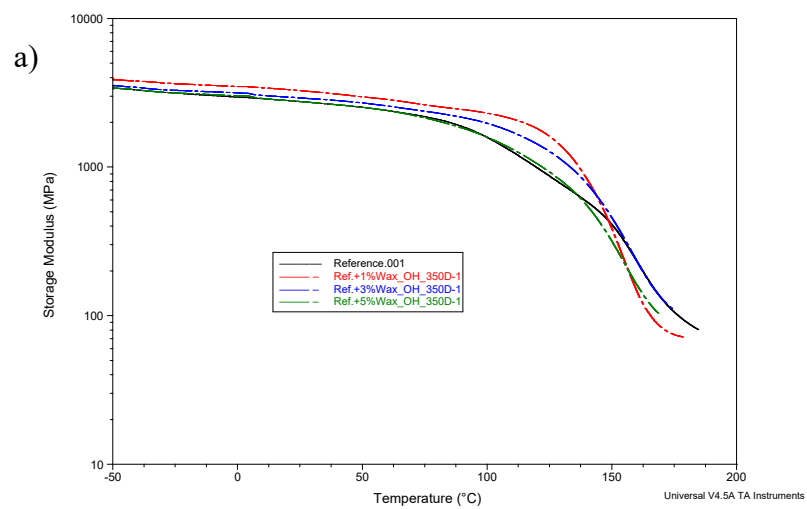


**Figure 7.11:** Storage modulus (a) and  $\tan(\delta)$  (b) plots of Tegomer H-Si 2311 modified formulations, compared to the pure Reference.





**Figure 7.12:** Storage modulus (a) and  $\tan(\delta)$  (b) plots of Tegomer H-Si 6440P modified formulations, compared to the pure Reference.



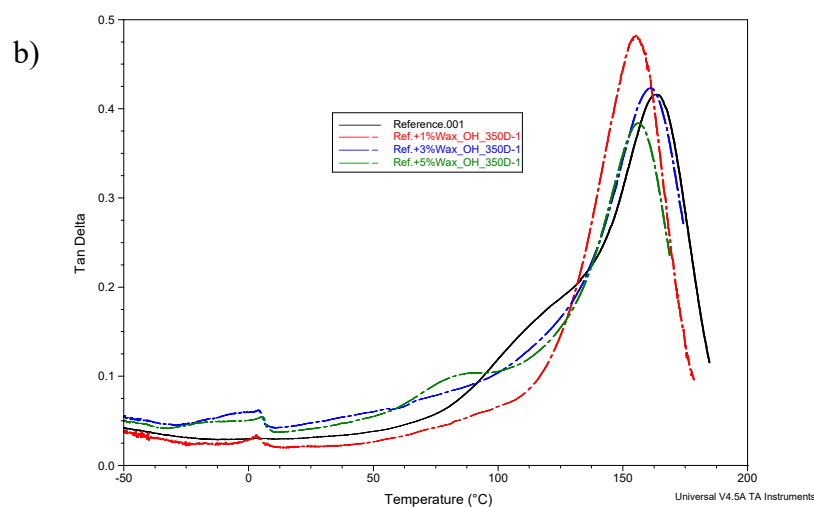


**Figure 7.13:** Storage modulus (a) and  $\tan(\delta)$  (b) plots of Wax OH 350D modified formulations, compared to the pure Reference.

The DMTA was performed in order to discover if the presence of hydroxyl groups in these siloxane structures could produce a regulation of the epoxy network effect similar to the trimethylolpropane (or similar polyols): the visible effects of this regulation are the narrowing of the  $\tan(\delta)$  peak and the presence of sharp glass transition in the storage modulus curve. The Reference with 1% in weight of Wax OH 350D shows this characteristics more pronounced.

### 7.3.3 RSA

The RSA was performed on the photocured samples of CDA\_1\_20% formulations containing 1% and 2% in weight of fumed silica, 1% in weight of Wax OH 350D and 5% in weight of Tegomer H-Si 2311. A brief analysis of the stress relaxation behaviour of the Reference with different poly-siloxanes was conducted.

The comparison between stress relaxation plots of modified CDA\_1\_20% samples is visible in figure 7.14. They are also compared to the Reference and the pure CDA\_1\_20% formulations.

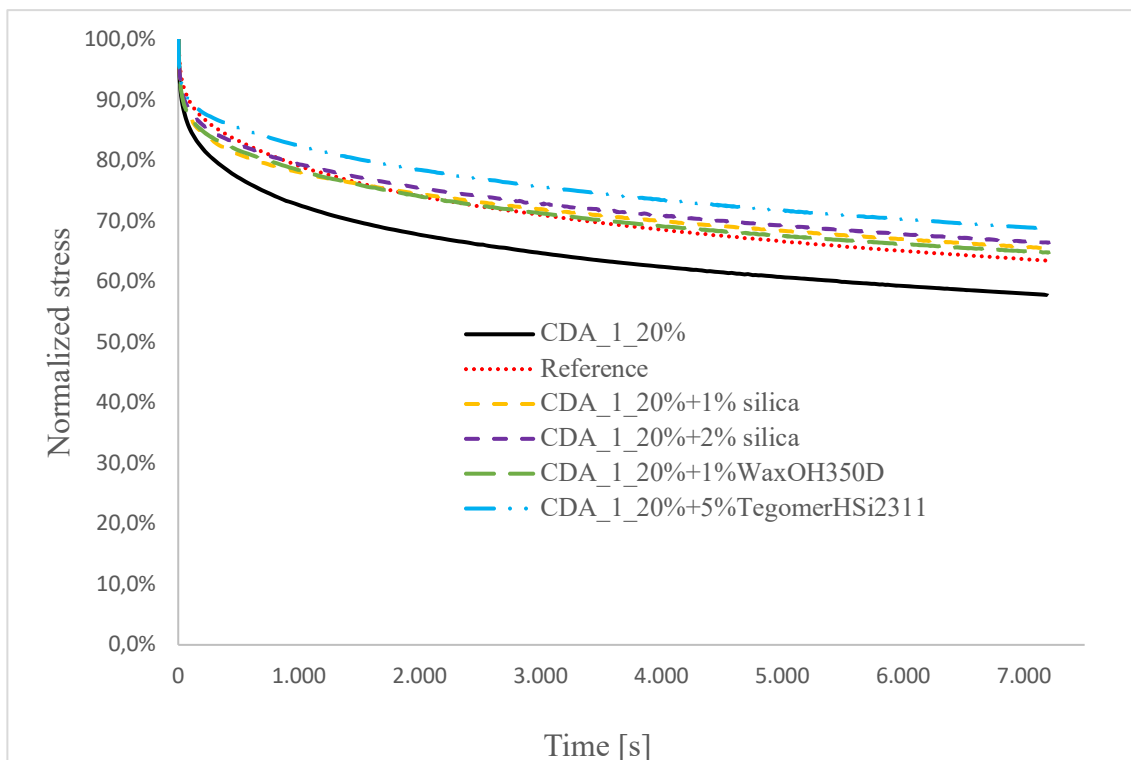


**Figure 7.14:** Stress relaxation curves of modified CDA\_1\_20% formulations, compared to the pure CDA\_1\_20% and the Reference.

The table 7.4 shows the max percentage of the stress relaxation reached by the cited formulations at the end of the test.

**Table 7.4:** Stress relaxation results of the CDA\_1\_20% formulations, and the Reference.

Name of formulation	Reference	CDA_1_20%	1%Silica	2%Silica	1%Wax OH 350D	5%Tegomer H-Si 2311
Time [s]	7200	7200	7200	7200	7200	7200
Max relaxation [%]	63,43	57,79	65,50	66,42	64,78	68,74

The stress relaxation behaviour of modified CDA\_1\_20% photopolymers results better than the pure CDA\_1\_20% and also than the Reference: the presence of nanosilica silica in the formulations especially leads to the best improvement for the photopolymers, thanks to the direct interaction of surface hydroxyl groups during the cationic photocuring of the resin, this should create a better link between the matrix and the reinforcement. The addition of 1% Wax 350D OH shows also good improvement of the CDA\_1\_20%, similar to the nanosilica addition. The resin containing the 5% of Tegomer H-Si shows an excellent reduction of stress relaxation, even better than the addition of 2% of fumed silica. The importance of the nanosilica hydroxyl groups in order to properly modify the mechanical properties of the cationic photocured polymers is again underlined by these stress relaxation results.

The stress relaxation curves of the Reference with different poly-siloxanes are represented and compared in the figure 7.15. In this case the normalized stress axis is limited between 60% and 100% for showing better the little difference between the formulations.



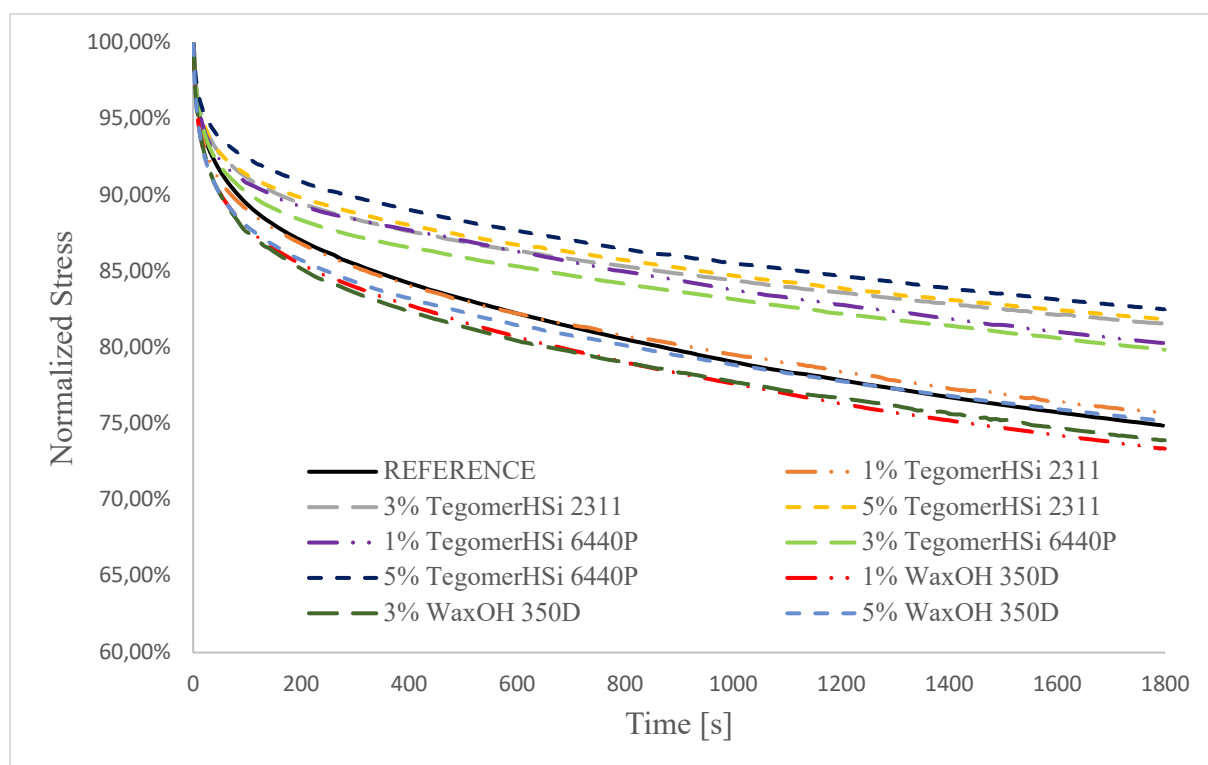


**Figure 7.15:** Stress relaxation curves of modified Reference samples, compared to the pure Reference.

The results are visible in table 7.5, in this case the time has been limited to 1800 seconds for shorter comparison of all formulations.

**Table 7.5:** Stress relaxation results of modified Reference formulations.

Name of formulation	Time [s]	Max relaxation [%]
Reference	1800	74,89
1%Tegomer H-Si 2311	1800	75,76
3% Tegomer H-Si 2311	1800	81,58
5%Tegomer H-Si 2311	1800	81,88
1%Tegomer H-Si 6440P	1800	80,31
3%Tegomer H-Si 6440P	1800	79,89
5%Tegomer H-Si 6440P	1800	82,53
1%Wax OH 350D	1800	73,39
3%Wax OH 350D	1800	73,94
5%Wax OH 350D	1800	75,21

In general the presence of siloxane in the Reference formulations does not increase the relaxation of the polymer, except the addition of 1% and 3% in weight of Wax OH 350D: the modified system results more rigid.

#### 7.3.4 Photo-DSC

The photo-DSC analysis was done in order to understand the reactivity of the formulations previously tested: the effects on the basic formulations of the presence of nanosilica particles and poly-siloxane with hydroxyl groups were investigated. The temperature selected is 80 °C, which ideally could represent the printing process temperature.

The table 7.6 and the table 7.7 summarise the main results obtained from these measurements: the table 7.6 refers to the modified CDA\_1\_20% formulations and the table 7.7 contains the results of the additions to the Reference.

**Table 7.6:** Photo-DSC data of the CDA\_1\_20% formulations.

Name of formulation	CDA_1_20%	2%Silica	1%Wax OH 350D	5%Tegomer H-Si 2311
Temp. [°C]	80	80	80	80
A [J/g]	354,6	391,5	355,5	303,7
t <sub>max</sub> [s]	13,7	13,8	16	15,2
h [mW/mg]	16,8	21,99	16,53	14,15
t <sub>95</sub> [s]	76,1	73,8	85,3	249,4

**Table 7.7:** Photo-DSC data of the Reference formulations.

Name of formulation	Temp. [°C]	A [J/g]	t <sub>max</sub> [s]	h [mW/mg]	t <sub>95</sub> [s]
Reference	80	284,3	20,5	10,07	81,4
1%Tegomer H-Si 2311	80	376,3	16,3	8,118	136,6
3%Tegomer H-Si 2311	80	354,2	17,6	6,812	113,2
5%Tegomer H-Si 2311	80	333	17,4	6,137	176,8
1%Tegomer H-Si 6440P	80	294,6	18,2	4,647	97,2
3%Tegomer H-Si 6440P	80	338,8	17,2	4,556	158,3
5%Tegomer H-Si 6440P	80	300,4	16,9	3,595	165,6
1%Wax OH 350D	80	382,9	19,2	5,37	164,1
3%Wax OH 350D	80	311,9	25,5	5,139	159,3
5%Wax OH 350D	80	341,5	31,6	3,74	236

The figure 7.16 shows the curves of CDA\_1\_20% with 2% in weight of nanosilica, with 1% in weight of Wax OH 350D and 5% in weight of Tegomer H-Si 2311. They are compared to each other and to the pure CDA\_1\_20%.

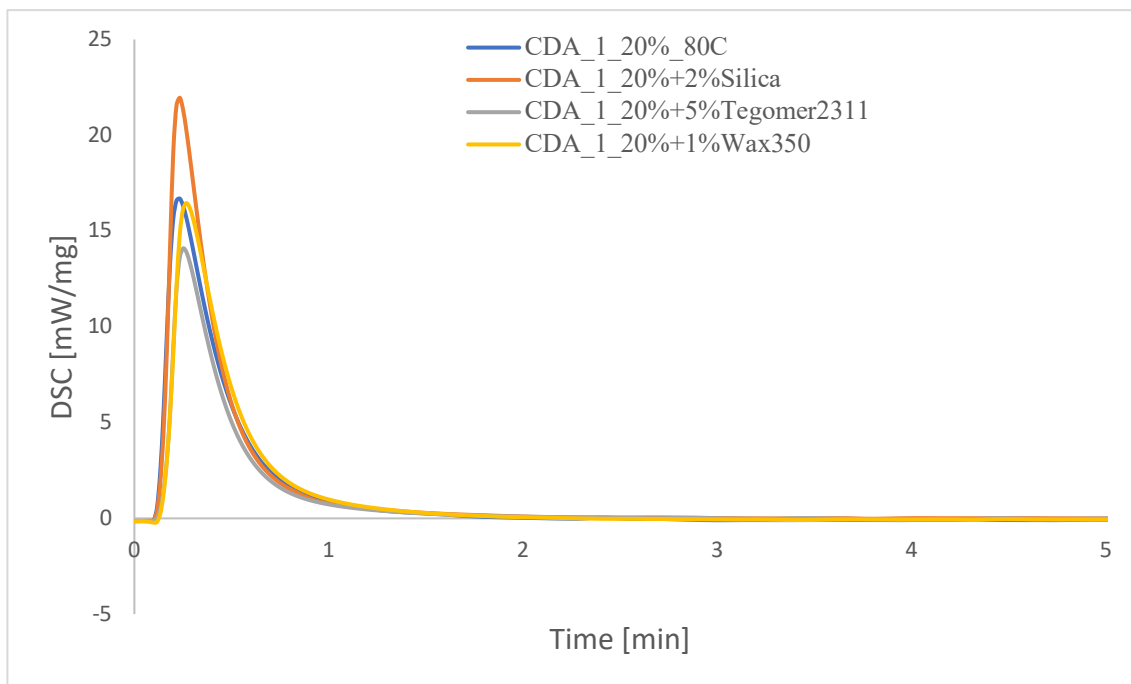


**Figure 7.16:** Photo-DSC plots comparison of CDA\_1\_20% formulations at 80 °C, time axis is limited to 5 minutes for showing better the differences.

The addition of nanosilica to the CDA\_1\_20% gives visible benefits also in this case: the reactivity of the resins expressed by the values of A and h in table 7.6 is higher than the pure one, the rate of polymerization is very similar. The higher reactivity could be explained again considering the hydroxyl groups on the silica surface as chain transfer agent during the cationic photoreaction. The addition of Wax OH 350D decreases the overall reactivity and polymerization rate of the pure CDA\_1\_20% system, the Tegomer H-Si 2311 has similar general effects but less pronounced than the other polysiloxane.

The figures 7.17, 7.18, 7.19 shows how the cationic photoreaction of the Reference changes with the addition (1%, 3% and 5% in weight each) of the three selected classes of polysiloxanes: the comparison of the Tegomer H-Si 6440P formulations is in figure 7.15, the figure 7.16 refers to Tegomer H-Si 2311 and the figure 7.17 contains the plots of Wax OH 350D formulations. The comparison between all the Reference formulations containing poly-siloxanes is visible in figure 7.20.

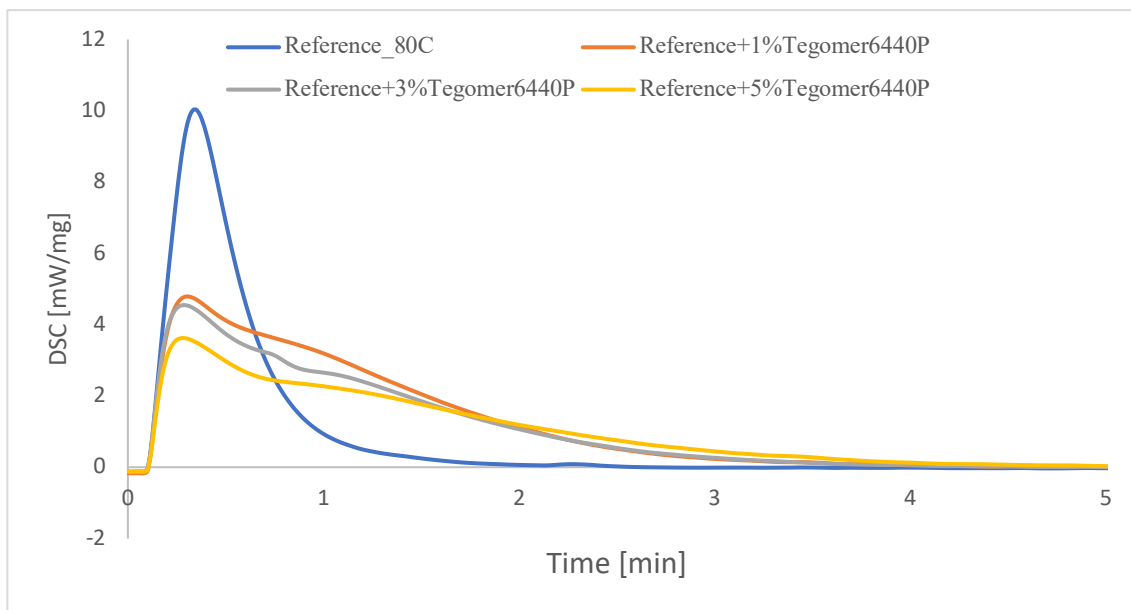


**Figure 7.17:** Photo-DSC graphs of the Reference formulations with different %wt of Tegomer H-Si 6440P, time axis limited to 5 minutes.

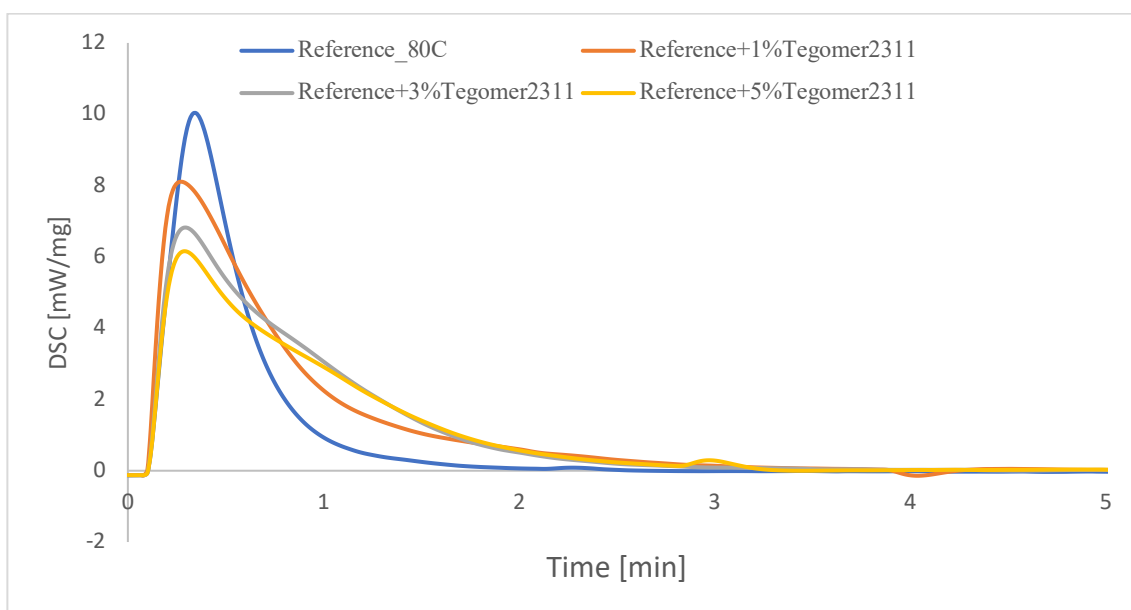


**Figure 7.18:** Photo-DSC graphs of the Reference formulations with different %wt of Tegomer H-Si 2311, time axis limited to 5 minutes.

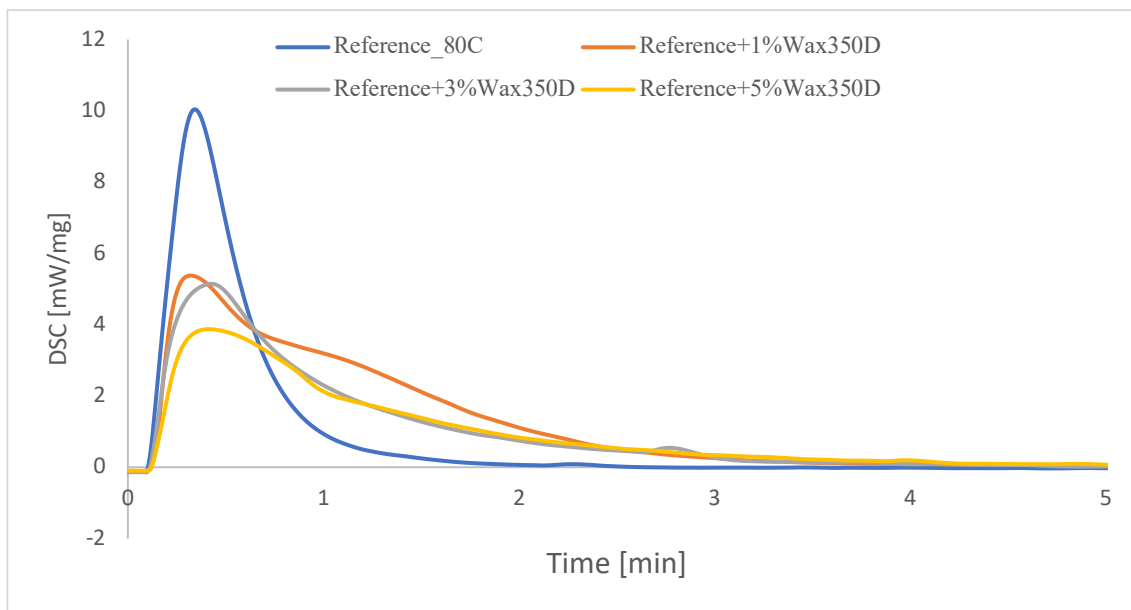


**Figure 7.19:** Photo-DSC graphs of the Reference formulations with different %wt of Wax OH 350D, time axis limited to 5 minutes.

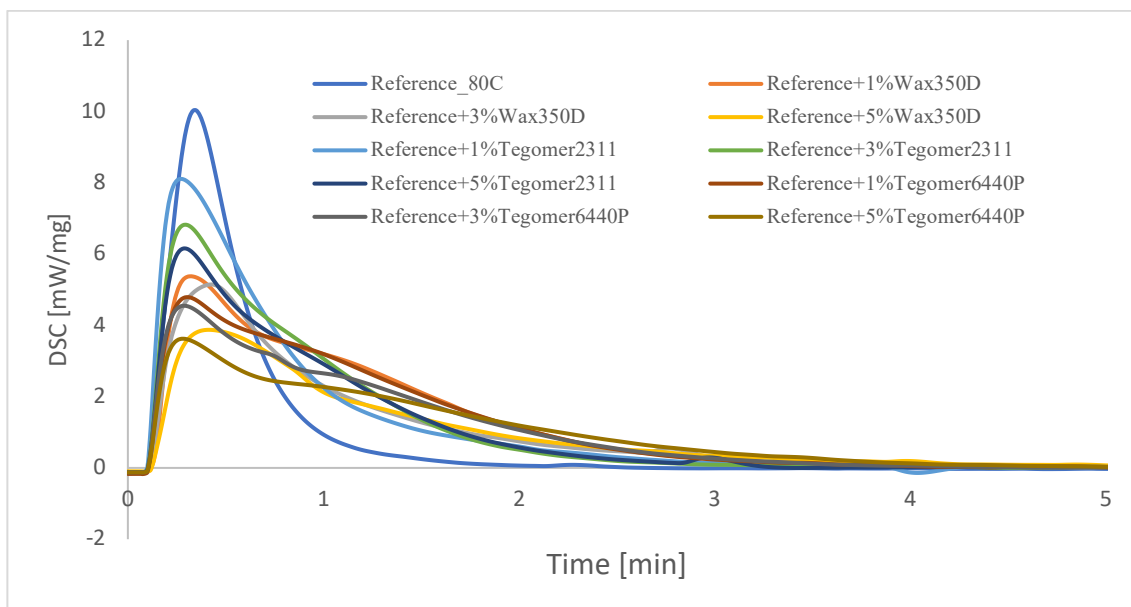


**Figure 7.20:** Photo-DSC curves comparison of all Reference modified formulations, time axis is limited to 5 minutes.

The figure 7.20 shows clearly the low efficiency of the selected poly-siloxanes in terms of enhancing the reactivity of the cationic photocuring: although the values of  $A$ , in table 7.7, are bigger and the values of  $t_{max}$  are lower than the pure Reference, the  $t_{95}$  are higher and the heights ( $h$ ) of the peaks are lower. In the case of higher concentration than 1% in weight of Wax OH 350D the cationic photopolymerization efficiency decreases dramatically (figure 7.17), on the contrary higher addition of the Tegomer H-Si 2311 and 6440P tends to increase the reactivity in presence of the poly-siloxane in the system, especially the Tegomer H-Si at 5% results closer to the Reference behaviour. In conclusion, regarding the reactivity of the system, the presence of this poly-siloxane with hydroxyl groups results to be negative, not showing the same CTA efficiency of trimethylolpropane.

### 7.3.5 Brief 3D printability study

After the results exposed in the previous paragraphs, the benefits derived from the addition of the nanosilica particles to the CDA\_1\_20% formulations are important: in this section a short 3D printability test is presented. Since the CDA\_1\_20% printability was already proven, the addition of 2% fumed silica to this formulations should not change the overall behaviour of the resin during the printing, on the contrary the reactivity thanks to the presence of nanoparticles should be higher as the photo-DSC analysis has shown.

The resin were processed in the same hot lithography machine, unfortunately the vat was ruined because of the previously printing jobs (see figure 6.5): so the 3D printability study was partial in this case.

First of all the irradiation tests were performed changing the laser speed at 80 °C: the laser speeds were 200, 350, 500 and 1000 mm/s, the profile drawn by the laser was the same disc as already described. The CDA\_1\_20% with 2% of fumed silica inside could form a complete disc even when the speed of laser was settled at 1000 mm/s, which resulted too fast for polymerized the pure CDA\_1\_20%. The disc obtained at 1000 mm/s was unsuitable for a real printing job because of low green strength, but if the vat temperature was raised at 100 °C, the photocured disc resulted more solid: the discs obtained are reported in figure 7.21.

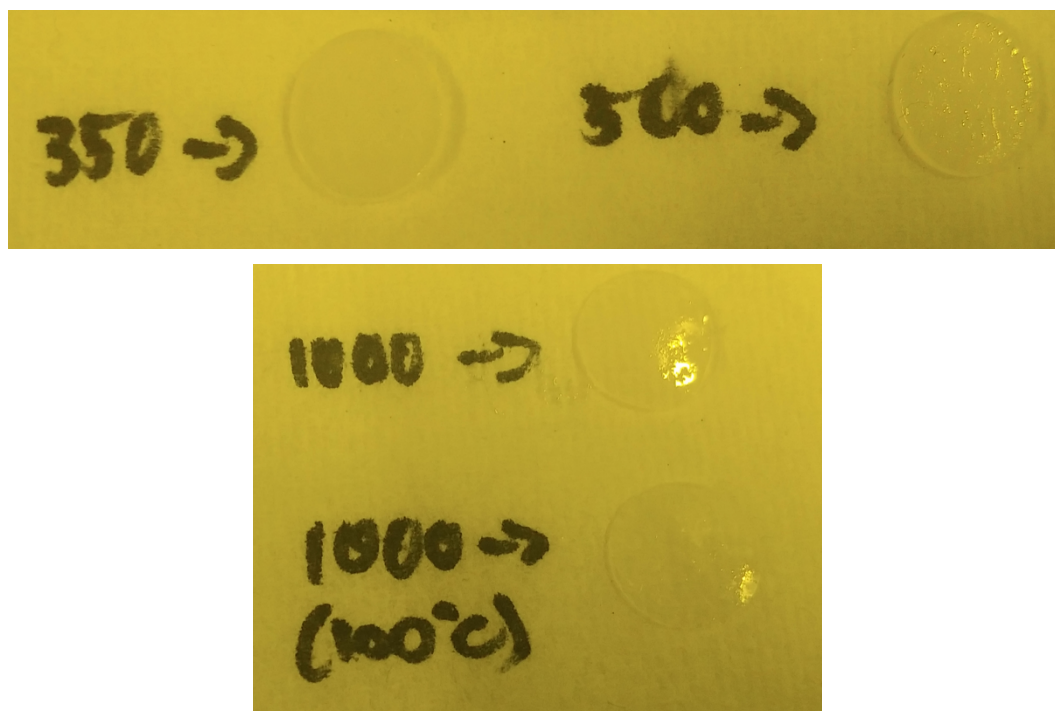


**Figure 7.21:** Discs from laser irradiation tests of CDA\_1\_20% with 2% silica nanoparticles formulation, the number in the photo is referred to the laser speed.

Because of the removal of the antiadhesion foil, the printing jobs at different laser speeds resulted difficult to be accomplished: the adhesion of layers to the building platform was insufficient and, most of the times, the first layers were stuck to the transparent vat. In this condition none suitable samples were printed, also because the silicone part of the vat was starting to break down due to thermal stress: finally only partial (because some layers were

missing) RSA sample was printed at 80 °C; the laser speed was 350 mm/s and the other process parameters were the same reported previously. The sample was post cured in oven at 250 °C for 4 hours.

The stress relaxation curve of this sample, compared to the one moulded in the silicone, is represented in figure 7.22. In this case the printed samples shows much higher stress relaxation than the UV photocured one, but this result has to be considered not representative because the 3D printing condition in the machine were not optimal.

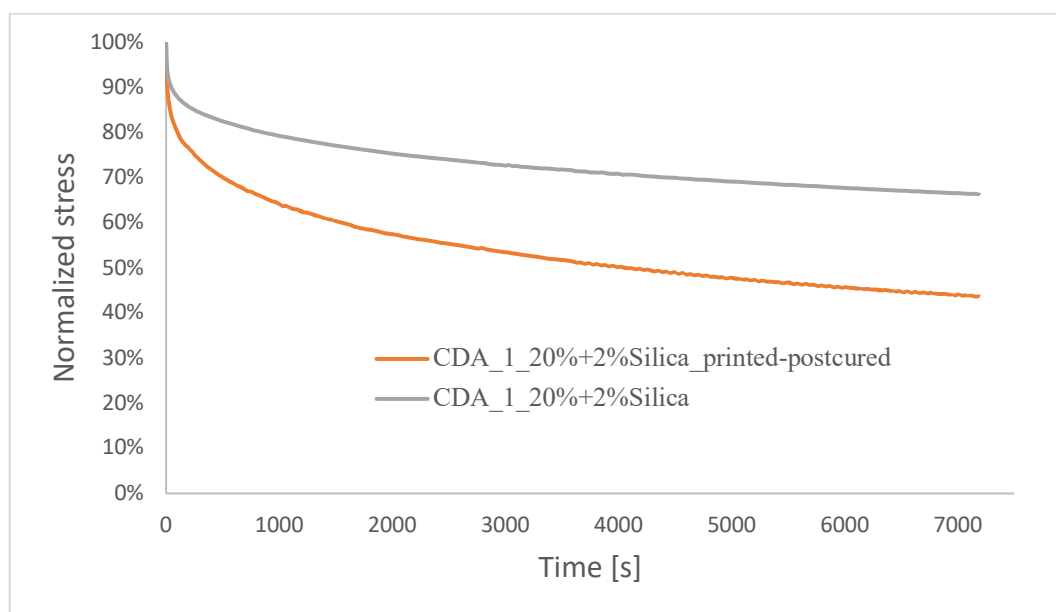


**Figure 7.22:** Stress relaxation behaviour of CDA\_1\_20% with 2% silica nanoparticles inside printed and post-cured, compared to the one photocured in UV oven.

#### 7.4 Preliminary conclusions

In this third part of the project the selection of a possible additive that could improve the mechanical properties of the CDA\_1\_20% photopolymer has been conducted. Among the different formulations prepared, the addition of 2% in weight of silica nanoparticles to the CDA\_1\_20% has resulted the best choice: the photopolymer gains elongation at break (more than 12%) without losing tensile strength (on the contrary increases) and stiffness (little changing in elastic modulus). The presence of this nanoparticles limits the stress relaxation in the photopolymer and it does not interfere with the network regulation due to the presence of trimethylolpropane: in addition the nanosilica thanks to the presence of hydroxyl groups on the surface directly participates to the cationic photocuring, as demonstrated by the photo-DSC analysis. The addition of rubber particles result less efficient: the desired toughening effect linked to the presence of core-shell rubber particles inside the resin is not visible at any composition; in addition the network regulation, operated by the trimethylolpropane, seems to be limited by these particles: the main cause could be related to inhomogeneous mixing and distribution of additives inside the formulation.

The selected poly-siloxanes, in which backbone structure hydroxyl groups are present, are added to the Reference formulations: the mechanical performances are, in some cases, slightly improved in terms of elongation at breaks, elastic modulus, tensile strength and stress relaxation

behaviour. The reactivity of the photocuring process studied by the photo-DSC is limited by the presence of these poly-siloxanes. The addition of two selected poly-siloxane (Tegomer H-Si 2311 and Wax OH 350D) to the CDA\_1\_20% formulations even though leads to general good mechanical reinforcement, this remains less efficient than one provided due to the presence of silica nanoparticles.

The CDA\_1\_20% remains printable in the hot lithography machine nevertheless the 2% in weight addition of the fumed silica (at least from irradiation tests): a more profound and intense study on printed samples must be conducted in order to understand the influences of the printing process on this resin formulation.

## 8. Final Conclusions

The division applied to the exposition of the experimental work has given the chance of showing homogeneously the main results and discussing independently each step of the project. Because of this reason, the general conclusion of the project based on the results obtained is presented here. The epoxy-based cationic photocurable formulation studied and tested in this work has given promising results: the modifications due to the presence of trimethylolpropane (chain transfer agent) have regarded crosslinked-network regulation, higher photocuring reactivity and rate, higher epoxy ring conversion and flexibilization of the material. The selected CDA\_1\_20% formulation has shown good processability in hot lithography based printer: in fact the mechanical properties of the printed samples were certainly improved. In order to counteract the intrinsic brittleness of the epoxy resin, the addition to CDA\_1\_20% of 2% weight percent of silica nanoparticles has revealed from all point of view a valid modification for the epoxy matrix. The general mechanical behaviour proves to be enhanced (almost doubled the elongation at break) and the overall photopolymerization of the resin has shown improvements due to the CTA function of the fumed silica. Even though the addition of this particles, the printability of the modified formulation has been confirmed: the study of mechanical properties of printed samples requires more profound studies. The main goal of the project has been reached: the printability of a cationic photocurable epoxy based resin has been proven thanks to the hot lithography machine.

Although issues and chances of improvement still need to be properly studied. The selection of a good chain transfer agent was more focused on the trimethylolpropane because of its efficient network regulation (from DMTA) and excellent contribution in terms of reactivity in the cationic photoreaction (paragraph 5.4). As further study, it would be interesting to manage the dissolution of the hyperbranched polymer like the Boltorn in this formulation and to study its CTA effects on the system. Expanding the research of new chain transfer agent in order to tune properly the characteristics of the photopolymers network would raise the number of possible final applications, particularly in the additive manufacturing field.

As already discussed in paragraph 6.5, the hot lithography method allows the CDA\_1\_20% system printability due to higher process temperature (80 °C): anyway some processing issues, as reported in the section 6.3.3, regard the bubbles formation in the vat and the interaction between the resin and the recoating unit. Nevertheless the existence of these problems, mechanical tests of printed samples and printing of a little object have proven the real printability of the formulation prepared: the 3D printing process influence on the characteristics of the polyme is generally positive. The process issues discussed could be overcome through



the variation of the vat setting: employing more thermal resistant joining method for covering the vat with the Teflon foil could avoid bubbles creation and, in order to use properly the recoating unit, a little liquid container could be built around the transparent vat.

General mechanical improvement of the epoxy resin, in this case, was obtained thanks to the addition of the fumed silica: higher concentration could be also tested at printing temperature higher than 100 °C, in order to reach reduce the viscosity of the formulation. Higher toughening effects could be reached considering the addition of different types of core-shell rubber particles, liquid rubber or siloxane, after reached the correct mixing homogeneity of the additive in the resin: in this project the selected rubber particles and polysiloxanes did not enhance in the desired way the toughness of the photopolymer.

In conclusion the characterization and the 3D printability study at high temperature of the epoxy-based formulations, photopolymerized through cationic photoreaction, have been accomplished: future applications of such photopolymers could be increase thanks to the combination of hot lithography machine and photochemistry implementation.

## 9. Bibliography

- [1]Sangermano M., Roppolo I., Chiappone A., 2018, *New Horizons in Cationic Photopolymerization*, **Polymers**, **v.10**, 136.
- [2]Mendes-Felipe C., Olivieira J., Etxebarria I., Vilas-Vilela J. L., Lanceros-Mendez S., 2019, *State-of-the-Art and Future Challenges of UV Curable Polymer-Based Smart Materials for Printing Technologies*, **Adv. Mater. Technol.**, **v.4**, 1-16.
- [3]Ligon S. C., Liska R., Stampfl J., Gurr M., Mülhaupt R., 2017, *Polymers for 3D Printing and Customized Additive Manufacturing*, **Chem. Rev.**, **v.117**, 10212-10290.
- [4]Bongiovanni R., Malucelli G., Sangermano M., Priola A., 2002, *Preparation of Coatings via Cationic Photopolymerisation: Influence of Alcoholic Additives*, **Macromol. Symp.**, **v.187**, 481-492.
- [5]Gorsche C., Seidler K., Harikrishna R., Kury M., Koch T., Moszner, Liska R., 2018, *Difunctional vinyl sulfonate esters for the fabrication of tough methacrylate-based photopolymer networks*, **Polymer**, **v.158**, 149-157.
- [6]Gorsche C., Griesser M., Gescheidt G., Moszner N., Liska R., 2014, *b-Allyl Sulfones as Addition-Fragmentation Chain Transfer Reagents: A Tool for Adjusting Thermal and Mechanical Properties of Dimethacrylates Networks*, **Macromolecules**, **v.47**, 7327-7336.
- [7]Dillman B., Jessop J. L. P., 2013, *Chain Transfer Agents in cationic Epoxide Polymerizations: Kinetic and Physical Effects*.
- [8]Sangermano M., Malucelli G., Morel F., Decker C., Priola A., 1999, *Cationic photopolymerization of vinyl ether systems: influence of the presence of hydrogen donor additives*, **European Polymer Journal**, **v.35**, 639-645.
- [9]Corcione C. E., Malucelli G., Frigione M., Maffezzoli A., 2009, *UV-curable epoxy systems containing hyperbranched polymers: Kinetics investigation by photo-DSC and real-time FT-IR experiments*, **Polymer Testing**, **v.28**, 157-164.

- [10]Gorsche C., Harikrishna R., Baudis S., Knaack P., Husar B., Laeuger J., Hoffmann H., Liska R., 2017, *Real Time-NIR/MIR-Photorheology: A Versatile Tool for the in Situ Characterization of Photopolymerization Reactions*, **Anal. Chem.**, **v.89**, 4958-4968.
- [11]Pfaffinger M., 2018, *Hot lithography-New Possibilities in Polymer 3D Printing*, **Laser Technik Journal**, 45-47.
- [12][https://www.tuwien.at/fileadmin/Assets/dienstleister/forschungsmarketing/messe/hm2018/flyer\\_TUW\\_cubicure\\_E.pdf](https://www.tuwien.at/fileadmin/Assets/dienstleister/forschungsmarketing/messe/hm2018/flyer_TUW_cubicure_E.pdf) [ultimo accesso marzo 2020].
- [13]Stretyer B., Buseti B., Harakály G., Liska R., Stampfl J., 2018, *Hot Lithography vs. room temperature DLP 3D-printing of a dimethacrylate*, **Additive Manufacturing**, **v.21**, 209-214.
- [14]Peer G., Dorfinger P., Koch T., Stampfl J., Gorsche C., Liska R., 2018, *Photopolymerization of Cyclopolymerizable Monomers and Their Application in Hot Lithography*, **Macromolecules**, **v.51**, 9344-9353.
- [15]Liu S., Fan. X., He C., 2016, *Improving the fracture toughness of epoxy with nanosilica-rubber core-shell nanoparticles*, **Composite Science and Technology**, **v.125**, 132-140.
- [16]Sprenger S., 2013, *Epoxy resins modified with elastomers and surface-modified silica nanoparticles*, **Polymer**, **v.54**, 4790-4797.
- [17]Kinloch A. J., Mohammed R. D., Taylor A. C., Eger C., Sprenger S., Egan D., 2005, *The effect of silica nano particles and rubber particles on the toughness of multiphase thermosetting epoxy polymers*, **J. Mater. Sci.** .
- [18]Hsieh T. H., Kinloch A. J., Masania K., Sohn Lee J., Taylor A. C., Sprenger S., 2010, *The toughness of epoxy polymers and fibre composites modified with rubber microparticles and silica nanoparticles*, **J. Mater. Sci.**, **v.45**, 1193-1210.
- [19]Sangermano M., Malucelli G., Amerio E., Priola A., Billi E., Rizza G., 2005, *Photopolymerization of epoxy coatings containing silica nanoparticles*, **Process in Organic Coatings**, **v.54**, 134-138.
- [20]Chemtob A., Croutxé-Barghorn C., Soppera O., Rigolet S., 2009, *Cationic Photopolymerization in Presence of Functionalized Silica Nanoparticles*, **Macromol. Chem. Phys.**, **v.210**, 1127-1137.
- [21]Liang Y. L., Pearson R. A., 2010, *The toughening mechanism in hybrid epoxy-silica-rubber nanocomposites (HERSNs)*, **Polymer**, **v.51**, 4880-4890.
- [22]Atif M., Bongiovanni R., Yang J., 2015, *Cationically UV-Cured Epoxy Composites*, **Polymer Reviews**, **v.55**, 90-106.
- [23]Ligon-Auer S. C., Schwentenwein M., Gorsche C., Stampfl J., Liska R., 2016, *Toughening of photo-curable polymer networks: a review*, **Polym. Chem.**, **v.7**, 257-286.
- [24]Chrusciel J., Lesniak E., 2015, *Modification fo epoxy resins with functional silanes, polysiloxanes, silsequioxanes, silica and silicates*, **Progress in Polymer Science**, **v.41**, 67-121.
- [25]Li S., Wang H., Liu M., Peng C., Wu Z., 2019, *Epoxy-functionalized polysiloxane reinforced epoxy resins for cryogenic application*, **J. Appl. Polym. Sci.**, **v.136**, 46930.
- [26]Crivello J. V., Reichmanis E., 2014, *Photopolymer Materials and Processes for Advanced Technologies*, **Chem. Mater.**, **v.26**, 553-548.
- [27]<https://cms-resources.coleparmer.com/t/chart555.jpg> [ultimo accesso marzo 2020].

- [28] [https://www.researchgate.net/profile/Barbara\\_Chan/publication/43180479/figure/fig2/AS:601790777131019@1520489510323/Jablonski-diagram-Color-images-available-online-at-wwwliebertonline-com-ten.png](https://www.researchgate.net/profile/Barbara_Chan/publication/43180479/figure/fig2/AS:601790777131019@1520489510323/Jablonski-diagram-Color-images-available-online-at-wwwliebertonline-com-ten.png) [ultimo accesso marzo 2020].
- [29]Streyrer B., Neubauer P, Liska R., Stampfl J., 2017, *Visible Light photoinitiator for 3D-Printing of Tough Methacrylate Resins*, **Materials**, v.10, 1445.
- [30]Crivello J.V., Jang M., 2003, *Anthracene electron-transfer photosensitizers for onium salt induced cationic photopolymerizations*, **Journal of Photochemistry and Photobiology A: Chemistry**, v.159, 173-188.
- [31]Capricho J. C., Fox B., Hameed N., 2019, *Multifunctionality in Epoxy Resins*, **Polymer Reviews**.
- [32]Chen C., Li B., Wang C., Iwasaki S., Kanari M., Lu D., 2018, *UV and Thermal Cure Epoxy Adhesives*, **Paint and Coatings Industry**, Faris Yilmaz, IntechOpen.
- [33]Sangermano M., Priola A., Malucelli G., Bongiovanni R., Quaglia A., Voit B., Ziemer A., 2004, *Phenolic Hyperbranched Polymers as Additives in Cationic Photopolymerization of Epoxy Systems*, **Macromol. Mater.**, v.289, 442-446.
- [34]Sangermano M., Amerio E., Di Gianni A., Priola A., Pospiech D., Voit B., 2007, *Hyperbranched Polymers in cationic UV curing*, **Macromol. Symp.**, v.254, 9-15.
- [35] [https://www.researchgate.net/profile/Sunpreet\\_Singh6/publication/312013986/figure/fig3/AS:451105114071042@1484563248326/Materials-category-for-AM-technologies-143.png](https://www.researchgate.net/profile/Sunpreet_Singh6/publication/312013986/figure/fig3/AS:451105114071042@1484563248326/Materials-category-for-AM-technologies-143.png) [ultimo accesso marzo 2020].
- [36]Schmidleit C., Kalaskar D. M., 2018, *Stereolithography*, **3D Printing**, Dragan Cvetković, IntechOpen.
- [37]Elbadawi M., 2018, *Polymeric Additive Manufacturing: The Necessity and Utility of Rheology*, **Polymer Rheology**, Jose Luis Rivera-Armenta and Beatriz Adriana Salazar Cruz, IntechOpen.
- [38][https://www.sigmaaldrich.com/content/dam/sigma-aldrich/docs/Aldrich/General\\_Information/photoinitiators.pdf](https://www.sigmaaldrich.com/content/dam/sigma-aldrich/docs/Aldrich/General_Information/photoinitiators.pdf) [ultimo accesso marzo 2020].
- [39]<https://assets.fishersci.com/TFS-Assets/CCG/Chemical-Structures/chemical-structure-cas-77-99-6.jpg-650.jpg> [ultimo accesso marzo 2020].
- [40][https://www.sigmaaldrich.com/content/dam/sigma-aldrich/structure8/043/mfcd00084446.eps/\\_jcr\\_content/renditions/mfcd00084446-medium.png](https://www.sigmaaldrich.com/content/dam/sigma-aldrich/structure8/043/mfcd00084446.eps/_jcr_content/renditions/mfcd00084446-medium.png) [ultimo accesso marzo 2020].
- [41][https://www.sigmaaldrich.com/content/dam/sigma-aldrich/structure3/195/mfcd00148879.eps/\\_jcr\\_content/renditions/mfcd00148879-medium.png](https://www.sigmaaldrich.com/content/dam/sigma-aldrich/structure3/195/mfcd00148879.eps/_jcr_content/renditions/mfcd00148879-medium.png) [ultimo accesso marzo 2020].
- [42][https://static.wixstatic.com/media/a35c7a\\_ed56c165f48a475e8917bec8d2c91ef6~mv2\\_d\\_1400\\_1534\\_s\\_2.png/v1/fill/w\\_912,h\\_1000,al\\_c,usm\\_0.66\\_1.00\\_0.01/a35c7a\\_ed56c165f48a475e8917bec8d2c91ef6~mv2\\_d\\_1400\\_1534\\_s\\_2.png](https://static.wixstatic.com/media/a35c7a_ed56c165f48a475e8917bec8d2c91ef6~mv2_d_1400_1534_s_2.png/v1/fill/w_912,h_1000,al_c,usm_0.66_1.00_0.01/a35c7a_ed56c165f48a475e8917bec8d2c91ef6~mv2_d_1400_1534_s_2.png) [ultimo accesso marzo 2020].
- [43]<https://image.slidesharecdn.com/a58642d4-c8b6-4f27-a709-b469c83e2c57-151020110757-lva1-app6892/95/150915-presentation-at-chinaadhesive-2015-3-638.jpg?cb=1445339323> [ultimo accesso 3 marzo 2020].



